

# **The Conceptual Design of a Four-seater, General Aviation Electric Aircraft**

By

**Priya Chouhan**

Department of Aerospace Engineering  
San Jose State University

Faculty Advisor

**Dr. Nikos J. Mourtos**

July, 2020

# TABLE OF CONTENTS

## **Chapter 1: Mission Specifications and Comparative Study**

<b>1.1 Introduction</b>	15
<b>1.2 Mission Specifications</b>	15
1.2.1 Mission Specifications	15
1.2.2 Mission Profile	16
1.2.3 Market Analysis	16
1.2.4 Technical and Economic Feasibility	17
1.2.5 Critical Mission Requirements	17
<b>1.3 Comparative Study of Similar Airplanes</b>	18
1.3.1 Mission Capabilities and Configuration Selection	18
1.3.2 Comparison of Important Design Parameters	22
1.3.3 Discussion	23
<b>1.4 Conclusion and Recommendations</b>	23
1.4.1 Conclusions	23
1.4.2 Recommendations	23

## **Chapter 2: Weight Sizing and Weight Sensitivities**

<b>2.1 Introduction</b>	24
<b>2.2 Mission Weight Estimation</b>	24
2.2.1 Database for Takeoff Weight and Empty Weight of Similar Airplanes	24
2.2.2 Determination of Regression Coefficients A and B	25
2.2.3 Determination of Mission Weights	25
<b>2.3 Take-off Weight Sensitivities</b>	29
2.3.1 Manual Calculation of Takeoff Weight Sensitivity	29
2.3.2 Manual Calculation of Range Sensitivity	30
2.3.3 Trade Studies	31
<b>2.4 Discussion</b>	32
<b>2.5 Conclusions and Recommendations</b>	33

## **Chapter 3: Performance Constraint Analysis**

<b>3.1 Introduction</b>	34
-------------------------	----

<b>3.2 Manual Calculation of Performance Constraints</b>	34
3.2.1 Stall Speed	34
3.2.2 Takeoff Distance	35
3.2.3 Landing Distance	38
3.2.4 Drag Polar Estimation	41
3.2.5 Climb Constraints	44
3.2.5.1 Sizing to FAR-23 rate-of-climb requirements:	44
3.2.5.2 Sizing to climb gradient requirements:	46
3.2.6 Maneuvering Constraints	48
3.2.7 Speed Constraints	49
<b>3.3 Matching Graph</b>	50
<b>3.4 Discussion</b>	51
<b>3.5 Conclusion</b>	52
<b><u>Chapter 4: Configuration Selection</u></b>	
<b>4.1 Introduction</b>	53
<b>4.2 Comparative Study</b>	53
4.2.1 Comparison of Weights, Performance, and Geometry of Similar Airplanes:	53
4.2.2 Configuration Comparison of Similar Airplanes	54
4.2.3 Discussion	57
<b>4.3 Selection of Propulsion System</b>	57
4.3.1 Selection of Propulsion System Type:	57
4.3.2. Determination of the number of engines/batteries to be used:	58
4.3.3 Integration of the propulsion system into the configuration	58
<b>4.4 Configuration Selection</b>	59
4.4.1 Wing Configuration	59
4.4.2 Empennage Configuration	60
4.4.3 Landing Gear Configuration	60
<b>4.5 Proposed Configuration</b>	60
<b><u>Chapter 5: Fuselage Design</u></b>	
<b>5.1 Introduction</b>	62
<b>5.2 Layout Design of the Cockpit</b>	62
5.2.1 The Layout of Cockpit Seating and Cockpit Controls:	62

5.2.3 Determination of Visibility from the Cockpit	63
<b>5.3 Layout Design of the Fuselage</b>	65
5.3.1 Aerodynamic Drag Considerations	66
<b>5.4 Discussion</b>	68

## **Chapter 6: Wing, High-Lift System & Lateral Control Design**

<b>6.1 Introduction</b>	69
<b>6.2 Wing Planform Design</b>	69
6.2.1 Sweep Angle - Thickness Ratio Combination	72
<b>6.3 Airfoil Selection</b>	73
<b>6.4 Wing Design Evaluation</b>	76
<b>6.5 Design of High-lift Devices</b>	77
<b>6.6 Design of the Lateral Control Surface</b>	81
<b>6.7 Wing Drawings</b>	82
<b>6.8 Conclusions and Recommendations</b>	83

## **Chapter 7: Design of the Empennage & the Longitudinal and Directional Controls**

<b>7.1 Introduction</b>	85
<b>7.2 Overall Empennage Design</b>	85
<b>7.3 Design of Horizontal Stabilizer</b>	88
<b>7.4 Design of Vertical Stabilizer</b>	90
<b>7.5 Design of Longitudinal and Directional Control</b>	92
<b>7.6 Cad Drawings</b>	93
<b>7.7 Discussion &amp; Conclusion</b>	94

## **Chapter 8: Landing Gear Design**

<b>8.1 Introduction</b>	95
<b>8.2 Estimation of the Center of Gravity Location for the Airplane</b>	95

<b>8.3 Landing Gear Design</b>	102
8.3.1 Number, Type, and Size of Tires	102
8.3.2 Preliminary Arrangement	102
<b>8.4 Discussion</b>	106

## **Chapter 9: Weight and Balance Analysis**

<b>9.1 Introduction</b>	108
<b>9.2 Component Weight Breakdown</b>	108
<b>9.3 Center of Gravity Location for Various Loading Scenarios</b>	109
<b>9.4 Discussion</b>	110

## **Chapter 10: Stability and Control Analysis**

<b>10.1 Introduction</b>	111
<b>10.2 Static Longitudinal Stability</b>	111
<b>10.3 Static Directional Stability</b>	113
<b>10.4 Conclusion</b>	114

## **Chapter 11: Drag Polar Estimation**

<b>11.1 Introduction</b>	115
<b>11.2 Airplane Zero-lift Drag</b>	115
<b>11.3 Low-speed Drag Increments</b>	117
11.3.1 High-Lift Device Drag Increments for Takeoff Flaps, Landing Flaps and Landing Gear	117
<b>11.4 Airplane Drag Polar</b>	117
<b>11.5 Discussion</b>	118
<b>11.6 Conclusion</b>	119

## **Chapter 12: Drawings, Environmental and Safety Considerations**

<b>12.1 Drawings</b>	120
12.1.1 Areas to improve:	123
<b>12.2 Environmental Considerations</b>	123

**12.3 Safety Considerations**

123

**References**

125

## TABLE OF SYMBOLS

Symbol	Definition	Dimensions
AR	Aspect Ratio	---
A, B	Regression Line Coefficients	---
b	Wing Span	ft
C	Fuel Fraction Parameter	---
c	Wing Chord	ft
$\bar{c}$	Wing Mean Geometric Chord	ft
$c_f$	Equivalent Skin Friction Coefficient	---
$C_D$	Drag Coefficient	---
$C_{D0}$	Zero Lift Drag Coefficient	---
CGR	Climb Gradient	rad
CGRP	Climb Gradient Parameter	rad
$C_L$	Lift Coefficient	---
$C_{L\alpha}$	Airplane Lift-Curve Slope	1/rad
$C_{L\alpha_W}$	Wing Lift-Curve Slope	1/rad
$d_f$	Fuselage Diameter	ft
D	Drag	lbs
$D_p$	Propeller Diameter	ft
$D_t$	Max. Tire diameter	ft
e	Oswald's Efficiency Factor	---
E	Endurance	hours
$E^*$	Specific Energy Density of Battery	Wh/kg
f	Equivalent Parasite Area	ft <sup>2</sup>
F	Weight Sensitivity Parameter	lbs

FAR	Federal Air Regulation	---
g	Acceleration of Gravity	ft/sec <sup>2</sup>
h	Altitude	ft
I <sub>p</sub>	Power Index	(hp/ft <sup>2</sup> ) <sup>1/3</sup>
i <sub>w</sub>	Wing Incidence Angle	deg
L	Lift	lbs
L/D	Lift-to-Drag Ratio	---
l <sub>f</sub>	Fuselage Length	ft
l <sub>m</sub>	Dist. c.g to Main Gear	ft
l <sub>n</sub>	Dist. c.g to Nose Gear	ft
k	Ratio of Airfoil Lift-Curve Slope to 2π	---
M <sub>ff</sub>	Mission Fuel Fraction	---
nm	Nautical Miles	nm
n <sub>p</sub>	Number of Propeller Blades	---
P	Power	hp
P <sub>bl</sub>	Blade Power Loading	hp/ft <sup>2</sup>
P <sub>n</sub>	Load on Nose Wheel Strut	lbs
<u>q</u>	Dynamic Pressure	psf
R	Range	nm or m
RC	Rate of Climb	Fpm or fps
RCP	Rate of Climb Parameter	hp/lbs
S	Wing Area	ft <sup>2</sup>
S <sub>wet</sub>	Wetted Area	ft <sup>2</sup>
S <sub>BS</sub>	Body Side Area	ft <sup>2</sup>
t/c	Thickness Ratio	---
TOP <sub>23</sub>	FAR 23 Takeoff Parameter	lbs <sup>2</sup> /ft <sup>2</sup> hp

V	True Airspeed	mph, knts
$\underline{V}$	Volume Coefficient	---
W	Weight	lbs
$\underline{X_{ac}}$	Distance from Leading Edge $\underline{c}$ to Aerodynamic Center	
$\lambda$	Taper Ratio	---
$\Lambda$	Sweep Angle	deg
$\Gamma$	Dihedral Angle	deg
$\eta_p$	Propeller Efficiency	---
$\pi$	Product, or 3.142	---
$\rho$	Air Density	slugs/ft <sup>3</sup>
$\sigma$	Air Density Ratio	---
x	Distance from the Leading Edge	ft
y	Span Wise Coordinate	ft
z	Vertical Distance from the Ground	ft

## LIST OF FIGURES

Figure 1.1: Mission profile	12
Figure 1.2: Global electric market trends [2]	13
Figure 1.3: Aerospace Sunflyer 4 aircraft model [6]	15
Figure 1.4: Pipistrel Panthera aircraft model [7]	16
Figure 1.5: Yuneec E430 aircraft model [8]	17
Figure 2.1: Regression Plot	22
Figure 2.2: Different Propulsion System Efficiencies [11]	24
Figure 2.4: Take-off Weight Vs Payload Weight	28
Figure 2.5: Take-off Weight Vs Lift-to-Drag ratio	29
Figure 2.6 Range Vs L/D	29
Figure 3.1: Maximum lift coefficient values for various types of airplanes [1]	32
Figure 3.4: FAR 23 landing distance definition	35
Figure 3.6: Relation between ground run and landing distance [1]	36
Figure 3.8: Equivalent parasite area Vs wetted area [1]	39
Figure 3.9: Range of values for W/P and W/S satisfying FAR 23.67 requirements	42
Figure 3.10: Range of values for W/P and W/S satisfying FAR 23.65 requirements	44
Figure 3.11: Range of values for W/P and W/S satisfying FAR 23.77 requirements	45
Figure 3.12: Combined range of values for W/P and W/S satisfying FAR 23 requirements	45
Figure 3.13: Airplane speed Vs power index	46
Figure 3.14: Allowable W/S and W/P to meet a given cruise speed	47
Figure 4.1: 3-Views of Pipistrel panthera [7]	51
Figure 4.2: 3-Views of Sunflyer 4 [6]	52
Figure 4.3: 3-Views of Yuneec E-430 [8]	52
Figure 4.4: 3-Views of Electro G2 [9]	53
Figure 4.5: 3-Views of Airbus Vahana [10]	54
Figure 4.6: T-tail configuration	57
Figure 4.7: 3D Models of the proposed configuration	58
Figure 5.1: Recommended sitting arrangement for civil airplanes [1]	59
Figure 5.2: Dimensions for civil cockpit controls [1]	60
Figure 5.3: Radial eye vector's definition [1]	61
Figure 5.4: Side view of the cockpit	62
Figure 5.5: Top view of the cockpit	62
Figure 5.6: Definition of geometric fuselage parameters [1]	62
Figure 5.7: Geometric fuselage parameters currently employed for different airplanes [1]	63
Figure 5.8: Length of the fuselage with respect to maximum take-off weight for different airplanes [15]	63
Figure 5.9: Side view of fuselage	65
Figure 5.10: Top view of fuselage	65
Figure 5.11: Isometric view of fuselage	65
Figure 6.1: Wing geometric data for various single engine airplanes [1]	67
Figure 6.2: Trapezoidal wing geometry [1]	68

Figure 6.3: Historical trend of thickness to chord ratio with respect to design mach number [15]	70
Figure 6.4: Airfoil geometry	70
Figure 6.5: NASA LS(1)-0417 airfoil profile [15]	71
Figure 6.6: NASA LS(1)-0417 airfoil performance graph [15]	71
Figure 6.7: NASA LS(1)-0413 airfoil profile	72
Figure 6.8: NASA LS(1)-0413 airfoil performance graph [16]	73
Figure 6.9: Summary of the effect of wing incidence angle	73
Figure 6.10: Flap geometry [1]	76
Figure 6.11: Effect of flap chord ratio and flap type on K [1]	76
Figure 6.12: Effect of thickness ratio and flap chord ratio on $c_{lf}$	77
Figure 6.13: Effect of flap chord ratio and flap deflection on K'	77
Figure 6.14: Aileron data for single engine propeller driven airplane	79
Figure 6.14: Front view of wing planform	80
Figure 6.15: Side view of wing planform	80
Figure 6.16: Approximate empty weight buildup [15]	81
Figure 7.1: Empennage moment arm	83
Figure 7.2: Horizontal tail volume and elevator data for single engine aircraft	84
Figure 7.3: Vertical tail volume, rudder and aileron data for single engine aircraft	84
Figure 7.4: Horizontal tail design planform parameters	86
Figure 7.5: Vertical tail design planform parameters	88
Figure 7.6: Isometric view of empennage planform with respect to wing	90
Figure 7.7: Front view of empennage planform	90
Figure 7.8: Top view of empennage planform	91
Figure 8.1: Landing gear parameters	92
Figure 8.2: Location of the CG of major components	95
Figure 8.3: Class-I weight and balance calculations	96
Figure 8.4: CG excursion diagram	98
Figure 8.5: Geometry for Static load tricycle gear	99
Figure 8.6: Longitudinal tip-over criterion for tricycle gear	100
Figure 8.7: Longitudinal tip-over criterion for the proposed aircraft	100
Figure 8.8: Lateral tip-over criterion	101
Figure 8.9: Lateral Tip-over criterion for the proposed aircraft	101
Figure 8.10: Longitudinal ground clearance criterion for tricycle gear [1]	102
Figure 8.11: Longitudinal ground clearance criterion for the proposed aircraft	102
Figure 8.12: Lateral ground clearance criterion for tricycle gear	103
Figure 8.13: Lateral ground clearance criterion for the proposed aircraft	103
Figure 9.1: CG excursion diagram	107
Figure 10.1: Longitudinal stability x-plot	114
Figure 10.2: Directional stability x-plot	115
Figure 11.1 Exposed planform definition	117
Figure 11.2: Cruise, takeoff and landing drag polar	120

Figure 12.1: Isometric view of the proposed aircraft	122
Figure 12.2: Side view of the proposed aircraft	122
Figure 12.3: Top view of the proposed aircraft	123
Figure 12.4: Front view of the proposed aircraft	123

## LIST OF TABLES

Table 1.1: Mission specifications	12
Table 1.2: Mission capabilities of Sunflyer 4	14
Table 1.3: Mission capabilities of Panthera	15
Table 1.4: Mission capabilities of Yuneec E-430	16
Table 1.5: Mission capabilities of Taurus Electro G2	17
Table 1.6: Mission capabilities of Airbus Vahana	18
Table 1.7: Similar aircraft datasheet	18
Table 2.1: Database for similar airplanes	21
Table 2.2: Specific energy density [12]	23
Table 2.3: Suggested values for several missions [1]	24
Table 2.4: Results of mission weights	26
Table 2.5: Takeoff weight and range sensitivity	28
Table 3.1: Required values for power loading	34
Table 3.2: Required values of wing loading at different values of lift coefficient	37
Table 3.3: Constants a and b based on skin friction coefficient [1]	39
Table 3.4: Values of constants c and d for various aircrafts	40
Table 3.5: First estimates for zero lift drag coefficient	40
Table 3.6: Drag polar for the proposed aircraft	41
Table 3.7: Range of values satisfying FAR 23.67 requirements	42
Table 3.8: Range of values satisfying FAR 23.65 requirements	43
Table 3.9: Range of values satisfying FAR 23.77 requirements	44
Table 3.10: Design parameters	48
Table 4.1: Comparison chart of similar airplanes	50
Table 4.2: Specific energy density of the proposed battery system[12]	55
Table 4.3: Configuration for the proposed design	56
Table 5.1: Fuselage dimensions	64
Table 6.1: Results of take-off and landing flap incremental maximum lift coefficients for two arbitrary values of $S_{wf}$	75
Table 6.2: Summary of flap geometry	78
Table 6.3: Wing parameters	79
Table 8.1: Component weight fractions for similar airplanes and the proposed aircraft	93
Table 8.2: Mission weights	93
Table 8.3: Subgroup component weight summary for the proposed aircraft	94
Table 8.4: Center of gravity location of major components	94
Table 8.5: Components weight and coordinate data for the proposed aircraft	96
Table 8.6: Loading scenarios	97
Table 9.1: Components with final weight and coordinate data	105
Table 9.2 : Final CG location for different loading scenarios	106
Table 10.1: Static longitudinal stability parameters [Appendix B]	113
Table 10.2: Static directional stability parameters [Appendix B]	115

Table 11.1 : Summary of components wetted area and total wetted area	118
Table 11.2: Flap drag increment for different flight conditions	119
Table 11.3: Drag polar equations	119
Table 11.4: Part I and part II L/D values	120
Table 12.1: Important design parameters	124

# Chapter 1

## Mission Specifications and Comparative Study

### 1.1 Introduction

The major source of energy in the aviation industry comes from fossil fuels, and the dominant fossil fuels used today by most industrialized and developing countries are oil, coal, and natural gas. More energy consumption leads to the rise in demand for fossil fuels in the next few decades, which results in increased prices, CO<sub>2</sub> emissions, and noise. There are plenty of ways to convert energy without fossil fuels, and many are being used, but not nearly to their full potential [1]. Hence, this report presents an electric four-seater aircraft as an alternative to conventional gasoline aircraft. The idea here is to save the environment from the harmful effects of fossil fuels by introducing an eco-friendly propulsion system with better aircraft design.

Electric aircraft have the following advantages:

1. Lower emissions
2. Suppression of noise during taxing and landing
3. Eco-friendly environment
4. Lower operating costs compared to ICE-powered vehicles
5. Improved efficiency

The challenge associated with electric aircraft is the battery specific energy density. To meet the mission requirements, an electric aircraft must be able to deliver sufficient power with the chosen battery system. It requires an electric motor that produces greater horsepower while keeping the weight minimum. In this design report, all the limitations will be carefully addressed and all the possible design solutions will be documented. The mission specifications of the proposed aircraft configuration will now be analyzed.

### 1.2 Mission Specifications

#### 1.2.1 Mission Specifications

The proposed aircraft is a light aircraft with a maximum capacity of 4 passengers. The mission requirement for the proposed aircraft design is given below.

**Table 1.1: Mission specifications**

<b>Power System</b>	Electric Propulsion
<b>Payload Capacity</b>	3
<b>Crew</b>	1
<b>Range</b>	400 nm (750km)
<b>Cruise Speed</b>	170 mph (272 km/h)
<b>Mach number</b>	0.23
<b>Cruise altitude</b>	10,000 ft
<b>Takeoff distance</b>	2500 ft
<b>Landing distance</b>	2000 ft
	General Aviation, FAR 23 Certifiable

### 1.2.2 Mission Profile

The mission phases and profile for the proposed design are shown below.

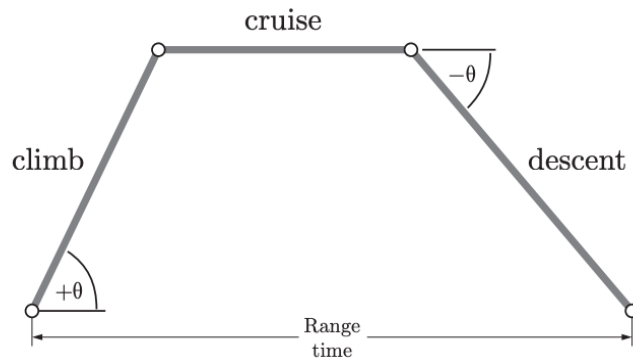


Figure 1.1: Mission profile

### 1.2.3 Market Analysis

General Aviation (GA) is a category of aviation that includes many aircraft subcategories. It covers certain commercial and private flights that can be carried out under both visual flight (VFR) and instrument flight (IFR) rules, such as light and ultra-light aircraft, sport aircraft, business aircraft, and helicopters. It basically represents the private transport component of aviation.

General aviation is a huge market that is evidently expanding fast. The total number of shipped GA aircraft doubled from 1,132 in 1994 to 2,262 units in 2016 [2]. The main concern for aviation industries is the increased demand and the price of fuel, which is basically impelling them to look for alternatives to

conventional fuel sources. Production of these fossil fuels is expected to rise, approximately doubling the amount of use of each fossil fuel. As the world population continues to grow and the limited amount of fossil fuels begins to diminish, it may not be possible to provide the amount of energy demanded by the world by only using fossil fuels to convert energy [4]. The main goal of the aircraft industry is to keep up the growth by offering the capability in an economical, safe and eco-friendly way. Environmental concern for global warming is a major factor to be considered in aircraft market analysis. The global electric market trend shows a projected market increase of 4.33% globally.

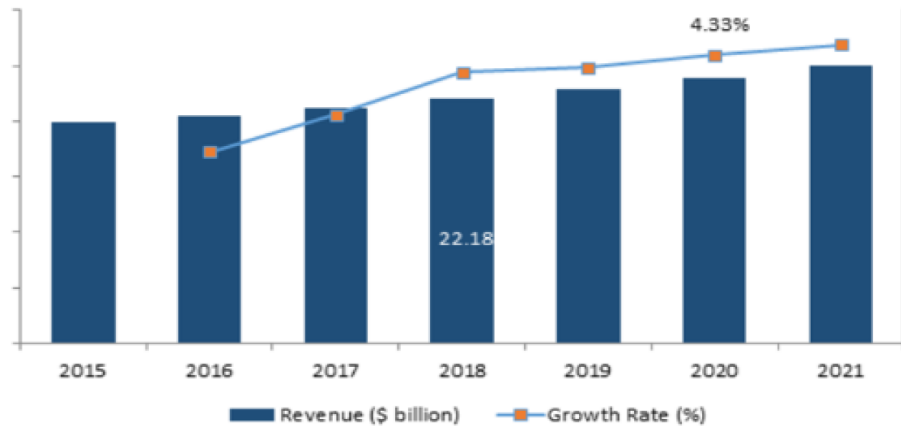


Figure 1.2: Global electric market trends [2]

### 1.2.4 Technical and Economic Feasibility

Currently, due to the low available energy density of the batteries, the weight of the battery required for the given mission tends to be heavy. Hence, only small general aviation aircrafts are feasible at this time. As research continues to push the limits of current battery technology, we anticipate that 5 years from now we can have better battery technology. The current generation batteries cannot be used to power large airliners. Therefore, the development of electric aircraft has been restricted to small general aviation aircraft and unmanned aerial vehicles (UAV). Thus, the proposed aircraft is suitable for medium-distance routes about 450 nautical miles and will carry four passengers including the pilot.

### 1.2.5 Critical Mission Requirements

A crucial thing to take into account when considering batteries is the weight they add to the aircraft. While the electric motor actually brings down the total takeoff mass of the aircraft, it is the batteries which make it skyrocket. A parameter to be considered when choosing the batteries must be their energy density. A bigger value indicates a greater energy for the same weight.

Compared to the current state-of-art with specific energy values of 150 to 250 Wh/kg, the mass-specific energy density would have to be increased at least by a factor of 5 to become useful. More realistically, this factor would have to be in the order of 10 to attract commercial interest for passenger aircraft. The critical requirements are those that are affected by the battery energy density which primarily includes the range and takeoff weight.

The critical mission requirements for the proposed design are as follows:

1. Takeoff weight
2. Range : 750 kms
3. Takeoff distance : 2500 ft

## 1.3 Comparative Study of Similar Airplanes

### 1.3.1 Mission Capabilities and Configuration Selection

#### 1. Bye Aerospace Sunflyer 4

The Sun Flyer 4 features a cantilever low wing, a four-seat enclosed cockpit under a bubble canopy, fixed tricycle landing gear with wheel pants and a single electric motor in tractor configuration [6].

**Table 1.2: Mission capabilities of sunflyer 4**

Power System	Electric
Payload Capacity	3
Crew	1
Range	4 hours
Cruise Speed	130mph
Takeoff Weight	2700lbs
Wing Area	120 sq ft



Figure 1.3: Aerospace Sunflyer 4 aircraft model [6]

## 2. Pipistrel Panthera

The Pipistrel Panthera is a lightweight, all-composite, highly efficient four-seat aircraft under development by Pipistrel of Slovenia. The sleek four-seater is powered by a Siemens 200 kW electric motor. [7].

**Table 1.3: Mission capabilities of Panthera**

Payload Capacity	3
Crew	1
Range	1200 km
Cruise Speed	163mph
Takeoff Weight	2640lbs
Wing Area	117 sq ft



Figure 1.4: Pipistrel Panthera aircraft model [7]

## 3. Yuneec E-430

The E430 is a Chinese two-seat electric aircraft designed for commercial production by the electric model aircraft manufacturer Yuneec International. It is a V-tailed, composite aircraft with high wing configuration[8].

**Table 1.4: Mission capabilities of yuneec E-430**

Payload Capacity	1
Crew	1
Range	227 km
Cruise Speed	56 mph
Takeoff Weight	1036 lbs
Wing Area	122 sq. ft



Figure 1.5: Yuneec E430 aircraft model [8]

#### **4. Pipistrel Taurus Electro G2**

The Taurus Electro G2 replaces the old gasoline-powered engine with the high-performance electric power train. It is a 2-seat glider with Li-Po batteries that can cover a range of 370 miles. It is a low wing configuration with a T-tail[9].

**Table 1.5: Mission capabilities of taurus electro G2**

Payload Capacity	1
Crew	1
Range	595 km
Cruise Speed	93 mph
Takeoff Weight	1200 lbs



Figure 1.6: Taurus G2 aircraft model [9]

#### 4. Airbus Vahana

The Airbus Vahana is an electric-powered eight-propeller VTOL personal air vehicle prototype by Airbus. [10].

**Table 1.6: Mission capabilities of airbus vahana**

Payload Capacity	2
Crew	None (self-piloted)
Range	100 km
Cruise Speed	140 mph
Takeoff Weight	1797 lbs



Figure 1.7: Airbus vahana aircraft model [10]

### 1.3.2 Comparison of Important Design Parameters

Table 1.7: Similar aircraft datasheet

<b>Aircraft Model</b>	<b>Sun Flyer 4</b>	<b>Pipistrel Panthera</b>	<b>Yuneec E-430</b>	<b>Pipistrel Taurus Electro G2</b>	<b>Airbus Vahana</b>
<b>Crew</b>	1	1	1	1	None (self piloted)
<b>Passengers</b>	3	3	1	1	2
<b>Wing Span</b>	12m	10.86m	13.8m	14.97m	6.25m
<b>Empty Weight</b>	862 kg	800 kg	250 kg	306kg	695kg
<b>Gross Weight</b>	1225 kg	1200kg	470 kg	550kg	815kg
<b>Powerplant</b>	1 electric motor 141hp (105kW)	Pure electric 195hp (145 kW)	Yuneec power drive 40kW	electric Li-Po	electric
<b>Cruise Speed</b>	150 mph (240km/h)	118 knots /218 kmph	56 mph 90 kmph	150 kmph	120 knots 140 mph 230 kmph
<b>Rate of Climb</b>	6.4 m/s	5.7m/s	3.5m/s	3.1m/s	-
<b>Wing Loading</b>	110kg/m <sup>2</sup>	-	41.3kg/m <sup>3</sup>	-	-
<b>Range Endurance</b>	4 hours	400 km 215 nm	227 km	370 mile 590 km	100km
<b>Surface ceiling</b>	-	4000m	-	2000m	3048 m 10000 ft

### **1.3.3 Discussion**

A comparative study of similar airplanes is performed as shown in Table (1.7). All the similar aircraft models are electric aircraft with different payload capacities.

The Pipistrel Panthera electro and Airbus Vahana are still under development. The comparison is mainly based on electric aircraft with different seating arrangements. Most of the aircraft above have a low wing design with a T-tail configuration except for the Yuneec E430 which is a high wing configuration. The proposed aircraft used a configuration like the Pipistrel Panthera. The low wing configuration does not require the use of struts for structural support.

The range is high for the Pipistrel and the Sun Flyer 4 compared to the other aircraft, whereas the proposed aircraft is expected to achieve a range of 800 km with more electric power. The proposed design structure can be made of more composites than aluminum alloys. The electric propulsion system reduces noise compared to conventional gas turbine engines. The need for energy efficiency, lower environmental impact, with low operating costs make this electric aircraft more desirable for the present aviation market.

## **1.4 Conclusion and Recommendations**

### **1.4.1 Conclusions**

A detailed report of the proposed design with the mission requirements and a comparative study of similar aircraft has been presented. The critical mission requirement is the range of the aircraft, as it depends on the battery energy density. Replacing fossil fuels completely with electric power is quite challenging so a study will be conducted by assuming a futuristic value for battery energy density. This proposed design is mainly for personal transportation with electric power. Summing up the entire discussion and comparison, an electric design is better in terms of safety, environmental protection, and lower operating and maintenance costs than a conventional design.

### **1.4.2 Recommendations**

Though the electric design has many advantages, practically achieving the design and utilizing electric power while keeping the battery weight minimum is challenging. The present aviation market needs a better electric propulsion system that can endure longer and carry more passengers.

# Chapter 2

## Weight Sizing and Weight Sensitivities

### 2.1 Introduction

This report presents weight sizing, weight sensitivities and range sensitivities for the proposed aircraft design. As the proposed aircraft is an electric propulsion design, no fuel related calculations are required in this report. The procedure from Roskam will be used for calculating the weight sizing and range sensitivities.

This report presents an estimation method for a given mission specification for the following weights:

- Takeoff Weight,  $W_{TO}$
- Empty Weight,  $W_E$
- Battery Weight,  $W_{BAT}$

### 2.2 Mission Weight Estimation

The mission weight estimates are primarily to determine the minimum aircraft weight, empty weight and battery weight needed to accomplish the given mission requirements.

#### 2.2.1 Database for Takeoff Weight and Empty Weight of Similar Airplanes

**Table 2.1: Database for similar airplanes**

Aircraft	Takeoff Weight ( $W_{TO}$ ), lbs	Empty Weight ( $W_E$ ), lbs
Pipistrel Taurus Electro G2	1212	674
Lange Antares 23E	1873	1124
Extra 330 LE	2094	1455
Sunflyer 4	2700	1900
Airbus Vahana	1797	1532
Pipistrel Panthera	2645	1764
Silent 2	6482	4321
Electrolight 2	6805	4062
NASA Scuba Stingray	3195	1438
Electrolight 2	6805	4062

### 2.2.2 Determination of Regression Coefficients A and B

Based on the above database for takeoff weights and empty weights, the following graph has been plotted using Excel:

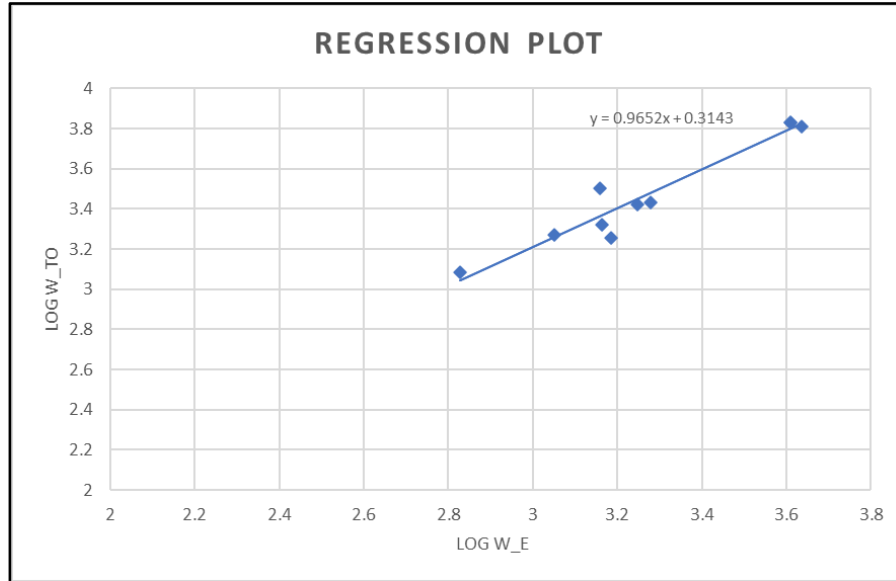


Figure 2.1: Regression plot

The Regression coefficients are calculated from the trend line equation:

$$y = 0.9652x + 0.3143 \quad (1)$$

The relationship between takeoff weight and empty weight in the regression plot is given by:

$$\text{Log } W_{\text{TO}} = A + B \text{ log } W_{\text{E}} \quad (2)$$

Comparing equation (1) & (2),

$$y = \text{Log } W_{\text{TO}}$$

$$x = \text{Log } W_{\text{E}}$$

Therefore,

$$A = 0.3143$$

$$B = 0.9652$$

### 2.2.3 Determination of Mission Weights

The Mission Weights are calculated manually by using the Roskam [1] procedure. The battery weight is calculated using the Hepperle's Range method.

### 2.2.3.1 Manual calculation of mission weights

The mission weights are calculated using the following steps:

- **Mission Payload Weight**

The mission requirements specify the passenger capacity of 4 including one pilot. The pilot is considered in the payload calculation.

The average weight of 175 lbs per person and 30 lbs of baggage is considered for commercial airplanes using Roskam data [1].

$$W_{PL} = 4 * (175 + 30)$$

$$W_{PL} = 820 \text{ lbs}$$

- **Battery Weight**

The Battery weight is calculated as per Martin Hepperle's Range Equation [12] as follows:

$$R = E * \eta * \left(\frac{1}{g}\right) * \left(\frac{L}{D}\right) * \left(\frac{W_{BAT}}{W_{TO}}\right) \quad (4)$$

The above equation clearly indicates the aircraft range is dependent on the lift-to-drag ratio, specific energy density, total system efficiency, and takeoff weight of the aircraft. Specific energy density is assumed for the calculation of battery weight. Table (2.2) shows a theoretical possible value of specific energy and expected values in the future based on a survey of battery systems conducted by Hepperle [12].

**Table 2.2: Specific energy density [12]**

Battery	Theoretical Value	Expected in the next 5-10 years
Li-Ion	390 Wh/kg	250 Wh/kg
Zn-air	1090 Wh/kg	400-500 Wh/kg
Li-S	2570 Wh/kg	500-1250 Wh/kg
Li-O <sub>2</sub>	3500 Wh/kg	800-1750 Wh/kg

The proposed aircraft is designed based on the future battery system. As per Table (2.2), it is reasonable to assume that energy density can reach close to 1500Wh/kg in the next ten years.

Figure 2.2 shows a different propulsion system efficiency chart. The battery propulsion system has the highest efficiency as compared to a conventional turboprop, turbofan and fuel cell.

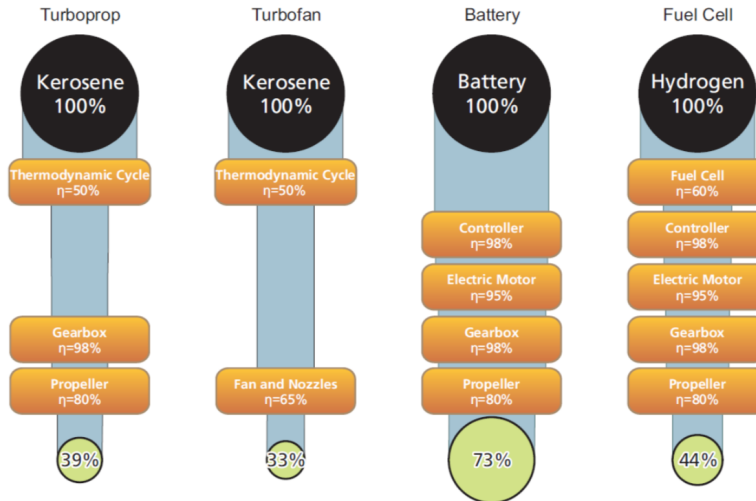


Figure 2.2: Different propulsion system efficiencies [11]

Based on Roskam [1], the L/D ratio is chosen for single-engine aircraft. A value of 10 is assumed based on similar aircraft.

Table 2.3: Suggested values for several missions [1]

Mission Phase No. (See Fig. 2.1)	L/D	Cruise			L/D	Loiter		
		$c_j$	$c_p$	$\eta_p$		$c_j$	$c_p$	$\eta_p$
Airplane Type		lbs/lbs/hr	lbs/hp/hr		lbs/lbs/hr	lbs/hp/hr		
1. Homebuilt	8-10*		0.6-0.8	0.7	10-12		0.5-0.7	0.6
2. Single Engine	8-10		0.5-0.7	0.8	10-12		0.5-0.7	0.7
3. Twin Engine	8-10		0.5-0.7	0.82	9-11		0.5-0.7	0.72
4. Agricultural	5-7		0.5-0.7	0.82	8-10		0.5-0.7	0.72

The summary of the calculated value from Appendix A is shown below.

$$W_{BAT} = 0.162 W_{TO}$$

- **Takeoff Weight**

The takeoff weight is calculated using the following equation:

$$W_{TO} = W_{OE} + W_F + W_{PL} + W_{BAT} \quad (5)$$

Based on the similar aircraft, we can guess the value of takeoff weight as:

$$W_{TO} = 3500 \text{ lbs}$$

- **Tentative Value of Operating Empty Weight**

The tentative operating empty weight is calculated by:

$$W_{OE\ tent} = W_{TO\ guess} - W_F - W_{PL} - W_{BAT} \quad (10)$$

- **Tentative Value for Empty Weight**

The tentative empty weight is calculated by:

$$W_{E\ tent} = W_{OE\ tent} - W_{tfo} \quad (11)$$

As per the Roskam data [1] for airplane design, the  $W_{tfo}$  can be 0.5% or more of  $W_{TO}$

Assuming it is 0.5% of takeoff weight then,

$$W_{tfo} = 0.005 W_{TO} \quad (12)$$

- **Allowable Value of Empty Weight**

$$W_E = \text{inv. Log}_{10} [(Log_{10} W_{TO} - A)/B]$$

$$\text{Log } W_{TO} = A + B * \log W_E \quad (13)$$

- **Comparing the Allowable and Tentative Empty Weight**

Comparing the allowable and tentative empty weights and adjusting the guess take-off weight by the iterative process until the difference is within 0.5% tolerance. The following mission weights are obtained using all the above-discussed equations. Calculations are attached in Appendix A.

**Table 2.4: Results of mission weights**

Take-off weight $W_{TO}$ (lbs)	3980
Payload weight $W_{PL}$ (lbs)	820
Empty Weight $W_E$ (lbs)	2535
Operating empty weight, $W_{OE}$ (lbs)	2523
Battery Weight, $W_{Bat}$ (lbs)	637

## 2.3 Take-off Weight Sensitivities

The outcomes from the last section depend on the values selected for the various parameters in the range equation. Once the preliminary sizing has been done, it is required to conduct sensitivity studies on some critical parameters.

### 2.3.1 Manual Calculation of Takeoff Weight Sensitivity

Take-off weight sensitivity will be obtained using regression coefficients A and B and other parameters like C and D. The parameters C and D are given by

$$W_E = C * W_{TO} - D \quad (14)$$

Where,

$$C = 1 - (1 + M_{res}) * (1 - M_{ff}) - M_{tfo} \quad (15)$$

Since, the proposed aircraft is electric so  $M_{res}$  and  $M_{ff}$  equals to zero

$$C = 0.995$$

And

$$D = W_{PL} + W_{crew} + W_{Bat} \quad (16)$$

$$D = 1457 \text{ lbs}$$

The value of **A = 0.3413** and **B = 0.9652** from the regression plot obtained from section 2.2.2

- **Sensitivity of Takeoff Weight to Payload Weight**

$$\frac{\delta W_{TO}}{\delta W_{PL}} = \frac{B * W_{TO}}{(D - C(1-B) * W_{TO})} \quad (17)$$

Where,

$$A = 0.3413, B = 0.9652$$

$$C = 0.995 \text{ and } D = 1457$$

$$W_{TO} = 3980 \text{ lbs from previous section}$$

By substituting all the values in the above equation, we get

$$\frac{\delta W_{TO}}{\delta W_{PL}} = 2.92$$

This means that for each pound of payload added, the airplane take-off weight will have to increase by 2.92 lbs. The factor 2.92 is called the growth factor due to payload.

- **Sensitivity of Takeoff Weight to Empty Weight**

$$\frac{\delta W_{TO}}{\delta W_E} = \frac{B * W_{TO}}{inv.Log_{10} [(Log_{10} W_{TO} - A) / B]} \quad (18)$$

By substituting values, we get

$$\frac{\delta W_{TO}}{\delta W_E} = 1.515$$

This means that take-off weight must be increased by 1.515lbs for each pound of increase in empty weight to keep the mission performance the same.

### 2.3.2 Manual Calculation of Range Sensitivity

- **Sensitivity of Range to Takeoff Weight**

The sensitivity of range to take-off weight is given by Hepperle[11] as

$$\frac{\partial R}{\partial W_{TO}} = - E^{**} \eta_{tot} * \left(\frac{L}{D}\right) * \left(\frac{1}{g}\right) * \left(\frac{W_{BAT}}{W_{TO}^2}\right) \quad (19)$$

- **Sensitivity of Range to Lift-to-Drag ratio**

$$\frac{\partial R}{\partial (L/D)} = (1 - f_e - f_p) * E^{**} \eta_{tot} * \left(\frac{1}{g}\right) \quad (20)$$

- **Sensitivity of Range to Battery Energy density**

$$\frac{\partial R}{\partial E^{**}} = (1 - f_e - f_p) * \left(\frac{L}{D}\right) * \eta_{tot} * \left(\frac{1}{g}\right) \quad (21)$$

The results of range sensitivities are obtained by using the above equations calculated manually attached in Appendix A. The results are as follows:

**Table 2.5 Takeoff weight and range sensitivity**

Sensitivity Parameters	Sensitivity Values
$\frac{\partial W_{TO}}{\partial W_{PL}}$	2.92 lbs
$\frac{\partial W_{TO}}{\partial W_E}$	1.515 lbs
$\frac{\partial R}{\partial W_{TO}}$	-0.188 km/lbs

$\frac{\partial R}{\partial(L/D)}$	74 km
$\frac{\partial R}{\partial E^*}$	0.50 km/Wh/kg

### 2.3.3 Trade Studies

The trade studies are performed for various parameters with respect to takeoff weight and range as shown below:

- **Takeoff Weight Versus Payload Weight**

Takeoff weight is directly proportional to payload weight from equation (5), the graph below clearly indicates that take-off weight increases with an increase in payload weight.

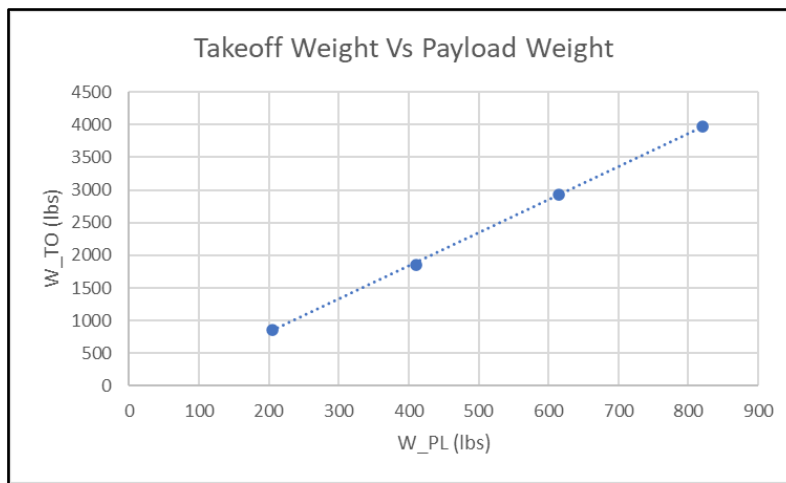


Figure 2.4: Take-off Weight Vs Payload Weight

- **Specific Energy Density Vs Range**

The specific energy density of the battery greatly affects the overall range of the aircraft. A bigger value indicates a greater energy for the same weight, thereby allowing the aircraft to cover more distance.

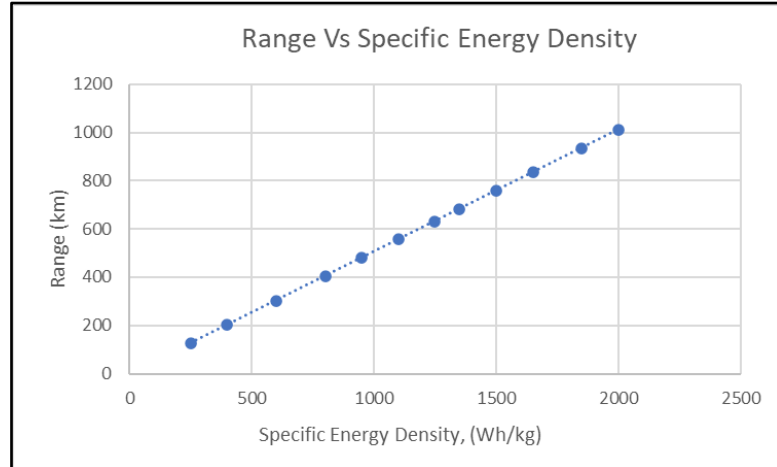


Figure 2.5: Take-off Weight Vs Lift-to-Drag ratio

- **Range Vs Lift-to-Drag Ratio**

The range is directly proportional to the lift-to-drag ratio, so the range increases with an increase in the lift-to-drag ratio.

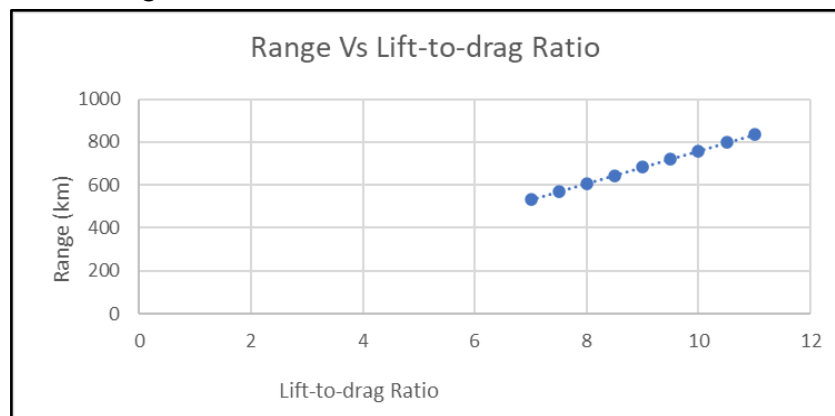


Figure 2.6 Range Vs L/D

## 2.4 Discussion

This chapter presented a class-I preliminary weight estimation for the electric aircraft. The regression coefficient plays a vital role in the calculation of aircraft-allowable weight. Assumptions have been made in the range equation, especially on the battery energy density, which would directly affect the overall aircraft range as the proposed configuration is an electric design. The assumptions seem to be reasonable, as per the current battery efficiency trends, attaining a value of 1500Wh/kg in the next 5-10 years seems possible. A trade study was performed between important parameters with respect to takeoff weight and range. This study shows dependence of range on battery energy density keeping the gross weight constant. The range follows a linear relationship with lift-to-drag ratio.

## **2.5 Conclusions and Recommendations**

The takeoff weight of the electric design is high as compared to the conventional aircraft due to the batteries that add more weight to the design. This weight can be reduced and the range of the aircraft can be improved by optimizing the battery technology. The range is directly proportional to the lift-to-drag ratio and the battery energy density, so appropriate values are assumed. The battery needs further research as the range and overall weight of an aircraft are directly affected by it.

# Chapter 3

## Performance Constraint Analysis

### 3.1 Introduction

In previous chapters, mission specifications, configuration selection and weight sizing of the proposed aircraft were introduced. This chapter presents a performance constraint analysis for the proposed design with the use of data obtained in previous chapters.

The following performance constraints will be analyzed in this report:

- Stall Speed
- Take-off Distance
- Landing Distance
- Cruise Speed
- Climb Rate
- Maneuvering

The main purpose of this report is to provide methods that allow the estimation of design parameters which have a major impact on the above-listed performance categories. Since the proposed aircraft is an electric propulsion design with a takeoff weight less than 6000 lbs, it falls into the FAR-23 certification category. Thus, all the performance constraint calculations will be determined based on the FAR-23 guidelines.

The proposed methods will determine a range of values for wing loading, thrust or power loading, and maximum lift coefficient. When all the constraint plots are consolidated into a single plot/matching graph, it is possible to size the takeoff wing loading and takeoff power loading to appropriate values for this aircraft.

### 3.2 Manual Calculation of Performance Constraints

#### 3.2.1 Stall Speed

A stall is a condition where the lift coefficient generated by an airfoil starts reducing as the angle of attack increases. As per the guidelines for FAR-23 certification, a single-engine airplane may not have a stall speed greater than 61 knots at take-off weight less than 6000 lbs. Since the proposed aircraft is below 6000 lbs and is an electric general aviation aircraft, the stall speed should be under 61 knots.

The power-off stall speed for the proposed aircraft can be derived from:

$$V_{stall} = \left( \frac{2 * (W/S)}{\rho * C_{Lmax}} \right)^{1/2} \quad (1)$$

The lift coefficient is influenced by the following factors:

- Wing and Airfoil Design
- Flap Type and Size
- Centre of Gravity Location

As per Roskam data [1] shown in figure 3.1, the single-engine airplane has a range of 1.3 to 1.9 for the maximum take-off lift coefficient.

Airplane Type	$C_{L_{max}}$	$C_{L_{max_{TO}}}$	$C_{L_{max_L}}$
1. Homebuilts	1.2 - 1.8	1.2 - 1.8	1.2 - 2.0
2. Single Engine Propeller Driven	1.3 - 1.9	1.3 - 1.9	1.6 - 2.3
3. Twin Engine Propeller Driven	1.2 - 1.8	1.4 - 2.0	1.6 - 2.5

Figure 3.1: Maximum lift coefficient values for various types of airplanes [1]

The density at an altitude of 10,000 ft is approximately 0.0056 lb/ft<sup>3</sup> [11].

Now we can determine the wing loading value by using equation (1) as follows:

$$\frac{60^2 * 0.0056 * 1.6}{2} > \left(\frac{W}{S}\right)_{\text{Take-off}} \quad (2)$$

$$\left(\frac{W}{S}\right)_{\text{Take-off}} \leq 31.6 \text{ psf}$$

$$\frac{60^2 * 0.0056 * 1.8}{2} > \left(\frac{W}{S}\right)_{\text{Landing}} \quad (3)$$

$$\left(\frac{W}{S}\right)_{\text{Take-off}} \leq 35.5 \text{ psf}$$

Combining equations 2 and 3, Wing loading should be less than 31.6 psf.

### 3.2.2 Takeoff Distance

According to Roskam [1], the takeoff distance of an aircraft is determined by the following factors:

- Takeoff Weight,  $W_{TO}$
- Takeoff Speed,  $V_{TO}$
- Thrust-to-Weight Ratio,  $(T/W)_{TO}$  or Weight-to-Power Ratio,  $(W/P)_{TO}$
- Aerodynamic Drag Coefficient
- Ground Friction Coefficient

The following figure (3.2) represents a definition of FAR-23 take-off distances used in the process of sizing the proposed airplane.

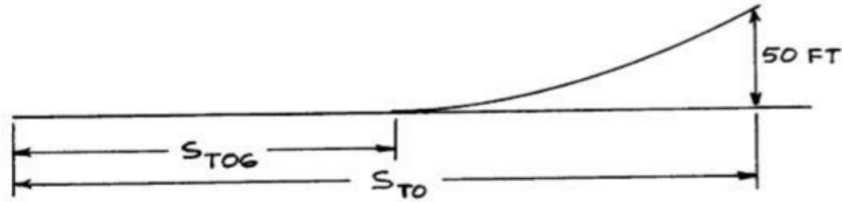


Figure 3.2: FAR 23 take-off distance definition

The take-off ground run,  $S_{TOG}$  is proportional to the take-off wind loading  $(W/S)_{TO}$ , take-off power loading  $(W/P)_{TO}$ , and maximum take-off lift coefficient,  $C_{LmaxTO}$  :

$$S_{TOG} \propto \left( \frac{(W/S)_{TO} * (W/P)_{TO}}{\sigma * C_{LmaxTO}} \right) = TOP_{23} \quad (4)$$

Here,

$$C_{LTO} = \frac{C_{LmaxTO}}{1.21}$$

The following equation is obtained from Roskam [1] for FAR 23 take-off ground run:

$$S_{TOG} = 4.9 TOP_{23} + 0.009 TOP_{23}^2$$

$$S_{TO} = 1.66 S_{TOG}$$

Combining the above two equations, the following equation is obtained for take-off field length:

$$S_{TO} = 8.134 TOP_{23} + 0.0149 TOP_{23}^2$$

Now, assume the take-off distance is 2500 feet as per the reference aircraft, which is under the FAR 23 requirement. So  $TOP_{23}$  for the proposed aircraft is given by:

$$TOP_{23} = 220 \text{ lbs}^2/\text{ft}^2 * \text{hp}$$

Summing up the ratio for 10,000 ft,  $\sigma = 0.7386$  [11]

Using equation (4), we get the take-off power in terms of wing loading as follows:

$$\left( \frac{(W/S)_{TO} * (W/P)_{TO}}{C_{LmaxTO}} \right) \leqslant TOP_{23} * \sigma$$

$$\left( \frac{(W/S)_{TO} * (W/P)_{TO}}{C_{LmaxTO}} \right) \leqslant 162 \text{ lbs}^2/\text{ft}^2 * \text{hp} \quad (5)$$

From equation(5), we can calculate the takeoff wing loading like tabulated below:

**Table 3.1: Required values for power loading**

$W/P_{TO}$	$C_{LmaxTO}$	1.2	1.6	1.8	2.0	2.4
10	$W/S_{TO}$	23.5	31.4	35.3	39.2	47.0
20		11.8	15.7	17.6	19.6	23.5
30		7.8	10.5	11.8	13.1	15.7
40		5.9	7.8	8.8	9.8	11.8
50		4.7	6.3	7.1	7.8	9.4
60		3.9	5.2	5.9	6.5	7.8
70		3.4	4.5	5.0	5.6	6.7
80		2.9	3.9	4.4	4.9	5.9

The below figure translates this tabulation into regions of  $(W/S)_{TO}$  and  $(W/P)_{TO}$  for the given values of  $C_{LmaxTO}$ , so that the takeoff distance requirement is satisfied. The design point should be below the  $C_L$  line for optimum design.

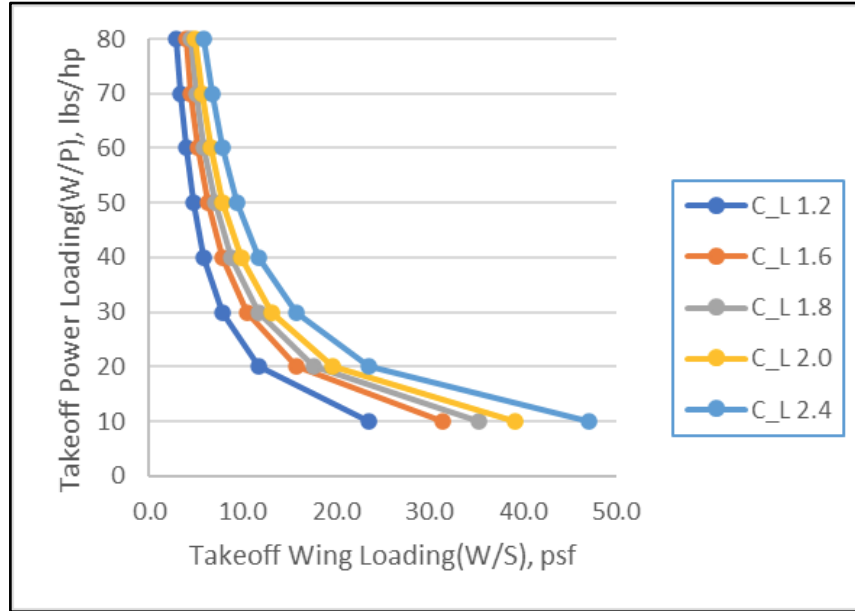


Figure 3.3: Effect of take-off wing loading and maximum take-off lift coefficient on take-off power loading

### 3.2.3 Landing Distance

According to Roskam [1], the landing distance is determined by the following factors:

- Landing Weight
- Approach Speed
- Deceleration Method Used
- Pilot Technique

The figure below represents a definition of FAR-23 landing distances used in the process of sizing Class-II aircraft.

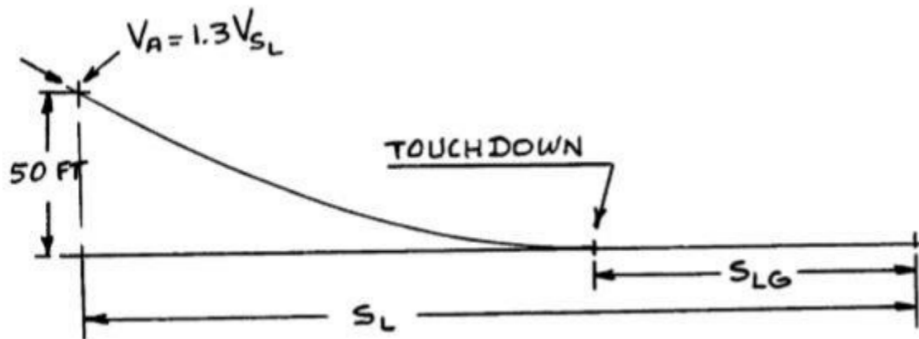


Figure 3.4: FAR 23 landing distance definition

As per Roskam data[1], the approach speed is defined as:

$$V_A = 1.3V_{SL} \quad (6)$$

The proposed aircraft is an electric propulsion thus the landing weight will be heavier than the conventional general aviation aircraft. The battery weight is basically dry weight. Therefore, it will not change during the flight envelope and due to that, the weight ratio of maximum landing weight to take-off weight can be assumed constant. From Roskam [1],  $W_L/W_{TO} = 1$  (maximum value)

For calculation of landing distance, the following assumptions will be made:

- Standard conditions
- Applied brakes to stop the aircraft
- Takeoff weight is 3980 lbs

The following figure shows the relation between the landing ground run ( $S_{LG}$ ) to the square of the stall speed ( $V_{SL}$ ).

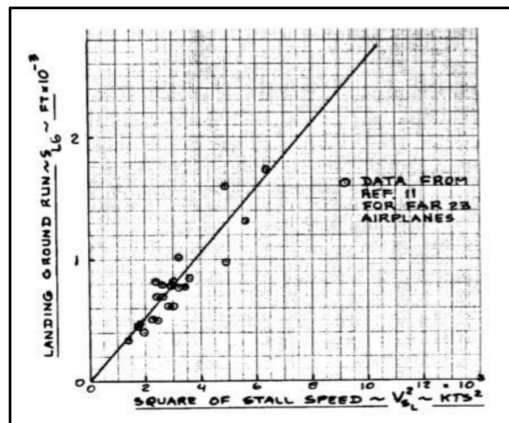


Figure 3.5: Effect of square of stall speed on landing ground run [1]

Figure (3.5) shows how the landing ground run,  $S_{LG}$  is related to the square of the stall speed,  $V_{SL}$

$$S_{LG} = 0.265 * V_{SL}^2 \quad (7)$$

Figure (3.6) shows the relation between total landing distance to the landing ground run.

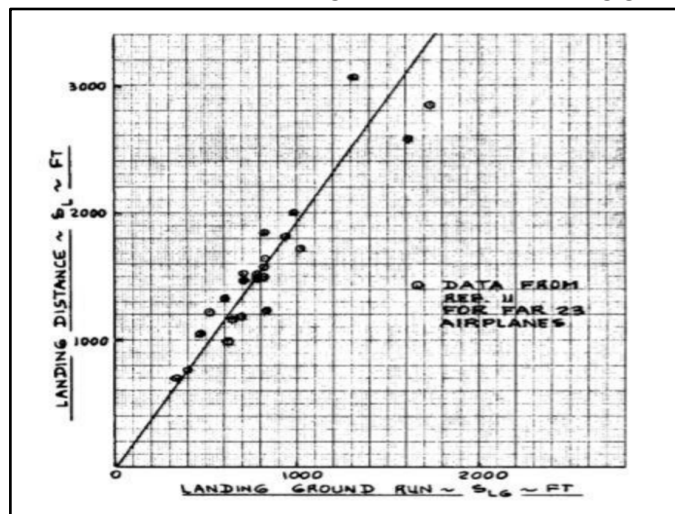


Figure 3.6: Relation between ground run and landing distance [1]

The above figures suggest the following relationship:

$$S_L = 1.938 * S_{LG} \quad (8)$$

Combining equations (7) and (8),

$$S_L = 0.5136 * V_{SL}^2 \quad (9)$$

Assume the landing field length of 2000 feet at 0 feet altitude. The design landing weight to take-off weight ratio is 1.

Therefore,

$$V_{SL} = \left( \sqrt{\frac{2000}{0.5136}} \right)$$

$$V_{SL} = 62.5 \text{ Knots}$$

With the help of equation (1), this translates into the following requirement:

$$\frac{2 * \left(\frac{W}{S}\right)_L}{0.002049 * C_{LmaxL}} = (V_S * 1.688)^2$$

$$\left(\frac{W}{S}\right)_L = 11.36 * C_{LmaxL} \quad (10)$$

Now, the landing weight to take-off weight ratio is 1, this yields:

$$\left(\frac{W}{S}\right)_{TO} = 11.36 * C_{LmaxL}$$

**Table 3.2: Required values of wing loading at different values of lift coefficient**

Wing loading at different values of lift coefficient			Wing loading				
	Wing loading, psf	Power loading, lbs/hp	@C <sub>L</sub> <sub>max</sub> 1.2	@C <sub>L</sub> <sub>max</sub> 1.6	@C <sub>L</sub> <sub>max</sub> 1.8	@C <sub>L</sub> <sub>max</sub> 2.0	@C <sub>L</sub> <sub>max</sub> 2.4
	W/S	W/P	1.2	1.6	1.9	2	2.4
	0	0	14	18	20.5	22.8	27
	5	10	14	18	20.5	22.8	27

	10	20	14	18	20.5	22.8	27
	15	30	14	18	20.5	22.8	27
	20	40	14	18	20.5	22.8	27
	25	50	14	18	20.5	22.8	27

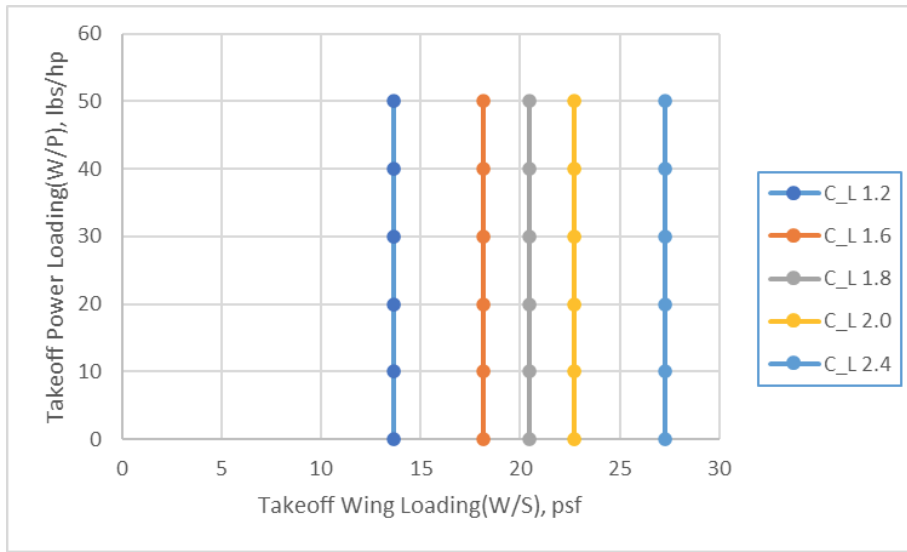


Figure 3.7: Allowable wing loading to meet landing distance requirement

### 3.2.4 Drag Polar Estimation

The drag coefficient is given by the following equation:

$$C_D = C_{D0} + \frac{C_L^2}{\pi * A * e} \quad (11)$$

The zero-lift drag coefficient can be expressed as:

$$C_{D0} = \frac{f}{S} \quad (12)$$

Now, it is possible to relate the equivalent parasite area to the wetted area from the figure (3.8).

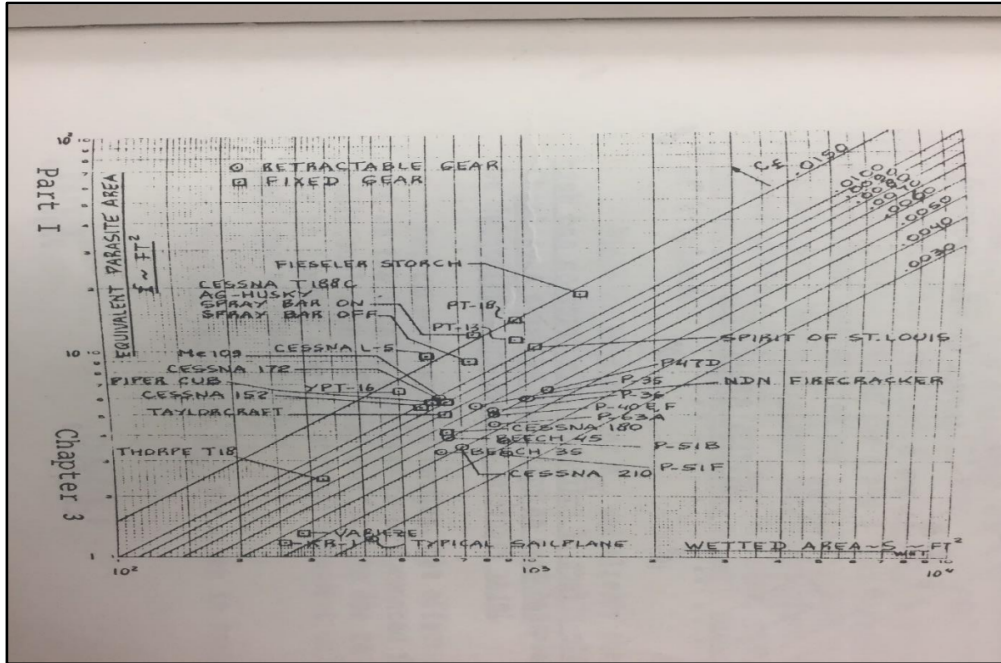


Figure 3.8: Equivalent parasite area Vs wetted area [1]

The relation between  $f$  and  $S_{wet}$  is given by:

$$\log_{10} f = a + b * \log_{10} S_{wet} \quad (13)$$

From figure (3.8), choosing a value of  $c_f = 0.0090$  (based on similar aircraft Sunflyer 4), and based on the skin friction value,  $a$  and  $b$  constants are chosen from the table presented below:

Table 3.3: Constants  $a$  and  $b$  based on skin friction coefficient [1]

Equivalent Skin Friction Coefficient, $c_f$	$a$	$b$
0.0090	-2.0458	1.0000
0.0080	-2.0969	1.0000
0.0070	-2.1549	1.0000
0.0060	-2.2218	1.0000
0.0050	-2.3010	1.0000
0.0040	-2.3979	1.0000
0.0030	-2.5229	1.0000
0.0020	-2.6990	1.0000

Constants  $a$  and  $b$  are a function of  $c_f$ ,

$c_f$	a	b
0.0090	-2.0458	1.000

Now, the relation between  $S_{wet}$  to  $W_{TO}$  is given by:

$$\log_{10} S_{wet} = c + d * \log_{10} W_{TO} \quad (14)$$

**Table 3.4: Values of constants c and d for various aircrafts**

Airplane Type	c	d
1. Homebuilts	1.2362	0.4319
2. Single Engine Propeller Driven	1.0892	0.5147
3. Twin Engine Propeller Driven	0.8635	0.5632
4. Agricultural	1.0447	0.5326
5. Business Jets	0.2263	0.6977
6. Regional Turboprops	-0.0866	0.8099

From Table (3.4), the value of c and d for a single-engine aircraft is given by:

$$c = 1.0892$$

$$d = 0.5147$$

On solving equation (14),

$$S_{wet} = 875 \text{ ft}^2$$

Further solving equation (13) gives value of f,

$$f = 7.9 \text{ ft}^2$$

Now, to find the zero-lift drag coefficient, Roskam [1] gives some estimated values in Table (3.5).

**Table 3.5: First estimates for zero lift drag coefficient**

Configuration	$\Delta C_{D_0}$	e
Clean	0	0.80 - 0.85
Take-off flaps	0.010 - 0.020	0.75 - 0.80
Landing Flaps	0.055 - 0.075	0.70 - 0.75
Landing Gear	0.015 - 0.025	no effect

Calculated value of zero-lift drag coefficient,  $C_{D0} = 0.0667$

Assuming the values of Aspect ratio (A) = 10 and e = 0.85 to find the ‘clean’ drag polar from equation (11) gives,

$$C_D = 0.0667 + 0.0374C_L^2 \quad (15)$$

For other configuration the values are as follows:

**Table 3.6: Drag polar for the proposed aircraft**

Flight Condition	$\Delta C_{D0}$	Aspect ratio	e	Drag Polar
Clean	0	10	0.85	$0.0667 + 0.0374C_L^2$
Take-off flaps	0.0165	10	0.80	$0.0832 + 0.0397C_L^2$
Landing flaps	0.0615	10	0.75	$0.1282 + 0.0424C_L^2$
Landing gear	0.0215	10	No effect	$0.150 + 0.0424C_L^2$

### 3.2.5 Climb Constraints

The proposed aircraft comes under FAR-23 climb requirements which are as follows:

- FAR 23.65 (*All Engines Operating*)  
The minimum climb rate at sea level is 300 fpm and a steady climb angle of 1:12 for land planes. (at Take-off)
- FAR 23.67 (*One Engine Inoperative*)  
For a multiengine airplane with take-off weight more than 6000 lbs, the steady climb rate must be at least  $0.027V_{so}^2$  fpm, at 5000 ft. altitude.
- FAR 23.77 (*All Engines Operating*)  
The steady climb angle shall be at least 1:30. (for balked landing)

#### 3.2.5.1 Sizing to FAR-23 rate-of-climb requirements:

The rate-of-climb is given by the following equation:

$$RC = \text{Rate of climb} = \frac{dh}{dt} = 33,000 * RCP \quad (16)$$

$$RCP = \text{Rate of climb parameter} = \left\{ \frac{\eta_p}{W/P} \right\} \cdot \left[ \frac{(W/S)^{1/2}}{19 * (C_L^{3/2} / C_D) * \sigma^{1/2}} \right] \quad (17)$$

**For FAR 23.65:** RC = 300 fpm

$$RCP = 33000^{-1} * RC$$

$$RCP = 0.0091 \text{ hp/lbs}$$

**For FAR 23.67:** The proposed aircraft is a single engine with takeoff weight  $\leq 6000$  lbs so it is not required to satisfy the constraints mentioned under the FAR 23.67 requirement.

The drag polar for proposed aircraft is already calculated as:

$$C_D = 0.0667 + 0.0374 C_L^2$$

With this drag polar at  $C_{Lmax} = 1.8$  and  $\eta_P = 0.85$  from Roskam [1].

From the above-mentioned equation (16), we need to maximize  $\frac{C_L^{3/2}}{C_D}$ , to get a higher value of RC.

On solving

$$\frac{C_L^{3/2}}{C_D} = 13$$

Now, solving for RCP equation gives final relation as

$$\frac{208}{2.3 + \sqrt{W/S}} = \frac{W}{P} \tag{18}$$

**Table 3.7: Range of values satisfying FAR 23.67 requirements**

W/S, psf	W/P Cont., lbs/hp	W/P Takeoff, lbs/hp
10	35	32
20	28	25
30	24	22
40	22	20

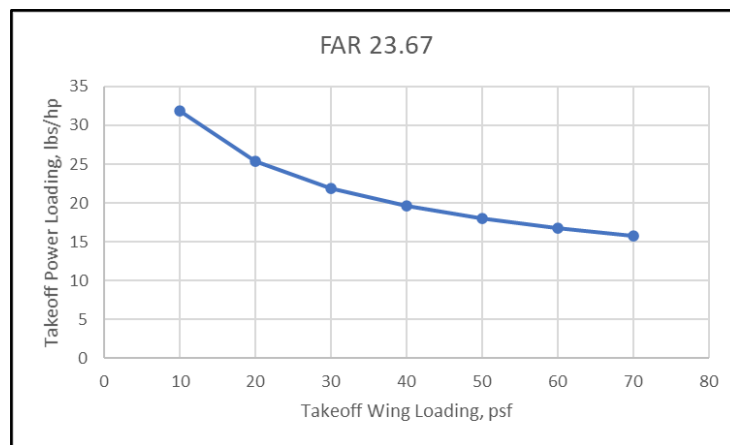


Figure 3.9: Range of values for W/P and W/S satisfying FAR 23.67 requirements

On the basis of typical piston engine data, the ratio of  $P_{TO}/P_{max.cont}$  was taken to be 1.1 [1]. The design point should be below the above-plotted line.

### 3.2.5.2 Sizing to Climb Gradient Requirements:

The design point should be below the figure plotted line. Climb gradient requirements are calculated based on the following equation:

$$CGRP = \frac{18.97 * \eta_p * \sigma^{1/2}}{(W/P) * (W/S)^{1/2}} = \frac{\{CGR + (L/D)^{-1}\}}{C_L^{1/2}} \quad (19)$$

**For FAR 23.65:**  $CGR = 1/12 = 0.0833$ .

The drag polar was already found as:

$$C_D = 0.0667 + 0.0374C_L^2$$

The value of  $C_{Lmax} = 1.8$  is already assumed. By taking a margin of 0.2:

$$C_{L\ climb} = 1.6$$

This yields  $L/D_{climb}$  from the above formula

$$\left(\frac{L}{D}\right)_{climb} = 9.84$$

$$\text{Which give, } CGRP = 0.146$$

This requirement now yields,

$$\frac{W}{P} * \left(\frac{W}{S}\right)^{1/2} = 110.3 \quad (20)$$

**Table 3.8: Range of values satisfying FAR 23.65 requirements**

W/S, psf	W/P Cont., lbs/hp	W/P Takeoff, lbs/hp
10	29.95626	27.23296
20	21.18227	19.25661
30	17.29525	15.72296
40	14.97813	13.61648



Figure 3.10: Range of values for W/P and W/S satisfying FAR 23.65 requirements

**For FAR-23.77:**

$$\text{CGR} = 1/30 = 0.0333 \quad (21)$$

It is already assumed that  $C_{L_{maxLanding}} = 1.8$ . And assuming that climb is carried out with the same margin as before:

$$C_{L_{climb}} = 1.6$$

The drag polar in this case is:

$$C_D = 0.1282 + 0.0424C_L^2$$

This yields  $L/D_{climb}$  from the above formula

$$\left(\frac{L}{D}\right)_{climb} = 6.75$$

Which give,

$$\text{CGRP} = 0.143$$

This requirement now yields,

$$\frac{W}{P} * \left(\frac{W}{S}\right)^{1/2} = 113 \quad (22)$$

**Table 3.9: Range of values satisfying FAR 23.77 requirements**

W/S, psf	W/P Takeoff, lbs/hp
10	30.6
20	21.6
30	17.7
40	15.3

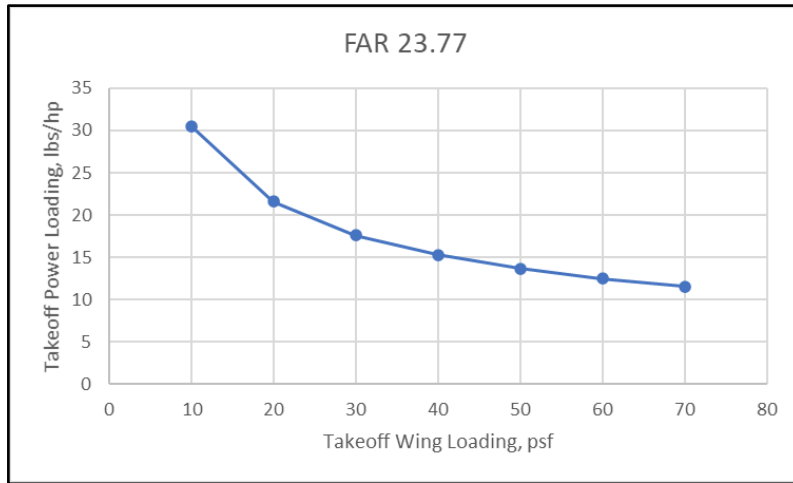


Figure 3.11: Range of values for W/P and W/S satisfying FAR 23.77 requirements

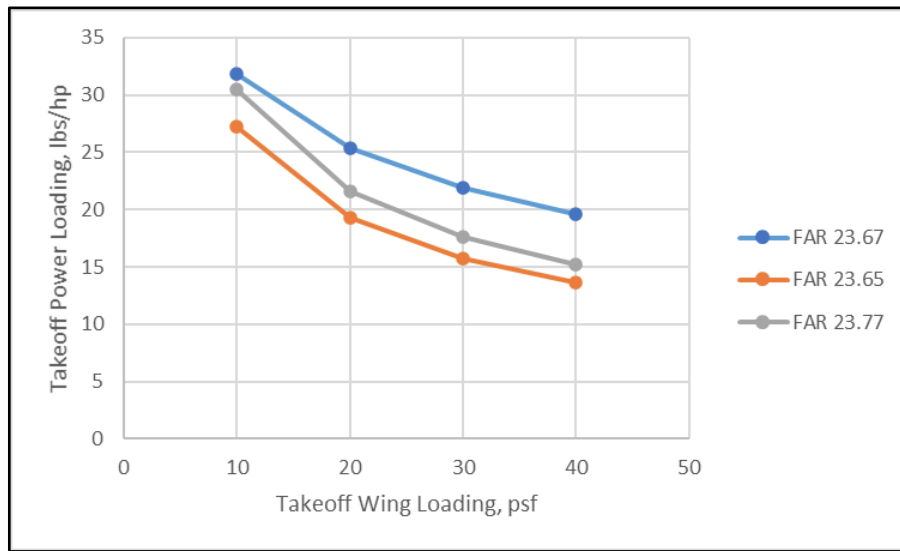


Figure 3.12: Combined range of values for W/P and W/S satisfying FAR 23 requirements

The design point in Figure (3.12) should be below the plotted lines.

### 3.2.6 Maneuvering Constraints

Since the proposed aircraft is a general aviation aircraft and the maneuvering requirements specified in Roskam [1] is only for utility, agricultural, aerobatic, and military airplanes, the proposed aircraft does not include those capabilities. So, the aircraft will not be sized to meet these requirements.

### 3.2.7 Speed Constraints

The cruise speed for any propeller-driven aircraft is calculated at 70 to 80 percent of total power. From this, it can be shown that the profile drag is higher than the induced drag [1].

$$C_{Di} = 0.1 C_{D0}$$

From Roskam [1], cruise speed is proportional to the factor called ‘the power index’  $I_p$ .

$$V_{cr} \propto \left( \frac{W}{S} \frac{W}{P} \right)^{1/3} \quad (23)$$

Where,

$$\left( \frac{W}{S} \frac{W}{P} \right)^{1/3} = I_p$$

The following figure will give the relationship between the power index and cruise speed:

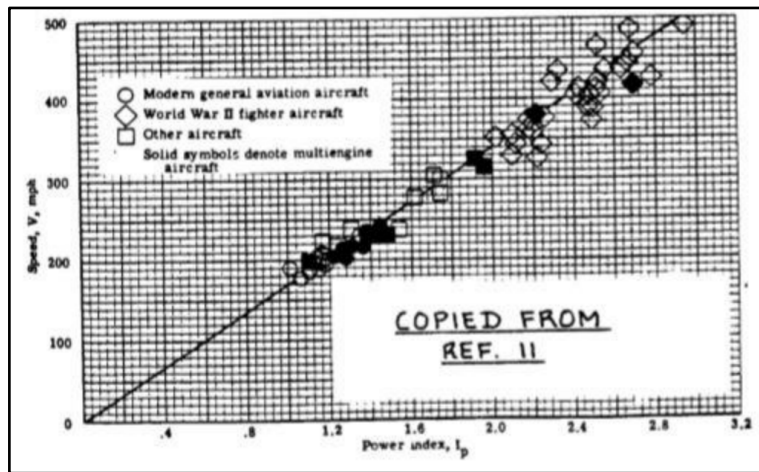


Figure 3.13: Airplane speed Vs power index

The cruise speed of propeller-driven aircraft is 150 knots (172 mph), at 85% power at 10,000 feet (cruising altitude), so from the above figure, power index  $I_p = 1.0$

At sea level,  $\sigma = 1$  [11]

Therefore, from equation (23)

$$\frac{W}{S} = 1.0 * \frac{W}{P} \quad (24)$$

The figure below shows the range of combinations of  $W/S$  and  $W/P$  for which the cruise speed requirement is met. The design point should be below the trendline.

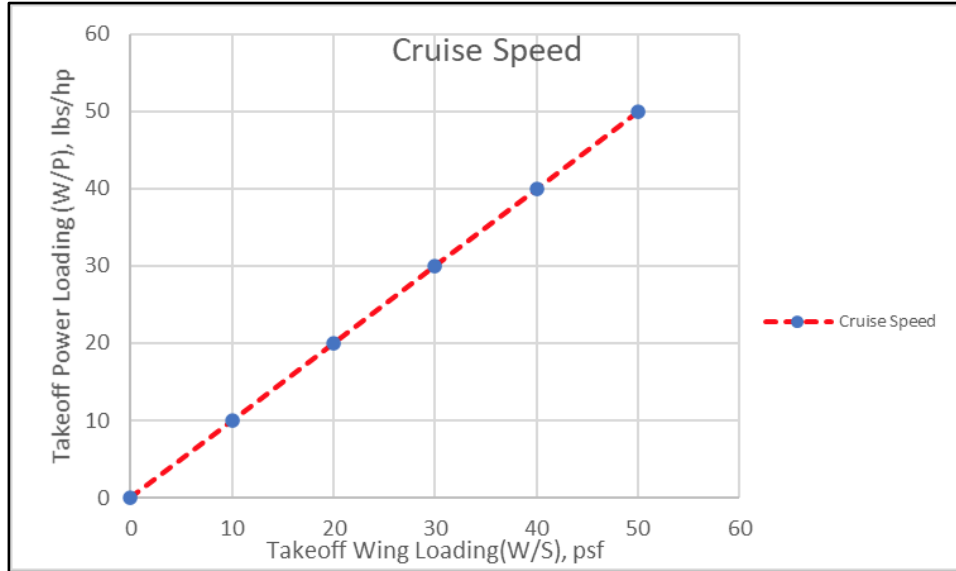


Figure 3.14: Allowable W/S and W/P to meet a given cruise speed

### 3.3 Matching Graph

It is now possible to determine the best combination of wing loading, power loading and lift coefficients from the matching process. The matching graph for the proposed aircraft is as follows:

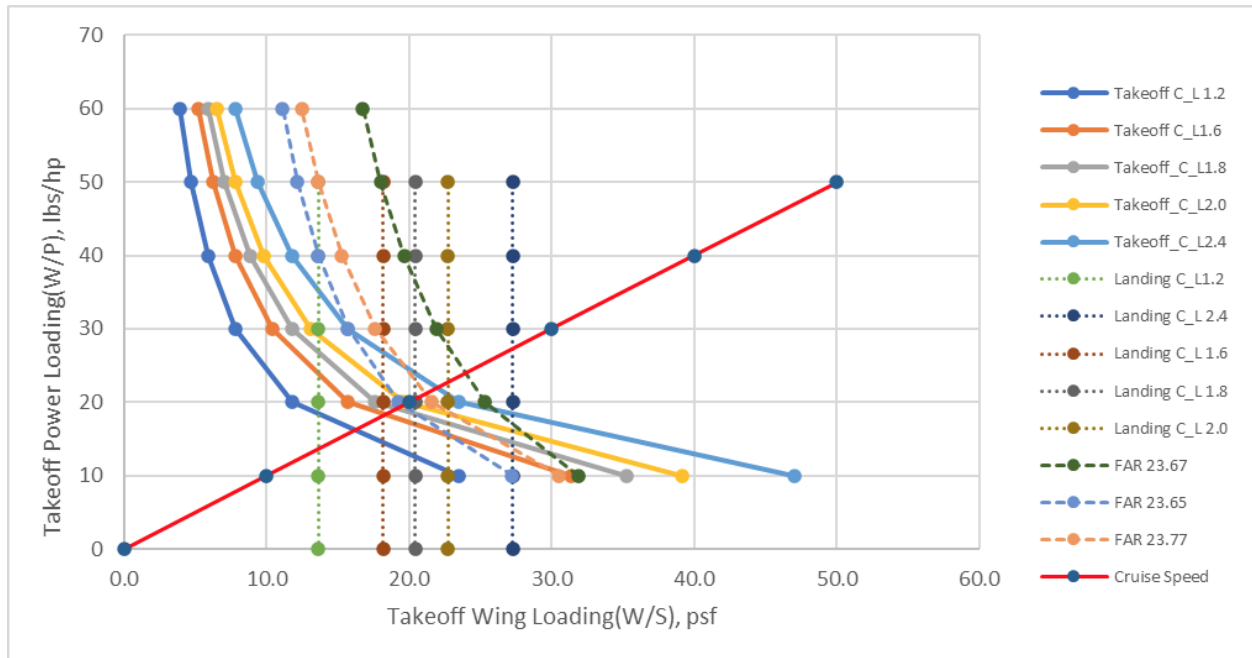


Figure 3.15: Performance sizing graph of manual calculations

The cleaned-up version of the above matching graph is as follows:

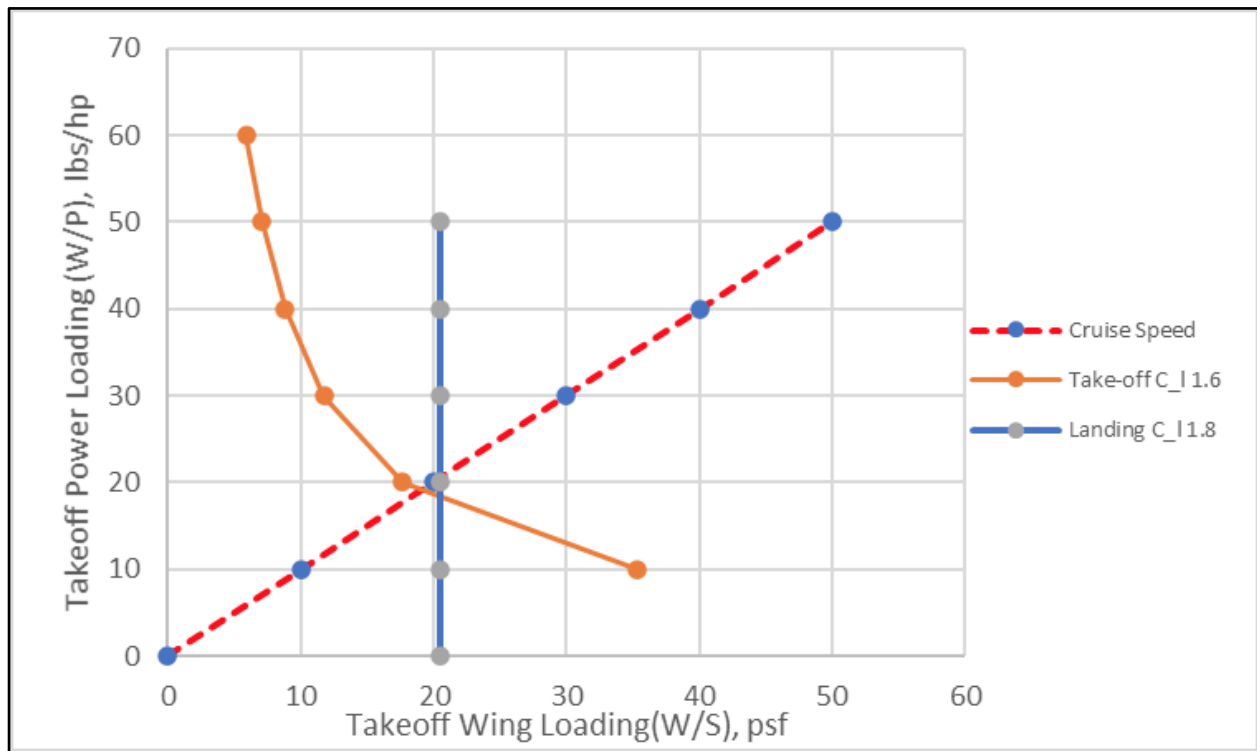


Figure 3.16: Cleaned-up version of matching plot

### 3.4 Discussion

In the above Excel plot, the design point is considered at a takeoff wing loading of 21 psf and takeoff power loading of 20 lbs/hp with a takeoff lift coefficient of 1.6 and landing lift coefficient of 1.6. With this design point, the airplane characteristics can be summarized as follows:

- Takeoff Weight: 3980 lbs
  - Empty Weight: 2535 lbs
  - Battery Weight: 637 lbs
- These are already known from the weight sizing chapter.

**Table 3.10: Design parameters**

Lift Coefficient, $C_L$	Clean	1.5
	Takeoff	1.6
	Landing	1.8

Aspect Ratio	10
Wing Loading, W/S, psf	20.5
Power Loading, W/P, lbs/hp	20
Wing Area, S, ft <sup>2</sup>	194
Take-off Power, hp	199

### 3.5 Conclusion

Examining the matching requirements of Figure 3.14, the design point seems like a reasonable choice. The most critical parameters are cruise speed, take-off and landing distances for the proposed design for the selection of design point. The required take-off power can be achieved by the proposed propulsion system.

# Chapter 4

## Configuration Selection

### 4.1 Introduction

This report presents the detailed selection process of the wing, empennage, integration of the propulsion system, landing gear disposition and overall configuration for the proposed design. Configuration design is very important in the design process as 90 percent of the life cycle cost gets locked during the early configuration phases of an aircraft [1].

A comparative study of configuration is performed for the Pipistrel Panthera, SunFlyer 4, Yuneec E-430, Pipistrel Taurus Electro G2, and Airbus Vahana to determine the best configuration for the proposed design that satisfies the given mission requirements. This report presents a configuration selection, which is based on mission requirements and compared with similar airplanes.

### 4.2 Comparative Study

#### 4.2.1 Comparison of Weights, Performance, and Geometry of Similar Airplanes:

**Table 4.1: Comparison chart of similar airplanes**

<b>Aircraft Model</b>	<b>Sun Flyer 4</b>	<b>Pipistrel Panthera</b>	<b>Yuneec E-430</b>	<b>Pipistrel Taurus Electro G2</b>	<b>Airbus Vahana</b>
<b>Crew</b>	1	1	1	1	None (self piloted)
<b>Passengers</b>	3	3	1	1	2
<b>Wing Span</b>	12m	10.86m	13.8m	14.97m	6.25m
<b>Empty Weight</b>	862 kg	800 kg	250 kg	306kg	695kg
<b>Gross Weight</b>	1225 kg	1200kg	470 kg	550kg	815kg
<b>Powerplant</b>	1 electric motor 141hp (105kW)	Pure electric 195hp (145 kW)	Yuneec power drive 40kW	electric Li-Po	electric

<b>Cruise Speed</b>	240km/hr (150 mph)	218 km/hr	90 km/hr (56 mph)	150 km/hr	230 km/hr (140 mph)
<b>Rate of Climb</b>	6.4 m/s	5.7m/s	3.5m/s	3.1m/s	-
<b>Wing Loading</b>	110kg/m <sup>2</sup>	-	41.3kg/m <sup>3</sup>	-	-
<b>Range Endurance</b>	4 hours	400 km 215 nm	227 km	370 mile 590 km	100km
<b>Surface ceiling</b>	-	4000m	-	2000m	3048 m 10000 ft

#### 4.2.2 Configuration Comparison of Similar Airplanes

- **Pipistrel Panthera**



Figure 4.1: 3-Views of pipistrel panthera [7]

- **Bye Aerospace Sunflyer 4**

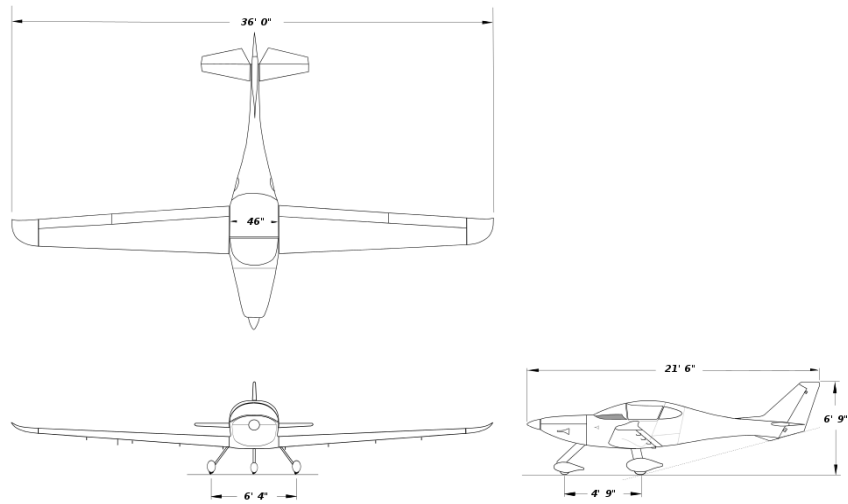


Figure 4.2: 3-Views of sunflyer 4 [6]

- **Yuneec E-430**



Figure 4.3: 3-Views of yuneec E-430 [8]

- **Pipistrel Electro G2**

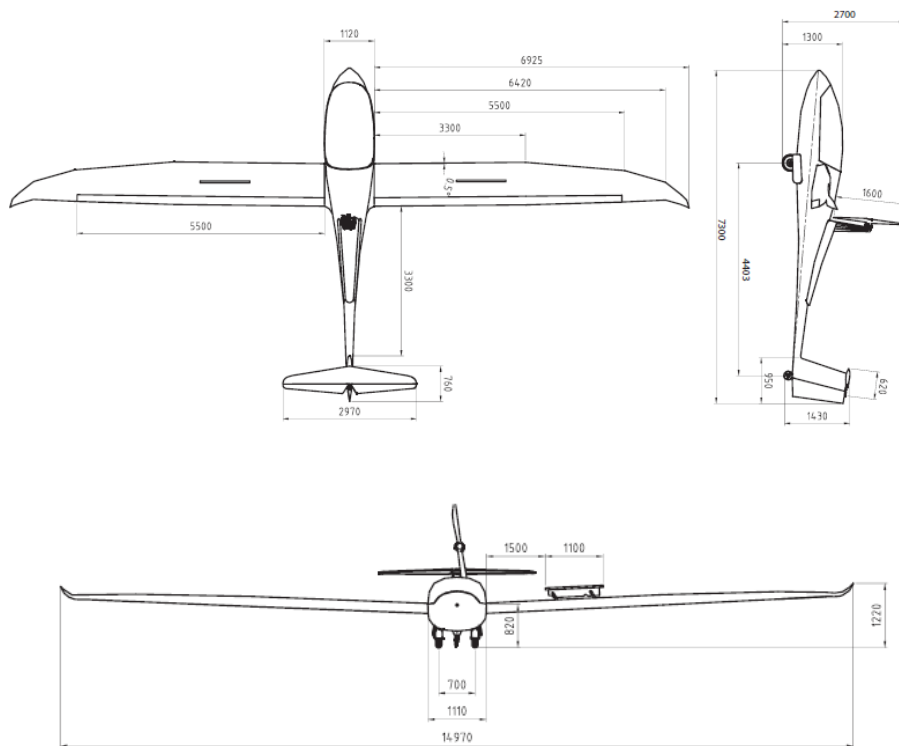


Figure 4.4: 3-Views of electro G2 [9]

- **Airbus Vahana**



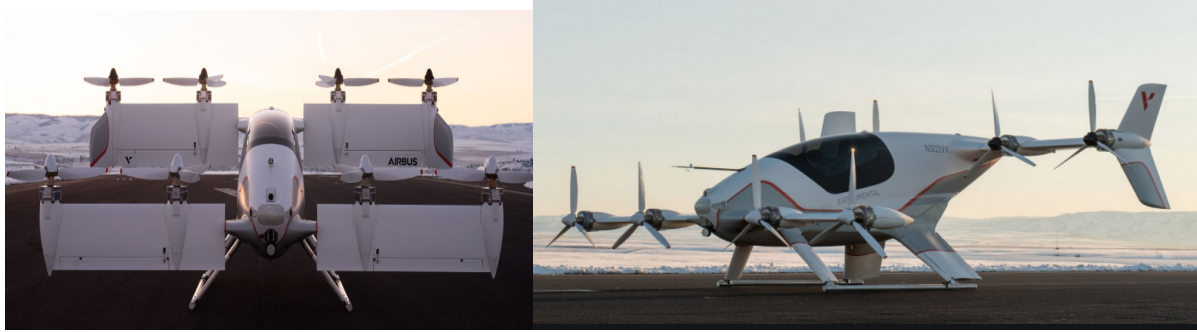


Figure 4.5: 3-Views of airbus vahana [10]

### 4.2.3 Discussion

In the previous section, 3-views are provided for each of five different airplanes that are similar to the proposed design. All five have different power efficiencies and seating capabilities. The propellers are tractor type and are simple in design and aerodynamically stable.

A key design parameter here is the wing configuration. The wing configuration of the five similar aircraft is cantilever construction, with most of them being low wing designs except for the Yuneec E-430, which is a high-wing design and Airbus Vahana which is a tandem tilt-wing design. Low wing aircraft have their wings attached to the bottom of the fuselage, so it is easy to refuel them. High-wing aircraft offer better lateral stability, while the low wing aircraft compensate by giving dihedral to the wings. Also, the landing gear can be retracted into the wings in the low wing configuration.

The next design parameter is the tail configuration. Two of the airplanes have a T-tail design whereas the Yuneec E-430 which has a V-tail and the Sunflyer has a conventional tail configuration. T-tails keep the stabilizers out of the engine wake, and give better pitch control.

The reference aircraft chosen for the proposed design is the Pipistrel Panthera.

## 4.3 Selection of Propulsion System

The three decisions that involves the selection and integration of the propulsion system are as follows:

1. Selection of the propulsion system type
2. Determination of the number of engines/batteries to be used
3. Integration of the propulsion system into the configuration

### 4.3.1 Selection of Propulsion System Type:

Since the proposed aircraft is an electric propulsion system, there are a couple of factors that need to be considered when selecting the battery technology.

These factors are as follows:

1. Energy density
2. Safety
3. Cost
4. Reliability

## 5. Maintainability

In aviation this means, lower fuel consumption, lower emissions and as such a cleaner flight with less impact on the environment.

### 4.3.2. Determination of the number of engines/batteries to be used:

The electric engine chosen for the proposed design is a Siemens brushless motor-SP 260D, as it can produce the required horsepower. It is a double winding motor with a 95% efficiency running at low rpm of 2500 and is lightweight. The power source for the proposed aircraft is electric so choosing the battery type becomes a critical task here. Lithium-air battery is chosen for this design with the following characteristics listed below.

**Table 4.2: Specific energy density of the proposed battery system[12]**

System	Theoretical specific energy	Expected in 2025	Environmental impact	Rechargeable
Li-O <sub>2</sub>	3500 Wh/kg	800-1750 Wh/kg	Zero Emission	Yes

### 4.3.3 Integration of the propulsion system into the configuration

The propulsion system will be integrated in the fuselage with an electric motor placed at the front and the batteries divided among the wings and the aft fuselage. The propeller is designed based on a relation between the maximum engine power, propeller diameter and the number of propeller blades for single-engine FAR-23 certified airplanes.

The diameter of the propeller is obtained from the following equation:

$$D_p = \left( \frac{4 * P_{max}}{\pi * n_p * P_{bl}} \right)^{1/2}$$

Where,

$D_p$  = Propeller Diameter

$P_{max}$  = 199 hp

$P_{bl}$  = 2.8 hp/ft<sup>2</sup>

$n_p$  = 3

On calculating,

$$D_p = 5.50 \text{ ft}$$

## 4.4 Configuration Selection

The proposed design is a land-based aircraft. The critical components in the general configuration selection are the fuselage, wings, engines, empennage and landing gear. Satisfying the mission requirement and comparing it with similar aircraft in the market, the overall configuration is selected as follows:

**Table 4.3: Configuration for the proposed design**

<b>Basing</b>	Land-based
<b>Fuselage Configuration</b>	Conventional
<b>Wing Configuration</b>	Low wing arrangement
	Cantilever wing
	Zero/negligible sweep
<b>Empennage Configuration</b>	Horizontal tail T-tail installation (mounted on vertical tail)
	Vertical tail Single vertical tail mounted on fuselage
<b>Landing gear Configuration</b>	Non-Retractable tricycle gear
	One nose wheel gear and two main gear mounted under fuselage

### 4.4.1 Wing Configuration

Wing configuration plays a significant role in the overall lift for the aircraft. This is the section where the key aspect of the wing will be thoroughly analyzed. Conventional aircraft have three wing placement options:

1. High
2. Low
3. Mid-wing

Each position has its own advantages and disadvantages. Since the proposed aircraft uses a **low wing configuration**, some advantages are listed below:

1. It will keep the aircraft afloat during an event of 'ditching'.
2. Low wing configuration is a lighter structure as it is below the fuselage, it doesn't have to carry more weight.
3. The low wing has an advantage of short landing gear which results in less weight and efficient use of undercarriage space



Figure 4.5: Low-wing design of the proposed aircraft

#### 4.4.2 Empennage Configuration

The T-tail configuration is chosen for the proposed aircraft. It offers excellent weight reductions and better tail efficiencies. As mentioned above, it is simple in design and reduces the interference that could result from the placement of the horizontal tail directly behind the main wing and the propeller slipstream.

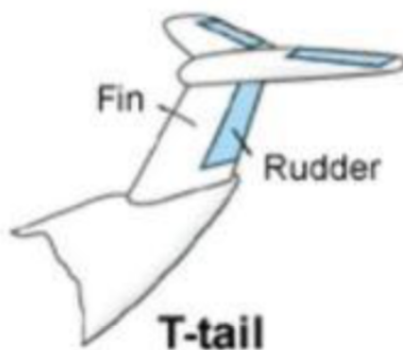


Figure 4.6: T-tail configuration

#### 4.4.3 Landing Gear Configuration

The landing gear will be non-retractable and conventional for tricycle configurations.

### 4.5 Proposed Configuration

The proposed configuration based on Table (4.2) has been conceptually designed in OpenVSP software and the 3D model sketches are shown below:

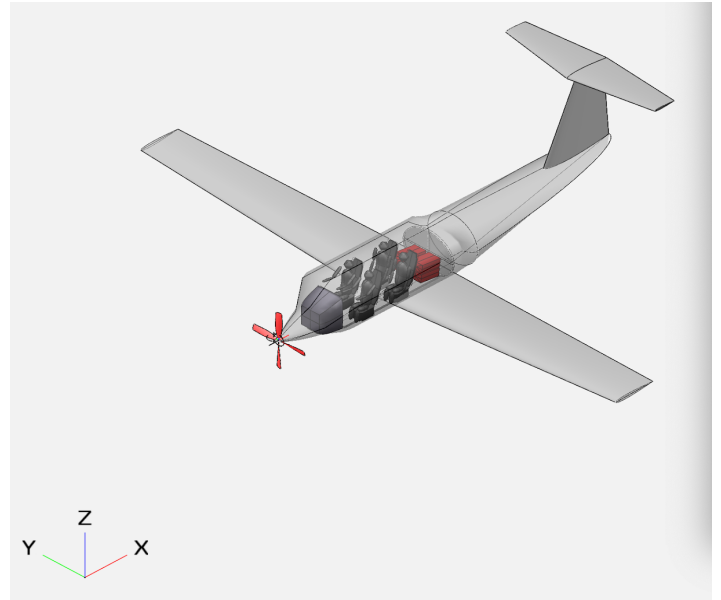
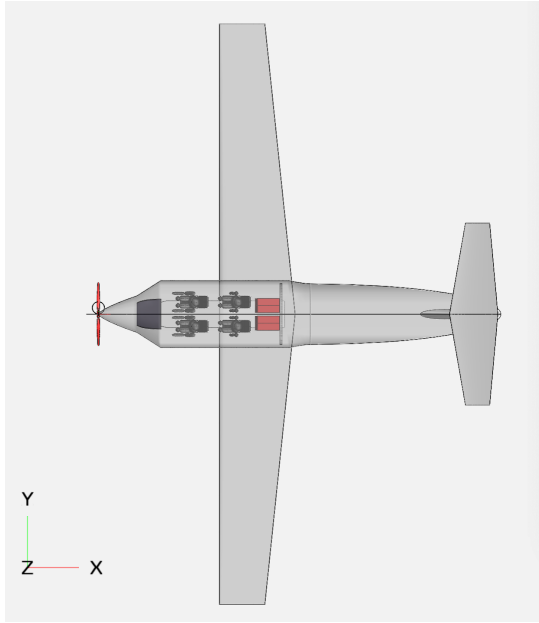


Figure 4.7: 3D Models of the proposed configuration

# Chapter 5

## Fuselage Design

### 5.1 Introduction

The preliminary estimates of mission weights and performance constraints are obtained in the previous chapters. This chapter presents the design of the fuselage using the mission requirements. The following factors are considered:

- Maximum Takeoff Weight
- Payload Capacity
- Landing Gear Location
- Wing Placement
- Engine Placement
- Fuel Storage

The purpose of this chapter is to layout the cockpit (also called the flight deck) and the fuselage. Section (5.2) will provide a design layout of the cockpit by considering the guidelines from Roskam [1]. Section (5.3) shows the fuselage design and discusses the effects of fuselage shape on drag. The passenger seating arrangements, seats, and windows will be considered when designing the fuselage.

### 5.2 Layout Design of the Cockpit

#### 5.2.1 The Layout of Cockpit Seating and Cockpit Controls:

Figure 5.1 shows the typical arrangement of the pilot seats and pilot controls for civil airplanes [1]. The proposed airplane is designed to use a wheel control system.

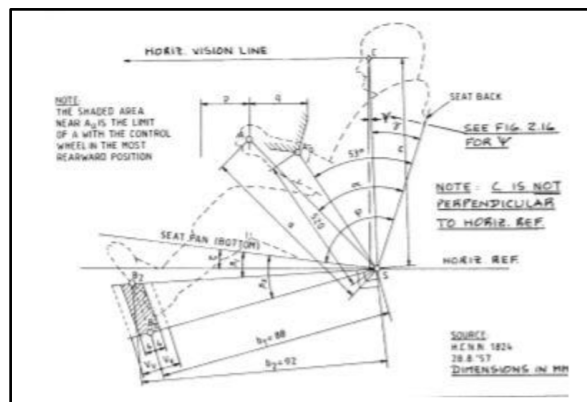


Figure 5.1: Recommended sitting arrangement for civil airplanes [1]

The geometric quantities in figure 5.1 are defined in Figure 5.2 with some adjustments and with all linear dimensions in cm and all angular dimensions are in degrees.

Symbol	Wheel Control
a	67 (+/- 4)
$\xi$	7° (+/- 2°)
p = Forward motion of point A:	18 (+/- 2)
q = Rearward motion of point A:	22 (+/- 2)
r = Sidewise motion of point A from center*:	-----
d = Distance between handgrips of wheel*:	38 (+/- 5)
s = Wheel rotation from center*:	85° (max.)
v = Distance between rudder pedal center lines*:	38 (+/- 12)
$\alpha$	64° (+/- 3°)
$\beta_1$	22°
$\beta_2$	10°
c	77 (+/- 2)
$\gamma$	21° (+/- 1°)
$\varphi$	102° (+/- 2°)
$V_v$ = Adjustment range of pedals from center position B:	7 (+/- 2)
$U_v$ = Forward and aft pedal motion from center position B*:	10 (+/- 2)
$S_h$ = Horizontal adjustment range of S from center position*:	< 10
$S_v$ = Vertical adjustment range of S from center position*:	8 (+/- 1)
* Not shown in Figure 2.7.	

Figure 5.2: Dimensions for civil cockpit controls [1]

### 5.2.3 Determination of Visibility from the Cockpit

The reasons why good visibility is essential are as follows:

- During takeoff and landing, the pilot must have a good view of the surroundings
- The pilot must be able to observe conflicting traffic

According to Jan Roskam, the visibility from the cockpit is defined as the angular area obtained by intersecting the airplane cockpit with radial vectors emanating from the eyes of the pilot. Even though the pilots see through both the eyes, it is customary to construct the visibility pattern by assuming the point C is the center of the vision as shown in the figure (5.3).

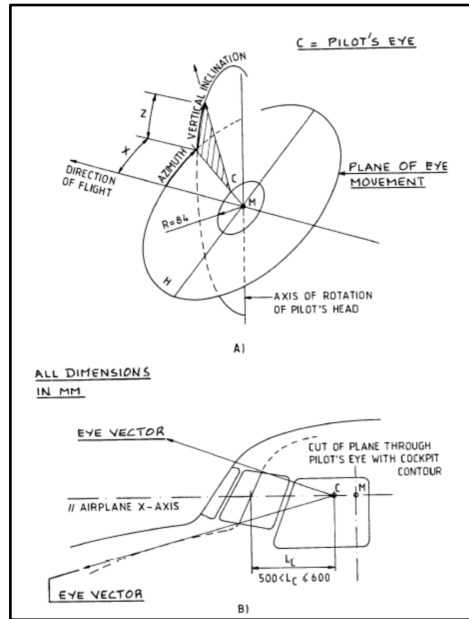


Figure 5.3: Radial eye vector's definition [1]

The layout design of the cockpit for the proposed aircraft.

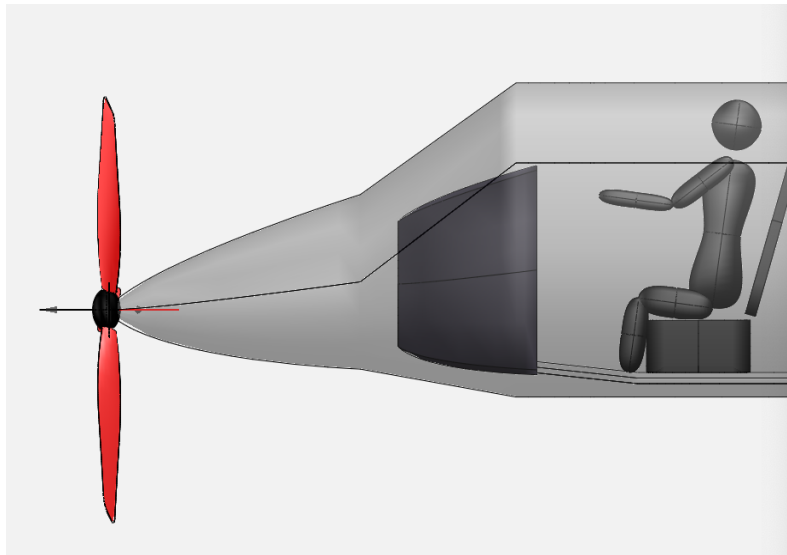


Figure 5.4: Side view of the cockpit

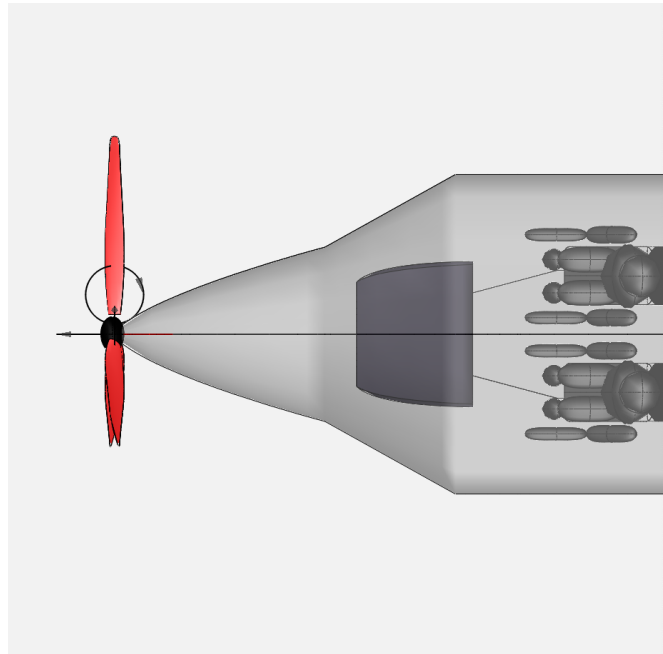


Figure 5.5: Top view of the cockpit

### 5.3 Layout Design of the Fuselage

The proposed design uses a fuselage layout design similar to the reference aircraft. Figure 5.6 shows important geometric parameters for the fuselage [1].

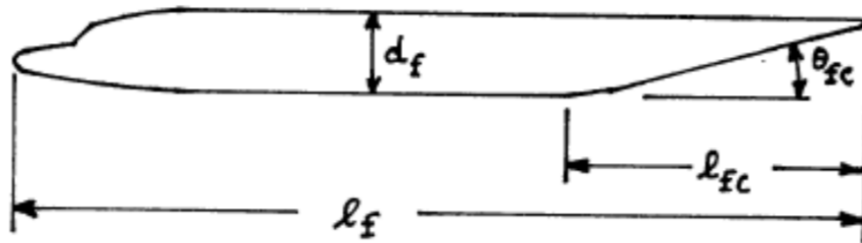


Figure 5.6: Definition of geometric fuselage parameters [1]

Figure 5.7 shows the range of values of the above geometric parameters for different airplanes.

Airplane Type	$l_f/d_f$	$l_{fc}/d_f$	$\theta_{fc}$ (deg)
Homebuilts	4 - 8	3*	2 - 9
Single Engine	5 - 8	3 - 4	3 - 9
Twins	3.6** - 8	2.6 - 4	6 - 13

Figure 5.7: Geometric fuselage parameters currently employed for different airplanes [1]

The length of the fuselage can be calculated using Raymer's equation as shown below. The takeoff weight obtained from the weight sizing is 3980 lbs and for the single engine aircraft, a and C are considered as 4.37 and 0.23.

$$\text{Length of the Fuselage} = a*(W_{TO})^C = 4.37 * 3980^{0.23} = 29.40\text{ft or } 8.96\text{m}$$

Length = $aW_0^C$	a	C
Sailplane—unpowered	0.86	0.48
Sailplane—powered	0.71	0.48
Homebuilt—metal/wood	3.68	0.23
Homebuilt—composite	3.50	0.23
General aviation—single engine	4.37	0.23
General aviation—twin engine	0.86	0.42
Agricultural aircraft	4.04	0.23
Twin turboprop	0.37	0.51

Figure 5.8: Length of the fuselage with respect to maximum take-off weight for different airplanes [15]

### 5.3.1 Aerodynamic Drag Considerations

The sizing of the fuselage depends on the aerodynamic drag considerations. A large percentage of the overall drag is produced by the fuselage. Therefore, the fuselage should be sized and shaped with minimum drag.

The following types of drag are generated by fuselage:

- Friction Drag
- Profile Drag
- Base Drag
- Compressibility Drag
- Induced Drag

**Friction Drag:** The wetted area is directly related to the length and perimeter of the fuselage and the friction drag is directly proportional to the wetted area. It can be minimized by using the following options:

- Shape the fuselage so that laminar flow is possible.
- Reduce the perimeter and length as much as possible.

**Profile and Base Drag:** Both are a function of the front and aft fuselage body shape, where blunt aft bodies and front bodies increase the flow separation which leads to a rise in profile and base drag. So, by improving the canopy and forebody shaping, the profile and base drag can be reduced.

**Compressibility Drag:** It does not have an effect until the fuselage experiences very high subsonic Mach numbers. Generally, compressibility drag comes from the presence of shocks on the fuselage. As the proposed design flies at low Mach numbers, there are no compressibility drag effects.

**Induced Drag:** The fuselage contributes to induced drag primarily because of its adverse effect on the wingspan load distribution [1].

### Fuselage Layout Design

The fuselage design of the proposed airplane is based on similar types of aircraft. For the FAR-23 airplanes, there is no fixed requirement of door and window placement, so it is assumed that the windows and doors are perpendicular to the seats. Based on the aerodynamic drag considerations and definition of fuselage geometric parameters given by Roskam [1], the proposed design fuselage parameters are tabulated below.

**Table 5.1: Fuselage Dimensions**

Fuselage Parameters	Dimension (ft)
Length of the Fuselage, $l_f$	29.40
Inner Diameter of the Fuselage, $d_f$	4.5
Fineness Ratio, $l_f/d_f$	6.53
Rear Fuselage Angle, $\theta_{fc}$	5 deg
Cabin Length	10.4
Nose Length	5
Tail Cone Length	14
Distance Between Two Seating Rows	2.7
Distance Between Two Adjacent Rows	0.25

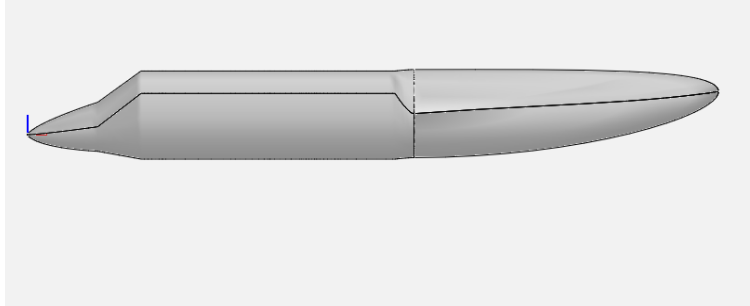


Figure 5.9: Side view of fuselage

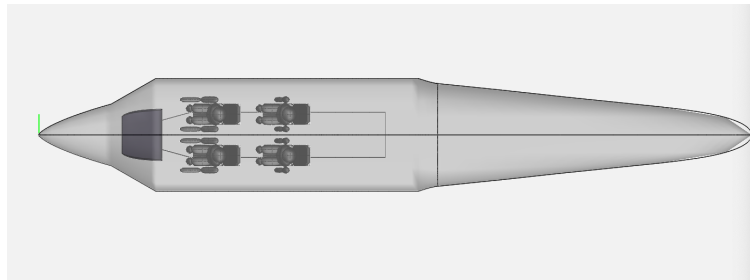


Figure 5.10: Top view of fuselage

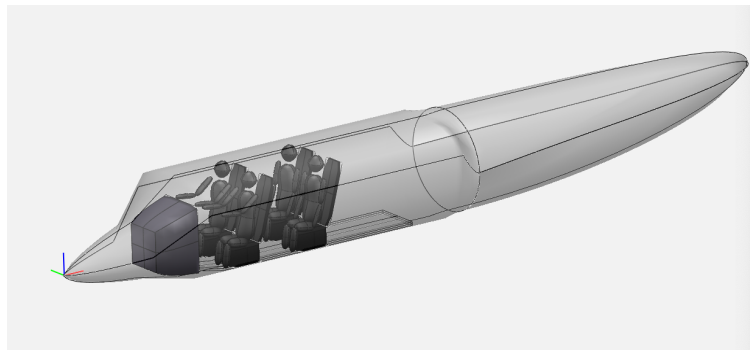


Figure 5.11: Isometric view of fuselage

## 5.4 Discussion

This chapter presented a detailed approach for designing the cockpit and fuselage of the proposed aircraft. The fuselage length was calculated using Raymer's Equation [15]. The diameter of the fuselage was taken from the reference aircraft. The calculated fineness ratio is within the range of values given by Roskam [1]. The layout of the cockpit and fuselage of the proposed aircraft were visualized using OpenVSP software.

# **Chapter 6**

## **Wing, High-Lift System & Lateral Control Design**

### **6.1 Introduction**

This chapter presents a wing planform design with a lateral control surface and high-lift devices based on the obtained weight sizing, performance sizing, and configuration selection.

The overall configuration for the proposed aircraft is conventional (tail aft) with a low wing configuration. Using the known characteristics from the previous chapter, the remaining planform design characteristics can be determined. The type of airfoil is selected based on the thickness-to-chord ratios required for the wing root and wing tip. The high-lift devices are selected based on the required maximum lift coefficients for cruise, takeoff, and landing obtained from the performance constraint analysis.

This chapter offers a detailed methodology for calculating the following characteristics of the wing planform design:

- Sweep Angle
- Dihedral Angle
- Incidence Angle
- Twist Angle
- Type of Airfoil
- Taper Ratio
- Thickness Ratio
- Lateral Control Surface Layout

### **6.2 Wing Planform Design**

The proposed aircraft uses a cantilevered low wing obtained from the configuration selection chapter. The area of the wing is calculated as 194 sq ft from a wing loading of 20.5 psf and an aspect ratio of 10 in the performance constraint analysis. The taper ratio and dihedral angle will be selected based on the reference aircraft data given by Roskam [1] as shown in the table below:

Type	Dihedral Angle, $\Gamma_w$ , deg.	Incidence Angle, $i_w$ , root/tip deg.	Aspect Ratio, A	Sweep Angle, $\Lambda_{c/4}$ , deg.	Taper Ratio, $\lambda_w$	Max. Speed, $V_{max}$ , kts	Wing Type
CESSNA Skywagon 107	1.7	1.5/-1.5	7.4	0	0.69	182	brcd/high
Cardinal RG	1.5	4.1/0.7	7.3	0	0.73	156	ctl/high
Skylane RG	1.7	0.8/-2.8	7.4	0	0.67	187	brcd/high
PIPER Cherokee Lance	7.0	2/-1	6.2	0	1.0	188	ctl/low
Cher. Warrior	7.0	2/-1	7.2	5	0.67	152	ctl/low
Turbo Sarat.SP	6.8	NA	7.3	0	0.68	195	ctl/low
Bellanca Skyrocket	2	2	6.7	0	0.57	287	ctl/low
Grunman Am. Tiger	5	1.4	7.1	0	1.0	148	ctl/low
Rockwell Commander 112A	7	2	7.0	-2.5	0.50	180	ctl/low
Trago Mills SAE-1	5	3/1	7.5	0	0.54	202	ctl/low
Scottish Aviation Bullfinch	6.5	1.2	8.4	0	0.57	150	ctl/low
Robin HR100/4	6.3	4.7	5.4	0	1.0	180	ctl/low
Socata Rallye 135E	7	4	7.6	0	1.0	148	ctl/low
Fuji FA-200	7	2.5	6.3	0	1.0	123	ctl/low
Gen Avia P13P	6	4	7.7	0	0.49	167	ctl/low

ctl = cantilever      brcd = braced (strutted)

Figure 6.1: Wing geometric data for various single engine airplanes [1]

The **taper ratio** is defined as the ratio of the tip chord length to the root chord length. A tapered wing is structurally and aerodynamically more efficient than a constant chord wing.

$$\lambda_w = \frac{C_{tip}}{C_{root}} \quad (1)$$

The proposed design uses a cantilevered low wing and by comparing it with similar aircraft in Figure 6.1 it is reasonable to assume taper ratio,  $\lambda_w = 0.50$ .

The **dihedral angle** is defined as the upward angle from the wing root to the wingtip of an aircraft wing. The proposed aircraft is a low wing configuration where the center of gravity is above the wing so a greater dihedral angle is required for lateral stability. The dihedral angle is chosen to be 7 degrees since it is fairly common among similar airplanes as shown in figure 6.1

The span of the wing is calculated by the following equation

$$b = \sqrt{AR * S} \quad (2)$$

$$b = \sqrt{10 * 194} = 44 \text{ ft}$$

Now, the root chord  $C_r$  is calculated as:

$$C_r = \frac{2 * S}{b * (1 + \lambda_w)} \quad (3)$$

$$C_r = 5.87 \text{ ft}$$

The tip chord can be calculated from equation (1),

$$C_t = \lambda_w * C_r \quad (4)$$

$$C_t = 2.90 \text{ ft}$$

The mean aerodynamic chord can be determined by using the following equation from Raymer [15]

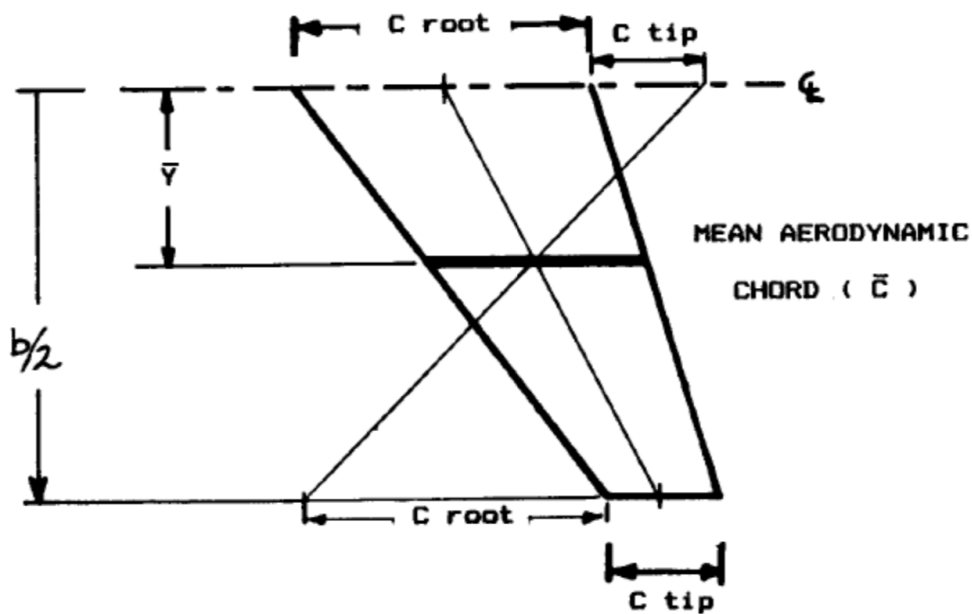
$$\underline{c} = \frac{2}{3} * C_r * \frac{1 + \lambda_w + \lambda_w^2}{1 + \lambda_w} \quad (5)$$

$$\underline{c} = 4.57 \text{ ft}$$

The spanwise location of the mean aerodynamic chord is determined as

$$\underline{Y} = \frac{b}{6} * \left( \frac{1 + 2\lambda_w}{1 + \lambda_w} \right) \quad (6)$$

$$\underline{Y} = 9.79 \text{ ft}$$



Figure

6.2: Trapezoidal wing geometry [1]

The typical wing aerodynamic center for subsonic aircraft is given as  $0.25\bar{c}$  from Raymer [15]

$$\text{Wing aerodynamic center} = 0.25 * \underline{c} = 1.14 \text{ ft} \quad (7)$$

The mean geometric chord is calculated by the below equation:

$$M_{gc} = S/b = 199/44.60 = 4.41 \text{ ft} \quad (8)$$

### Leading-edge spars

Along root chord =  $0.20 \cdot c_r$

Along tip chord =  $0.20 \cdot c_t$

### Trailing edge spars

Along root chord =  $0.745 \cdot c_r$

Along tip chord =  $0.745 \cdot c_t$

## 6.2.1 Sweep Angle - Thickness Ratio Combination

The wing geometric data for a single-engine airplane is presented in Figure 6.1. All single-engine airplanes have zero or negligible sweep, the proposed aircraft will, therefore, feature the zero-sweep angle. The other reason for selecting a zero-sweep angle is due to the fact that the proposed aircraft is not designed for a supersonic application.

Airfoil thickness has a direct effect on drag, maximum lift, stall characteristics, and structural weight. The thickness to chord ratio is determined from Figure (6.3). As thickness ratio increases, the coefficient of lift also increases at low speed. The thickness ratio also influences the critical Mach number. As the thickness ratio decreases, the critical Mach number increases.

The following thickness ratios are assumed at the design Mach number of 0.23 for the proposed design:

At the wing centerline,  $(t/c)_{\text{center}} : 0.14$

At the wingtip,  $(t/c)_{\text{tip}} : 0.13$

At the wing root,  $(t/c)_{\text{root}} : 0.17$

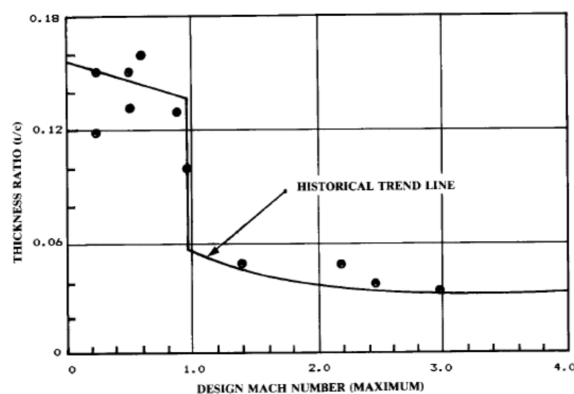


Figure 6.3: Historical trend of thickness to chord ratio with respect to design mach number [15]

### 6.3 Airfoil Selection

The geometry of an airfoil can be seen from the following figure:

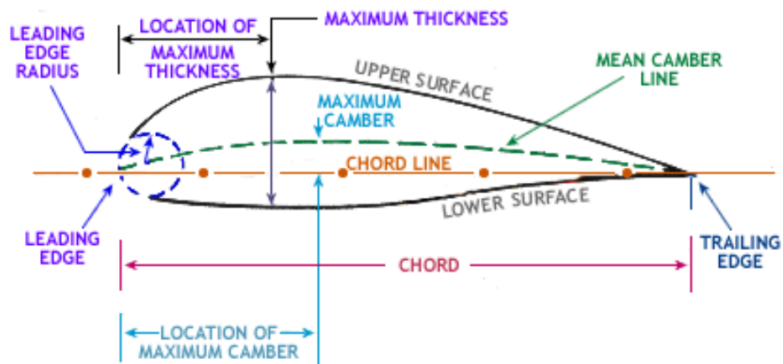


Figure 6.4: Airfoil geometry

- **Type of Airfoil**

NASA LS airfoil is selected for the electric design as it has superior lift characteristics. It is an airfoil profile widely used in vehicle design especially in aircrafts for subsonic and transonic speed regimes.

**Wing Root:** NASA LS(1)-0417 airfoil

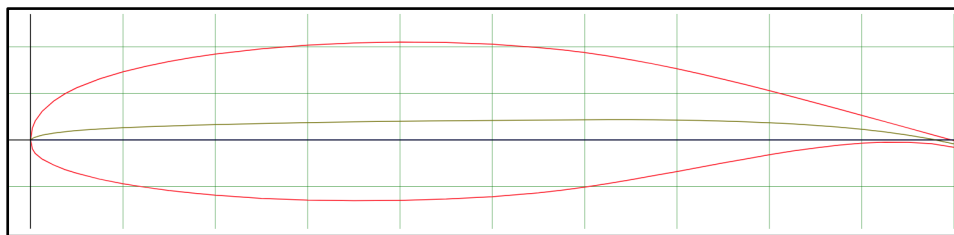


Figure 6.5: NASA LS(1)-0417 airfoil profile [15]

The following graphs were taken at Reynolds number = 1,000,000 and  $N_{crit} = 9$  [15]

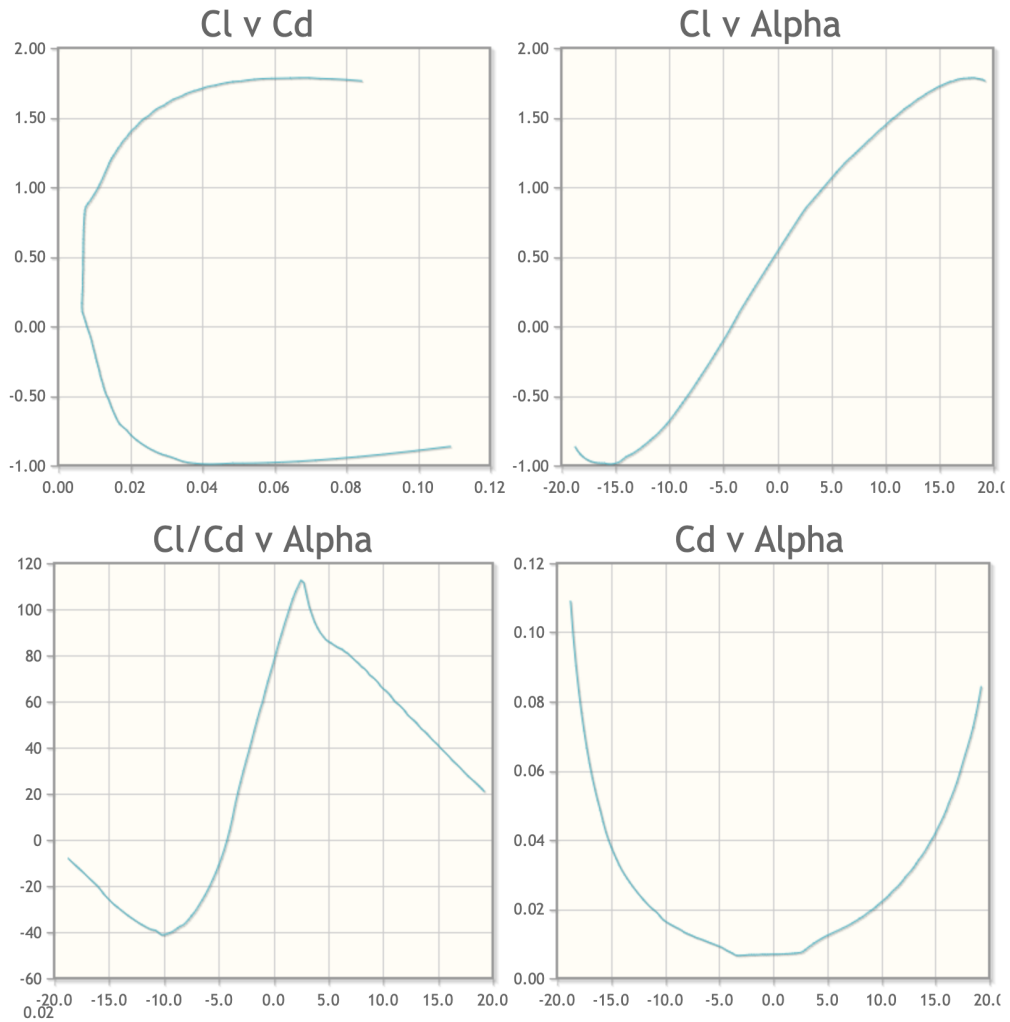


Figure 6.6: NASA LS(1)-0417 airfoil performance graph [15]

From Figure 6.6, it can be noted that the maximum lift coefficient increases with an increase in Reynold's number and note that the actual calculations of Reynolds number will be carried out in the next sections. The graphs of  $C_L$  versus  $\alpha$  for the NASA LS-0417 airfoil show that the proposed wing root airfoil can produce  $C_L$  of 1.76 at an angle-of-attack of 19.25 degrees.

**Wing Tip:** NASA LS(1)-0413 Airfoil

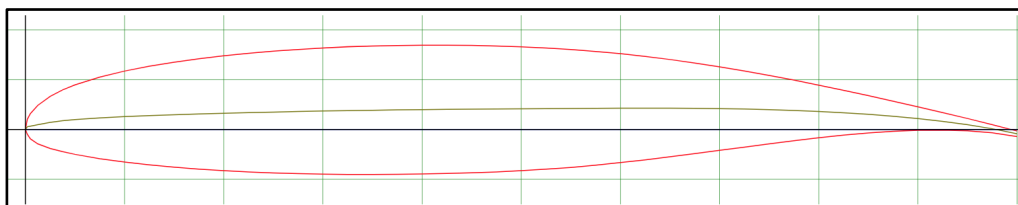


Figure 6.7: NASA LS(1)-0413 airfoil profile

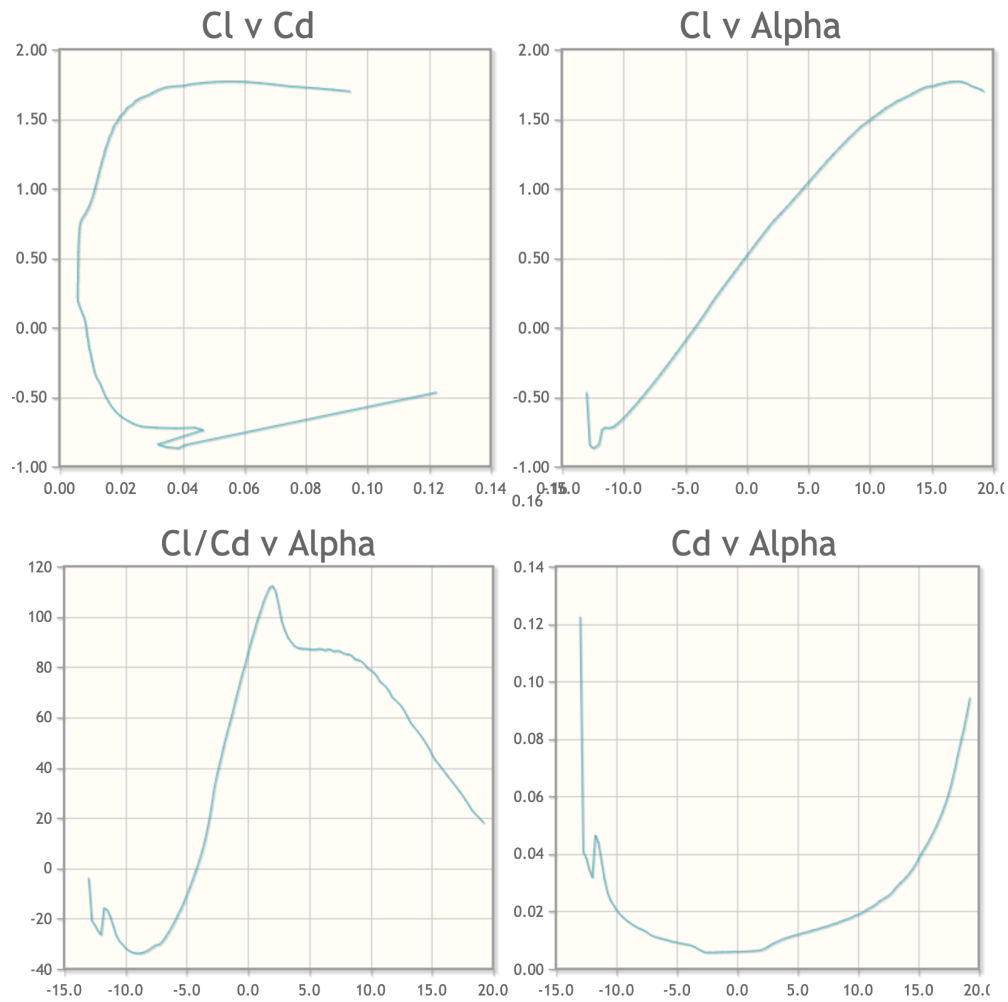


Figure 6.8: NASA LS(1)-0413 airfoil performance graph [16]

From Figure 6.8, the graph of  $C_L$  versus  $\alpha$  for the NASA LS airfoil show that the proposed wing tip airfoil can produce  $C_L$  of 1.70 at an angle-of-attack of 19.25 degrees. Substantial improvement in  $c_{l \max}$  for LS airfoils throughout the Reynolds number range were seen when compared to the NACA 4 and 5 digit airfoils and 65 series airfoils

- **Incidence Angle**

The angle of incidence is defined as the angle of the wing chord line with respect to the longitudinal axis of the fuselage. The Roskam data [1] summarizes the effect of wing incidence angle as shown in Figure 6.9.

Item	Large $i_w$	Small $i_w$
Cruise drag	High	Low
Cockpit visibility	Good	Watch out
Landing attitude in terms of nose gear hitting runway first	Watch out	No problem

Figure 6.9: Summary of the Effect of Wing Incidence Angle

Based on the above figure and comparable aircraft data from Figure 6.1, it is reasonable to have an incidence angle of 2 degrees which results in low cruise drag.

## 6.4 Wing Design Evaluation

To verify whether the airfoils chosen are capable of providing the appropriate value of  $C_{Lmax}$  to satisfy the value of 1.5 needed for clean flight, it is necessary to perform a procedure for calculating the  $C_{Lmax}$ . The maximum lift coefficient of the wing for the proposed design which is a short-coupled aircraft is given by Roskam[1] as,

$$C_{LmaxW} = 1.06 * C_{Lmax} \quad (9)$$

$$C_{LmaxW} = 1.59$$

There is no sweep in the proposed aircraft, so

$$C_{LmaxW} = K_\lambda * \frac{(C_{1maxr} + C_{1maxt})}{2}$$

$$C_{1maxr} + C_{1maxt} = 3.34 \quad (10)$$

The value of section maximum lift coefficients at the root,  $C_{1maxr}$  and at the tip  $C_{1maxt}$ , can be calculated using Reynolds number at the root and tip.

$$\text{At the root: } R_{nr} = \frac{\rho * V * C_r}{\mu} \quad (11)$$

$$\text{At the tip: } R_{nt} = \frac{\rho * V * C_t}{\mu} \quad (12)$$

Using the values

$$\rho = 0.002378 \text{ Slugs/ft}^3,$$

$$\mu = 3.737 \times 10^{-7} \text{ lbs/ft}^3 \text{ at sea-level [13]}$$

$$V = 170 \text{ mph.}$$

$C_r$  and  $C_t$  are obtained as 5.87 ft and 2.90 ft from Equation 3 & 4.

By substituting the above values in equations 11 and 12, we get the Reynolds number at sea-level as follows:

$$\text{At the root: } R_{n_r} = \frac{0.002378 * 250 * 5.87}{3.737 * 10^{-7}} = 8.55 * 10^6$$

$$\text{At the tip: } R_{n_t} = \frac{0.002378 * 250 * 2.90}{3.737 * 10^{-7}} = 5.13 * 10^6$$

The Reynolds number was used to choose the plot for both the root and tip airfoil's section coefficient of lift. The peaks on both these plots correspond to  $C_{1_{max_r}}$  and  $C_{1_{max_t}}$  for this wing planform, which turns out to be 1.76 and 1.7 respectively.

$$C_{1_{max_r}} + C_{1_{max_t}} = 3.46 \quad (13)$$

The value obtained is higher than the required value of 3.34 from equation 10, so the current wing planform satisfy the  $C_{L_{max}}$  requirement for this aircraft as long as NASA LS(1)-0417 airfoil is used.

## 6.5 Design of High-lift Devices

A high lift device is a component on an aircraft's wing that increases the lift on the wing. These devices are of two types:

- Trailing edge devices i.e. Flaps
- Leading-edge devices i.e. Slats

The high lift devices are selected based on the required maximum take-off lift coefficient and maximum landing lift coefficient. The clean lift coefficient, maximum take-off lift coefficient and maximum landing lift coefficient already obtained in the performance analysis are as follows:

- Clean:  $C_{L_{max}} = 1.5$
- Take-off:  $C_{L_{max_{TO}}} = 1.6$
- Landing:  $C_{L_{max_L}} = 1.8$

The incremental values of the maximum lift coefficient required to be produced by the high-lift devices can be determined by the following equations.

$$\text{Take-off : } \Delta C_{L_{max_{TO}}} = 1.05 (C_{L_{max_{TO}}} - C_{L_{max}}) = 1.05 * (1.6 - 1.5) = 0.105 \quad (14)$$

$$\text{Landing : } \Delta C_{L_{max_L}} = 1.05 (C_{L_{max_L}} - C_{L_{max}}) = 1.05 * (1.8 - 1.5) = 0.315 \quad (15)$$

The required incremental section lift coefficient value with flaps down can be calculated as:

$$\Delta c_{1_{max}} = \frac{(\Delta C_{L_{max}}) * (\frac{S}{S_{wf}})}{K_A} \quad (16)$$

Where,

$$K_A = (1 - 0.08 * \cos^2 \Lambda_{c/4}) \cos^{3/4} \Lambda_{c/4} \quad (17)$$

The factor  $K_A$  accounts for the effect of sweep angle in the flaps down. As the proposed design uses  $\Lambda_{c/4} = 0$  so,

$$K_A = 1 - 0.08 = 0.92$$

Assuming two arbitrary values for  $S_{wf}/S$  as per Roskam [1] procedure, the following values of take-off flaps and landing flaps are obtained using equation (16) and  $K_A$  value,

**Table 6.1: Results of take-off and landing flap incremental maximum lift coefficients for two arbitrary values of  $S_{wf}$**

$S_{wf}/S$	0.3	0.6
Take-off Flaps, $\Delta c_{1_{max}}$	0.38	0.19
Landing Flaps, $\Delta c_{1_{max}}$	1.14	0.57

### Assumptions:

It is observed that the required flap lift increments are not very high. Therefore, plain flaps will be enough for the proposed design. The following assumptions are made for the geometry of the flap based on the Roskam data [1].

$$\frac{z_{fh}}{c} = 0.1, \quad \frac{c_f}{c} = 0.25, \quad \delta_{f_{TO}} = 15 \text{ deg}, \quad \delta_{f_L} = 40 \text{ deg}$$

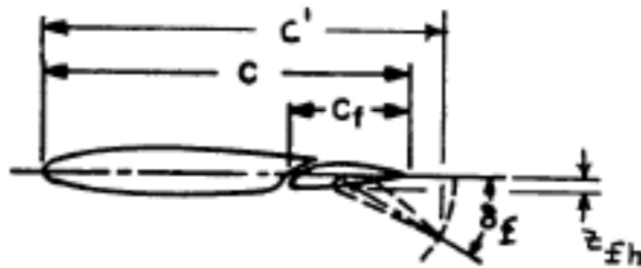


Figure 6.10: Flap geometry [1]

The required incremental section lift coefficient value which the flap must generate can be calculated as:

$$\Delta c_1 = (1/K) * \Delta c_{1_{max}} \quad (18)$$

Where the factor  $K=0.75$  for the plain flap from Figure (6.11)

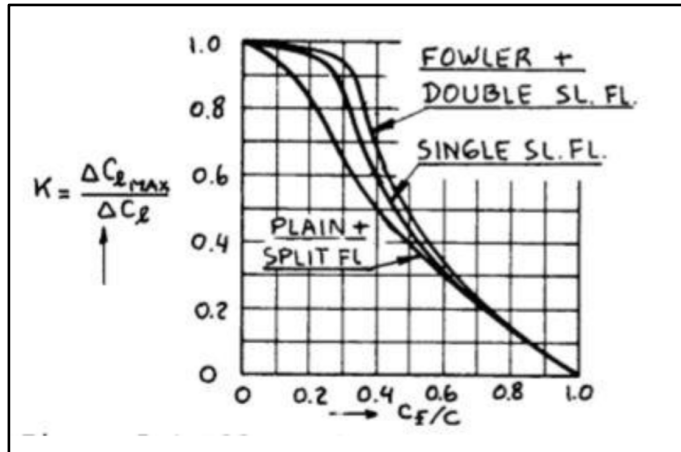


Figure 6.11: Effect of flap chord ratio and flap type on K [1]

The ability of the flaps to be able to meet these requirements is based on the deflection angle  $\delta_f$  and its effect on the wings incremental section coefficient of lift. Equation 19 shows this relationship. The value of  $c_{1\delta_f}$  and  $K'$  is assumed from Figures 6.12 and 6.13 from Roskam[1]. The incremental section lift coefficient  $\Delta c_1$ , for the plain flap, is calculated as:

$$\Delta c_1 = c_{1\delta_f} * \delta_f * K' \quad (19)$$

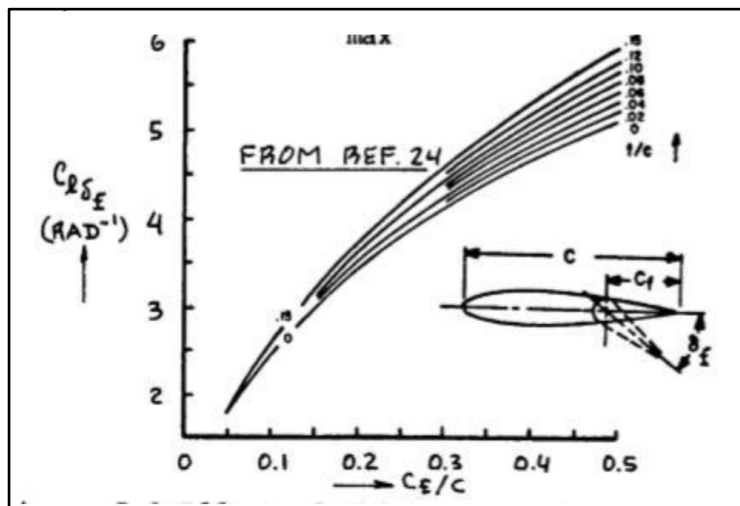


Figure 6.12: Effect of thickness ratio and flap chord ratio on  $c_{1\delta_f}$

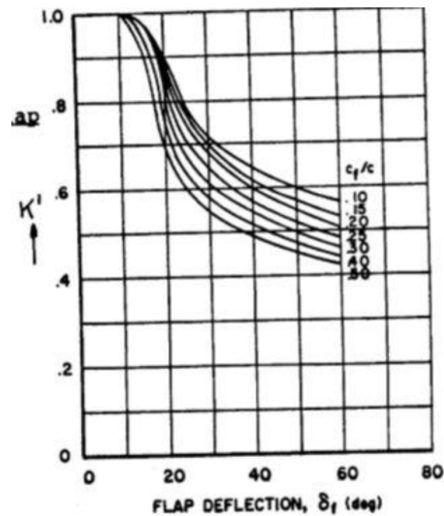


Figure 6.13: Effect of flap chord ratio and flap deflection on  $K'$

- **For Take-off:**

At  $\delta_{f_{TO}} = 15 \text{ deg}/0.2618 \text{ rad}$ , the value of  $K' = 0.98$  and  $c_{1\delta_f} = 4 \text{ rad}^{-1}$  is found from the figure (6.12) and (6.13)

From Equation 19,  $\Delta c_1 = 4.0 * 0.2618 * 0.98 = 1.026$

From Equation 18,  $\Delta c_{1_{max}} = 0.75 * 1.026 = 0.77$

- **For Landing:**

At  $\delta_{f_{TO}} = 40 \text{ deg}/0.6981 \text{ rad}$ , the value of  $K' = 0.58$  and  $c_{1\delta_f} = 4 \text{ rad}^{-1}$  is found from the figure (6.12) and (6.13)

From Equation 19,  $\Delta c_1 = 4.0 * 0.6981 * 0.58 = 1.61$

From Equation 18,  $\Delta c_{1_{max}} = 0.75 * 1.61 = 1.207$

It can be seen that the value of  $\Delta c_1$ , for take-off and landing, is more than needed with the previously assumed values of  $s_{wf}/s$  in Table 6.1. Thus, the plain flaps are sufficient to produce the required lift coefficient.

**Summary:**

The following parameters summarize the geometry of the flap:

**Table 6.2: Summary of flap geometry**

Type of the Flap	Plain Flap
The Ratio of Wing Flap Area to the Wing Area, $\frac{S_{wf}}{S}$	0.3
The Ratio of Flap Chord to Wing Chord, $\frac{c_f}{c}$	0.25
The Ratio of $\frac{z_{fh}}{c}$	0.1
Take-off Flap Angle	15 deg
Landing Flap Angle	40 deg

## 6.6 Design of the Lateral Control Surface

The lateral control surfaces are responsible for the lateral stability of the aircraft. The ailerons are used to generate a rolling motion and hinge on the outboard portion of a wing. The lift force of the wing is applied to the aerodynamic center which is at some distance from the aircraft center of gravity. These unequal forces create torque and the aircraft rotates about its center of gravity.

The data for a single-engine airplane is given in Roskam [1] as follows:

Type	Wing Area S ft <sup>2</sup>	Wing Span b ft	Vert. Tail Area S <sub>v</sub> ft <sup>2</sup>	S <sub>r</sub> /S <sub>v</sub>	x <sub>v</sub> ft	$\bar{V}_v$	Rudder Chord root/tip fr.c <sub>v</sub>	S <sub>a</sub> /S	Ail. Span Loc. in/out fr.b/2	Ail. Chord in/out fr.c <sub>w</sub>
CESSNA Skywagon 207	174	35.8	16.0	0.44	18.0	0.046	.46/.46	0.10	.61/.94	.25/.22
Cardinal RG	174	35.5	17.4	0.37	13.5	0.038	.35/.43	0.11	.65/.97	.38/.37
Skylane RG	174	35.8	18.6	0.37	15.8	0.047	.41/.42	0.11	.47/.96	.17/.24
PIPER Cherokee Lance	175	32.8	13.8	0.31	15.3	0.037	.26/.30	0.064	.56/.88	0.20
Warrior	170	35.0	11.5	0.36	13.2	0.026	.29/.32	0.078	.48/.96	.27/.24
Turbo Saratoga SP	178	36.2	15.9	0.29	15.2	0.038	.23/.38	0.057	.52/.84	0.19
Bellanca Skyrocket	183	35.0	18.1	0.33	13.2	0.037	.28/.40	0.076	.60/1.0	.25/.22
Grumman Tiger	140	31.5	8.4	0.43	12.6	0.024	.36/.46	0.055	.56/.92	0.24
Rockwell Commander	152	32.8	17.0	0.28	11.4	0.039	.30/.46	0.072	.64/.97	.27/.36
Trigo Mills SAB-1	120	30.7	17.1	0.40	18.6	0.086	.35/.54	0.080	.58/.97	.25/.29
Scottish Aviation Bullfinch	129	33.8	22.7	0.39	11.9	0.062	.35/.56	0.073	.61/.93	.23/.30

Figure 6.14: Aileron data for single engine propeller driven airplane

The data in the above table suggest that following aileron dimensions are appropriate:

Aileron chord ratio: 0.24 – 0.26

Aileron span ratio: 0.57 – 0.94

## 6.7 Wing Drawings

The wing parameters are as follows:

**Table 6.3: Wing parameters**

Wing Area	194 ft <sup>2</sup>
Aspect Ratio	10
Wing Span, b	44 ft
Sweep Angle	0 deg
Airfoil Thickness at the Wing Centerline	0.14
Airfoil Thickness at the Wing Tip	0.12
Taper Ratio	0.50
Dihedral	7 deg
Root Chord, C <sub>r</sub>	5.87 ft
Tip Chord, C <sub>t</sub>	2.90 ft
Mean Aerodynamic Chord, $\bar{c}$	4.57 ft
Spanwise Location of $\bar{c}$	9.75 ft
Wing Aerodynamic Center, X <sub>ac</sub>	1.14 ft
Aileron Chord Ratio	0.25
Aileron Span Ratio	0.70

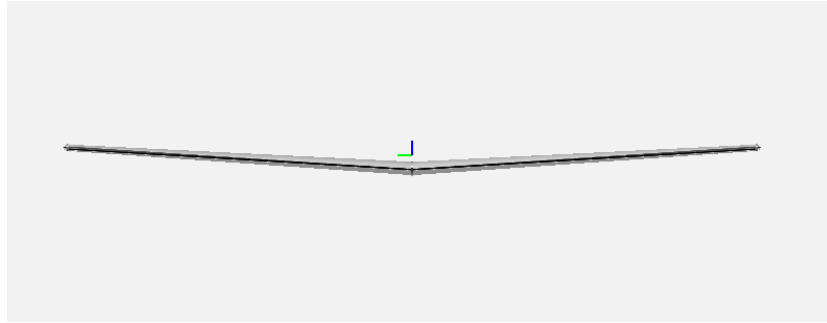


Figure 6.14: Front view of wing planform

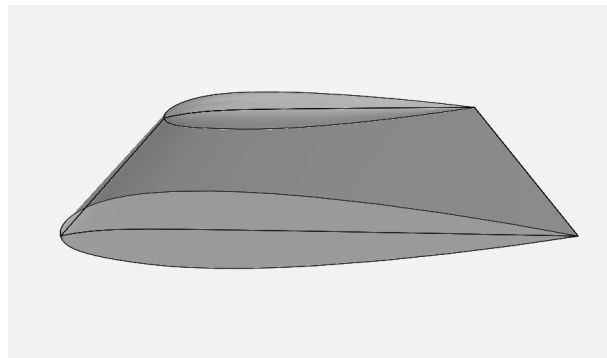


Figure 6.15: Side view of wing planform

- **Placement of Wing on the Fuselage:**

It depends on the CG of the wing and CG of the fuselage,

Fuselage CG =  $0.40 \times \text{length} = 11.76 \text{ ft}$

Wing CG =  $0.40 \times c_{\text{bar}} = 1.83 \text{ ft}$

Location of the wing on fuselage approximately:

$11.76 - 1.83 = 9.93 \text{ ft}$  (distance from nose to leading edge of the wing)

Item	Fighters	Transports and bombers	General aviation	Multiplier <sup>a</sup>	Approximate location
Wing	9.0	10.0	2.5	$S_{\text{exposed planform ft}^2}$	40% MAC
Horizontal tail	4.0	5.5	2.0	$S_{\text{exposed planform ft}^2}$	40% MAC
Vertical tail	5.3	5.5	2.0	$S_{\text{exposed planform ft}^2}$	40% MAC
Fuselage	4.8	5.0	1.4	$S_{\text{wetted area ft}^2}$	40-50% length
Landing gear <sup>b</sup>	.033	.043	.057	TOGW (lb)	-
Installed engine	.045 Navy				
	1.3	1.3	1.4	Engine weight (lb)	-
"All-else empty"	.17	.17	.10	TOGW (lb)	40-50% length

<sup>a</sup>Results are in pounds.  
<sup>b</sup>15% to nose gear; 85% to main gear.

Figure 6.16: Approximate Empty Weight Buildup [15]

## 6.8 Conclusions and Recommendations

The wing for the proposed aircraft is designed and compared with a benchmark provided in Roskam. It is a single engine airplane that flies at low Mach number, therefore, does not require sweep (zero sweep). The

taper ratio is chosen as 0.50 which gives the root and tip chord of around 5.87 feet and 2.90 feet respectively. Almost all the general aviation low wing aircraft have dihedral which gives lateral stability to the aircraft. The dihedral angle taken for the proposed design is 7 degrees. Based on the geometry of wing and flight parameters chosen, plain flaps are the recommended high-lift devices because they provide substantial lift. Additionally, the wings have enough volume to store the batteries. They need to be properly insulated to avoid any risk of fire due to a battery explosion.

# Chapter 7

## Design of the Empennage & the Longitudinal and Directional Controls

### 7.1 Introduction

The empennage, also known as tail, provides stability during flight. Almost all aircraft have an empennage integrating vertical and horizontal surfaces which stabilize the flight dynamics of yaw and pitch. Based on previous chapters, this chapter presents a methodology for designing an empennage with longitudinal and directional controls. The selection of the following tail parameters will be presented:

- Aspect Ratio
- Taper Ratio
- Sweep Angle
- Thickness Ratio
- Airfoil
- Incidence Angle
- Dihedral Angle

### 7.2 Overall Empennage Design

- **Location of Empennage**

The location of the empennage components on the airplane will be decided in this section. The main objective of the tail is to counter the moments produced by the wing and the tail. By keeping the empennage area as small as possible, the airplane weight and drag will be reduced as much as possible. The location of the empennage amounts to deciding the empennage moment arms  $X_v$ ,  $X_h$ , and  $X_c$ .

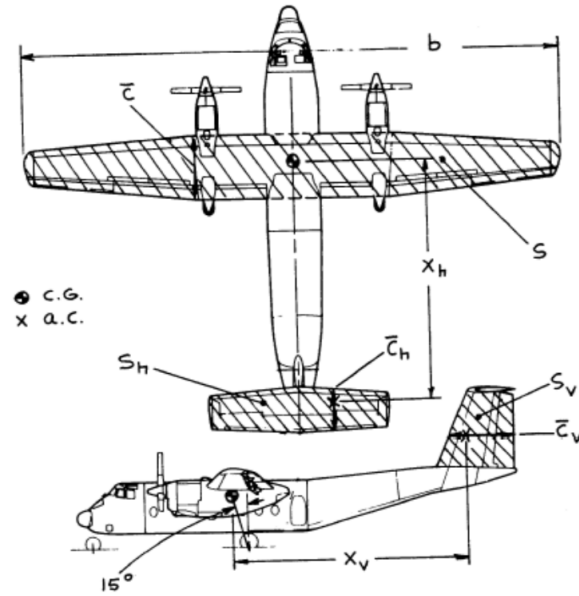


Figure 7.1: Empennage Moment Arm

The  $X_v$  and  $X_h$  are defined in the above figure, whereas  $X_c$  is related to the canard moment arm. There is no canard in the proposed configuration, so the location of empennage is determined only for the tail.

For the proposed aircraft, the value of  $X_v$  and  $X_h$  is estimated from Figure 7.2 and 7.3 as:

$$X_v = 13.5 \text{ ft} \quad (1)$$

$$X_h = 11.5 \text{ ft} \quad (2)$$

- **Size of Empennage**

The lift produced by the tail is directly proportional to the tail area and the tail effectiveness is proportional to the product of the tail area and tail moment arm which leads to the tail volume coefficient. Therefore, the tail sizing is all about determining the tail area using the tail volume coefficient and obtained tail moment arm as shown below.

$$\text{Horizontal Volume coefficient: } V_h = \frac{x_h * S_h}{S * \bar{c}} \quad (3)$$

$$\text{Vertical Volume coefficient: } V_v = \frac{x_v * S_v}{S * b} \quad (4)$$

The tail volume coefficient is assumed from Roskam data [1] of comparable aircraft as shown in Figure 7.2 for the horizontal tail and Figure 7.3 for the vertical tail as follows:

$$\underline{V_h} = 0.50$$

$$\underline{V_v} = 0.04$$

Type	Wing Area S ft <sup>2</sup>	Wing mc $\bar{c}$ ft	Wing Airfoil root/tip NACA*	Hor. Tail Area S <sub>h</sub> ft <sup>2</sup>	S <sub>e</sub> /S <sub>h</sub>	x <sub>h</sub> ft	$\bar{V}_h$	Elevator Chord root/tip fr.c <sub>h</sub>
CESSNA Skywagon 207	174	4.55	2412	44.9	0.45	16.2	0.92	.48/.47
Cardinal RG	174	4.79	64A215/64A412	35.0	1.00	14.3	0.60	stabilator
Skylane RG	174	4.52	2412	38.8	0.41	14.3	0.71	.47/.39
PIPER Cherokee								
Lance	175	5.25	65,415	34.6	1.00	16.1	0.61	stabilator
Warrior	170	4.44	65,415	26.5	1.00	13.5	0.48	stabilator
Turbo Saratoga SP	178	4.71	NA	36.2	1.00	16.2	0.70	stabilator
Bellanca Skyrocket	183	5.30	63,215	42.6	0.38	13.8	0.61	.36/.42
Grumman Tiger	140	4.44	NA	37.6	0.28	12.6	0.76	0.39
Rockwell Commander	152	4.58	63415	31.2	0.34	10.9	0.49	.33/.44
Trago Mills SAH-1	120	3.94	2413.6	22.0	0.46	17.8	0.83	0.46
Scottish Aviation Bullfinch	129	3.97	63,615	27.5	0.58	11.9	0.63	0.45

Figure 7.2: Horizontal tail volume and elevator data for single engine aircraft

Type	Wing Area S ft <sup>2</sup>	Wing Span b ft	Vert. Tail Area S <sub>v</sub> ft <sup>2</sup>	S <sub>r</sub> /S <sub>v</sub>	x <sub>v</sub> ft	$\bar{V}_v$	Rudder Chord root/tip fr.c <sub>v</sub>	S <sub>a</sub> /S	Ail. Span Loc. in/out fr.b/2	Ail. Chord in/out fr.c <sub>w</sub>
CESSNA Skywagon 207	174	35.8	16.0	0.44	18.0	0.046	.46/.46	0.10	.61/.94	.25/.23
Cardinal RG	174	35.5	17.4	0.37	13.5	0.038	.35/.43	0.11	.65/.97	.38/.37
Skylane RG	174	35.8	18.6	0.37	15.8	0.047	.41/.42	0.11	.47/.96	.17/.24
PIPER Cherokee										
Lance	175	32.8	13.8	0.31	15.3	0.037	.26/.50	0.064	.56/.88	0.20
Warrior	170	35.0	11.5	0.36	13.2	0.026	.29/.52	0.078	.48/.96	.27/.24
Turbo Saratoga SP	178	36.2	15.9	0.29	15.2	0.038	.23/.58	0.057	.52/.84	0.19
Bellanca Skyrocket	183	35.0	18.1	0.33	13.2	0.037	.28/.40	0.076	.60/1.0	.25/.22
Grumman Tiger	140	31.5	8.4	0.43	12.6	0.024	.36/.46	0.055	.56/.92	0.24
Rockwell Commander	152	32.8	17.0	0.28	11.4	0.039	.30/.46	0.072	.64/.97	.27/.36
Trago Mills SAH-1	120	30.7	17.1	0.40	18.6	0.086	.35/.54	0.080	.58/.97	.25/.29
Scottish Aviation Bullfinch	129	33.8	22.7	0.39	11.9	0.062	.35/.56	0.073	.61/.93	.23/.30

Figure 7.3: Vertical tail volume, rudder and aileron data for single engine aircraft

Using the equations (3) and (4), the horizontal and the vertical tail areas are calculated as:

$$S_h = \frac{(V_h) * S * c}{x_h} = 46.25 \text{ ft}^2$$

$$S_v = \frac{(V_v) * S * b}{x_v} = 26 \text{ ft}^2$$

### 7.3 Design of Horizontal Stabilizer

The design of horizontal stabilizer includes the selection of the following parameters:

- **Aspect Ratio**

The Aspect ratio of a horizontal stabilizer is determined as 50% of the wing aspect ratio which is given by:

$$AR_h = 0.50 * AR = 0.50 * 10 = 5$$

The calculated aspect ratio is within the given range of values of single engine aircraft by Roskam as shown in Figure 7.4. The aspect ratio is given by:

$$AR_h = \frac{b_h^2}{S_h}$$

Therefore, the span of the horizontal stabilizer is calculated as follows:

$$b_h = \sqrt{5 * 46.25} = 15.20 \text{ ft}$$

Type	Dihedral Angle, $\Gamma_h$ deg.	Incidence Angle, $i_h$ deg.	Aspect Ratio, $A_h$	Sweep Angle, $\Delta_c/4_h$ deg.	Taper Ratio, $\lambda_h$
Homebuilts	+5 - -10	0 fixed to variable	1.8 - 4.5	0 - 20	0.29 - 1.0
Single Engine Prop. Driven	0	-5 - 0 or variable	4.0 - 6.3	0 - 10	0.45 - 1.0
Twin Engine Prop Driven	0 - +12	0 fixed to variable	3.7 - 7.7	0 - 17	0.48 - 1.0
Agricultural	0 - +3	0	2.7 - 3.4	0 - 10	0.59 - 1.0
Business Jets	-4 - +9	-3.5 fixed	3.2 - 6.3	0 - 35	0.32 - 0.57
Regional Turbo-Props.	0 - +12	0 - 3 fixed to variable	3.4 - 7.7	0 - 35	0.39 - 1.0
Jet Transports	0 - +11	variable	3.4 - 6.1	18 - 37	0.27 - 0.62
Military Trainers	-11 - +6	0 fixed to variable	3.0 - 5.1	0 - 30	0.36 - 1.0
Fighters	-23 - +5	0 fixed to variable	2.3 - 5.8	0 - 55	0.16 - 1.0
Mil. Patrol, Bomb and Transports	-5 - +11	0 fixed to variable	1.3 - 6.9	5 - 35	0.31 - 0.8
Flying Boats, Amph. and Float Airplanes	0 - +25	0 fixed	2.2 - 5.1	0 - 17	0.33 - 1.0
Supersonic Cruise Airplanes	-15 - 0	0 fixed to variable	1.8 - 2.6	32 - 60	0.14 - 0.39

Figure 7.4: Horizontal tail design planform parameters

- Taper Ratio

The taper ratio of the horizontal stabilizer is assumed to be 0.5 from the given comparable aircraft data by Roskam as shown in Figure 7.4. The root chord of the horizontal stabilizer can be determined by using the following equation:

$$c_{r_h} = \frac{2 * S_h}{b_h(1 + \lambda_h)}$$

$$c_{r_h} = 4.05 \text{ ft}$$

The tip chord of the horizontal stabilizer is calculated as:

$$c_{t_h} = \lambda_h * c_{r_h}$$

$$c_{t_h} = 2.02 \text{ ft}$$

Mean aerodynamic chord,  $\underline{c_h} = 3.15 \text{ ft}$

Mean aerodynamic chord location,  $\underline{Y}_h = 3.37$  ft

- **Sweep Angle:**

The sweep angle is the angle between the perpendicular to the centerline and the leading edge of the wing. It is assumed as 10 deg for the proposed aircraft.

- **Thickness Ratio:**

The selection of thickness ratio is important to ensure that the critical Mach number for the tails is higher than that of the wing. As per Roskam [1], the typical thickness ratio for the horizontal tail in use is 0.10 to 0.20. The thickness ratio for the horizontal tail is assumed to be 0.12 for the proposed design.

- **Airfoil:**

The horizontal tail airfoil needs to provide positive and negative lift based on the center of gravity location during the mission and thus airfoil needs to be symmetric. The airfoil NACA 0012 is selected for both root and the tip based on the thickness ratio.

- **Dihedral:**

The tail dihedral angle is used for lateral stability adjustment and control adjustment. The dihedral angle of the horizontal stabilizer is assumed to be 0 degrees by comparison to the similar aircraft data provided by Roskam [1].

- **Incidence angle:**

The incidence angle of the horizontal tail is assumed as zero.

## 7.4 Design of Vertical Stabilizer

The design of vertical stabilizer includes the selection of following parameters:

- **Aspect Ratio**

T-tail aircraft have lower vertical aspect ratios to reduce the weight impact of the horizontal tail's location on top of the vertical tail. The Aspect ratio of the vertical stabilizer for the proposed design is obtained from the similar aircraft data shown in Figure 7.5 as 1.6.

$$AR_v = 1.6$$

The calculated aspect ratio is within the given range of values of single engine aircraft by Roskam [1] as shown in Figure 7.5. The aspect ratio is given by:

$$AR_v = \frac{b_v^2}{S_v}$$

Therefore, the span of the vertical stabilizer is calculated as follows:

$$b_v = \sqrt{1.6 * 26} = 6.44 \text{ ft}$$

Type	Dihedral Angle, $\Gamma_v$ deg.	Incidence Angle, $i_v$ deg.	Aspect Ratio, $\lambda_v$	Sweep Angle, $\Delta_c/4_v$ deg.	Taper Ratio, $\lambda_v$
Homebuilts	90	0	0.4 - 1.4	0 - 47	0.26 - 0.71
Single Engine Prop. Driven	90	0	0.9 - 2.2	12 - 42	0.32 - 0.58
Twin Engine Prop Driven	90	0	0.7 - 1.8	18 - 45	0.33 - 0.74
Agricultural	90	0	0.6 - 1.4	0 - 32	0.43 - 0.74
Business Jets	90	0	0.8 - 1.6	28 - 55	0.30 - 0.74
Regional Turbo-Props.	90	0	0.8 - 1.7	0 - 45	0.32 - 1.0
Jet Transports	90	0	0.7 - 2.0	33 - 53	0.26 - 0.73
Military Trainers	90	0	1.0 - 2.9	0 - 45	0.32 - 0.74
Fighters	75 - 90	0	0.4 - 2.0	9 - 60	0.19 - 0.57
Mil. Patrol, Bomb and Transports	90	0	0.9 - 1.9	0 - 37	0.28 - 1.0
Flying Boats, Amph. and Float Airplanes	90	0	1.2 - 2.4	0 - 32	0.37 - 1.0
Supersonic Cruise Airplanes	75 - 90	0	0.5 - 1.8	37 - 65	0.20 - 0.43

Figure 7.5: Vertical tail design planform parameters

- **Taper Ratio**

The taper ratio of the vertical stabilizer is assumed to be 0.4 from the given comparable aircraft data by Roskam [1] as shown in Figure 7.5. The root chord of the vertical stabilizer can be determined by using the following equation:

$$c_{r_v} = \frac{2 * S_v}{b_v(1 + \lambda_v)}$$

$$c_{r_v} = 5.76 \text{ ft}$$

The tip chord of the vertical stabilizer is calculated as:

$$c_{t_v} = \lambda_v * c_{r_v}$$

$$c_{t_v} = 2.3 \text{ ft}$$

Mean aerodynamic chord,  $c_v = 4.27 \text{ ft}$

Mean aerodynamic chord location,  $Y_v = 1.38 \text{ ft}$

- **Sweep Angle:**

As the proposed aircraft travels at low subsonic speeds, a low sweep angle is preferred for the vertical tail. The quarter chord sweep angle of the vertical tail is assumed as 15 degrees from the comparable aircraft data as shown in Figure 7.5

- **Thickness ratio:**

As per Roskam [1], the typical thickness ratio for vertical tail in use is 0.09 to 0.18. The thickness ratio for the vertical tail is assumed to be 0.12 for the proposed design.

- **Airfoil:**

The airfoil needs to be selected based on the selected thickness ratio and to maintain the symmetry of the aircraft about the fuselage longitudinal axis, the airfoil should be symmetric. NACA 0012 is selected for the proposed design.

- **Dihedral:**

The dihedral angle of the vertical stabilizer is assumed to be 90 degrees by comparing to the similar aircraft data as shown in Figure 7.5.

- **Incidence angle:**

The incidence angle of the vertical tail is assumed as 0 deg.

## 7.5 Design of Longitudinal and Directional Control

Using Figures 7.2 and 7.3, the control surface parameters are chosen and added to the design. For the horizontal and vertical tail, the chosen values are:  $\frac{S_e}{S_h} = 0.45$ ,  $\frac{S_r}{S_v} = 0.40$

Where,  $S_h$  = horizontal Stabilizer area = 46.25 ft<sup>2</sup>

$S_v$  = Vertical Stabilizer area = 26 ft<sup>2</sup>

On calculating,  $S_e = 20.81$  ft<sup>2</sup> and  $S_r = 10.5$  ft<sup>2</sup>

## 7.6 Cad Drawings

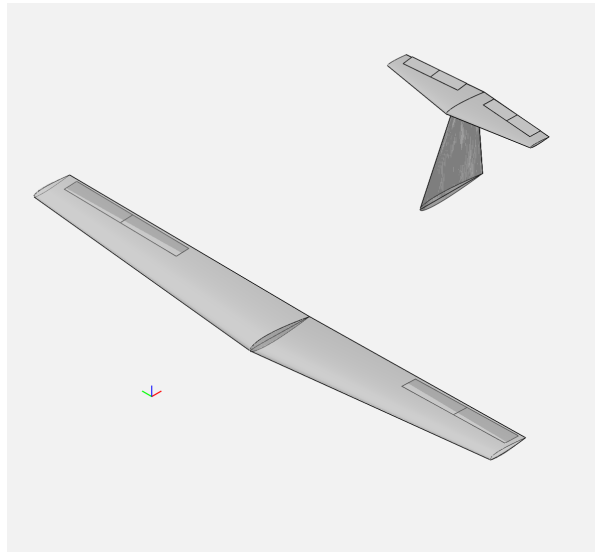


Figure 7.6: Isometric view of empennage planform with respect to wing planform

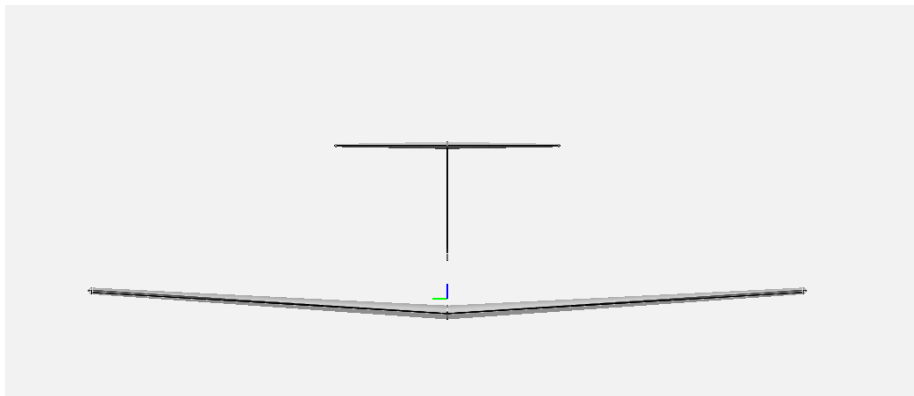


Figure 7.7: Front view of empennage planform

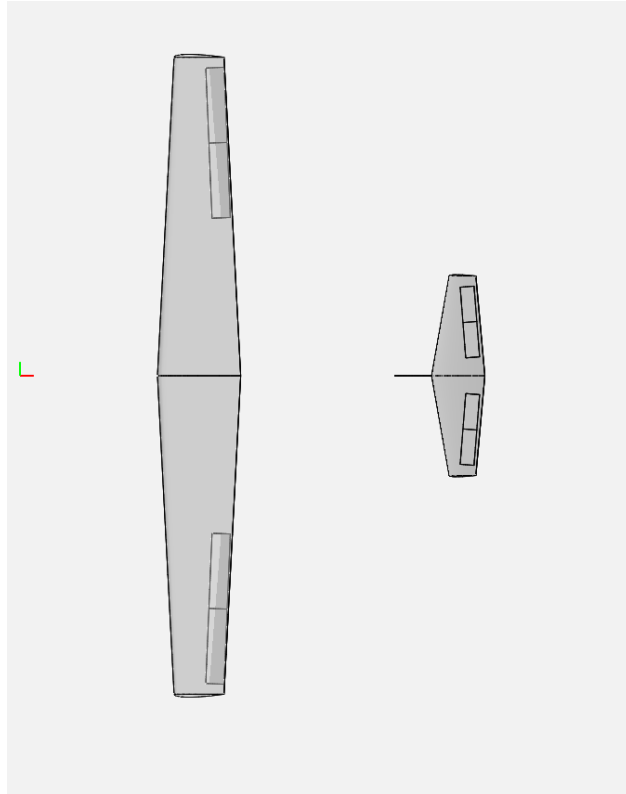


Figure 7.8: Top View of empennage planform

## 7.7 Discussion & Conclusion

The T-tail arrangement provides a suitable conventional configuration for the electric design. The chosen control surface ratios are consistent with the ratios provided by Roskam. The empennage is modeled after guessing the volume coefficient for the horizontal and vertical stabilizers. The locations are decided by guessing the moment arms for both stabilizers. This is subject to change depending on the stability and control analysis of the airplane.

# Chapter 8

## Landing Gear Design

### 8.1 Introduction

The landing gear arrangement previously introduced in the configuration chapter will consist of a fixed tricycle landing gear. The following landing gear parameters are decided here:

- Type, size, and number of tires
- Preliminary arrangement

The landing gear preliminary parameters can be seen in the following figure:

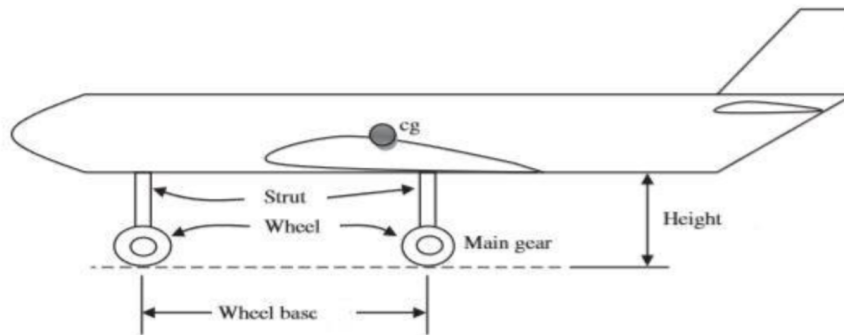


Figure 8.1: Landing Gear Parameters

Some of the advantages of selecting a fixed tricycle landing gear are: fewer parts, less weight, low cost, design is easy, and more longitudinally stable. In order to size the landing gear, the center of gravity will need to be determined. The CG range is obtained from the estimated weight and balance for an assumed disposition of the landing gear. Once it is obtained, the landing gear is designed satisfying two geometric criteria, tip-over, and ground clearance. The landing gear design requires an iteration process until the actual CG location of the aircraft is obtained.

### 8.2 Estimation of the Center of Gravity Location for the Airplane

Before proceeding into the landing gear analysis, it is better to get a rough idea of the center of gravity of the airplane. In this section, the CG location of the major subgroups of the proposed aircraft is determined using the weight fraction analysis. At this stage, the initial component weight breakdown is calculated using the obtained take-off weight. The class-I method of Roskam [1] for weight estimation highly relies on the assumption that it is possible to express each component weight as a fraction of takeoff weight ( $W_{TO}$ ) or empty weight ( $W_E$ ) or flight design gross weight ( $GW$ ). For almost all the civil airplanes, take-off weight and flight design gross weight are the same.

The following table lists the major weight fractions for similar airplanes:

**Table 8.1: Component weight fractions for similar airplanes and the proposed aircraft**

Type	Cessna 210	Beech J-35	Cessna 210 J	Proposed Electric Aircraft
Wing Grp/GW	0.09	0.131	0.099	0.106
Emp. Grp/GW	0.024	0.02	0.025	0.023
Fuselage Grp/GW	0.109	0.069	0.12	0.099
Landing Gear/GW	0.071	0.071	0.056	0.066
Fixed equip/GW	0.199	0.201	0.171	0.190
Empty Weight/GW	0.094	0.115	0.099	0.103

The mission weights obtained in chapter 3 are as follows:

**Table 8.2: Mission weights**

Takeoff Weight $W_{TO}$ (lbs)	3980
Payload Weight $W_{PL}$ (lbs)	820
Empty Weight $W_E$ (lbs)	2535
Battery Weight, $W_{Bat}$ (lbs)	637

Using the averaged weight fractions from Table 8.1, the following preliminary component weights are obtained for the proposed aircraft.

### Component Weight Breakdown

**Table 8.3: Subgroup component weight summary for the proposed aircraft**

<b>Component</b>	<b>Class-I Estimation (lbs)</b>	<b>Adjustments</b>	<b>Class-I Weight (lbs)</b>
Wing	425	35	460
Empennage	92	8	99
Fuselage	395	33	428
Landing Gear	263	22	285
Powerplant	758	63	821
Fixed Eqp	409	34	443
Empty Weight	2342	195	2535
Payload			820
Battery Weight			637
Takeoff Weight			3980

The sum of the first column yields an empty weight of 2342 lbs instead of the desired 2535 lbs. The difference is due to round-off errors in the weight fractions used. This difference is distributed to overall items in proportion to their component weights i.e. the wing adjusted number is arrived at by multiplying 195 lbs by  $425/2342$ . Similarly, all other component weights are adjusted.

The location of the center of gravity of major components is calculated as follows:

**Table 8.4: Center of gravity location of major components**

<b>Component</b>	<b>Lengths or MAC</b>	<b>Relation</b>	<b>CG (ft)</b>	<b>CG from the nose (ft)</b>
------------------	-----------------------	-----------------	----------------	------------------------------

Fuselage	29.4	$0.39 * l_f$	11.466	11.466
Wing	4.57	$0.40 * c_w$	1.828	11.758
VT	4.27	$0.30 * c_v$	1.281	26.411
HT	2.56	$0.30 * c_h$	0.768	27.608
Empty weight	29.4	$0.45 * l_f$	13.23	13.23

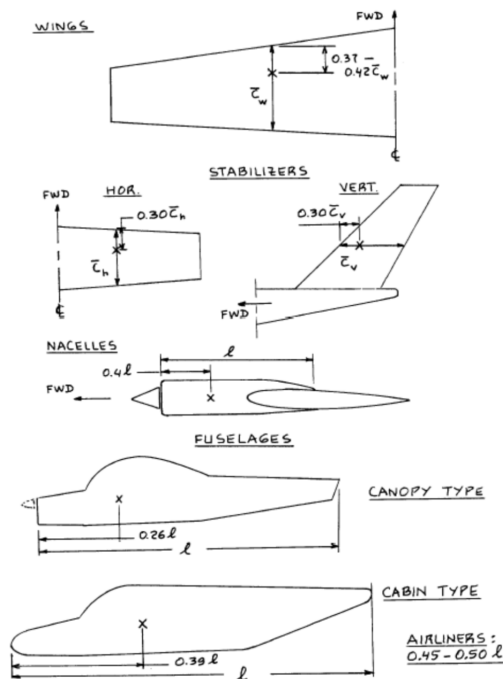


Figure 8.2: Location of the CG of major components

The component's weight and coordinate data for the proposed aircraft are shown in Table 8.5 by assuming the disposition of the landing gear. At this stage taking x coordinate data, the range of the CG is determined.

No.	Type of Component	$W_i$	$x_i$	$W_i x_i$	$y_i$	$W_i y_i$	$z_i$	$W_i z_i$
		lbs	in.	inlbs	in.	inlbs	in.	inlbs
1.	Fuselage group	$W_1$	$x_1$	$W_1 x_1$	$y_1$	$W_1 y_1$	$z_1$	$W_1 z_1$
2.	Wing group							
3.	Empennage group							
4.	Engine group							
5.	Landing gear group							
6.	Fixed equipm't group							
	Empty weight: $W_E = \sum_{i=1}^{i=6} W_i$					$x_{cg_{W_E}} = (\sum_{i=1}^{i=6} W_i x_i) / W_E$		
7.	Trapped fuel and oil							
8.	Crew							
	Operating weight empty: $W_{OE} = \sum_{i=1}^{i=8} W_i$					$x_{cg_{W_{OE}}} = (\sum_{i=1}^{i=8} W_i x_i) / W_{OE}$		
9.	Fuel							
10.	Passengers							
11.	Baggage							
12.	Cargo							
13.	Military load							
	Take-off weight: $W_{TO} = \sum_{i=1}^{i=13} W_i$					$x_{cg_{W_{TO}}} = (\sum_{i=1}^{i=13} W_i x_i) / W_{TO}$		
Note: Locations for $y_{cg}$ and for $z_{cg}$ are found from similar equations.								

Figure 8.3: Class-I weight and balance calculations

Table 8.5: Components weight and coordinate data for the proposed aircraft

Type of Component	Weight(lbs)	x(ft)	Wx (ft.lbs)
Wing	460	11.75	5408.68
Empennage	99	27.01	2673.941
Fuselage	428	11.46	4907.448
Landing Gear: Nose	57	5.88	335.16
Landing Gear: Main	228	17.64	4021.92
Powerplant	800	4.41	3528
Fixed Equipment	443	11.46	5079.438
Empty Weight	2535	13.23	33538.05
Passengers: Front Row	350	11	3850
Passengers: Rear	350	12	4200

Row			
Luggage	120	17	2040
Trapped Fuel and Oil	18	10	180
Batteries	620	11.758	7289.96
Takeoff Weight	3980		

The CG locations for different loading scenarios is calculated as follows:

**Table 8.6: Loading Scenarios**

<b>Loading Scenarios</b>	<b>CG location from the nose (ft)</b>	<b>Weight(lbs)</b>
Empty Weight	13.23	2535
Empty Weight + Front Row passengers	12.95	2885
Empty Weight + Rear row passengers	13.08	2885
Empty Weight + Passengers	12.85	3235
Empty weight + baggage	13.40	2655
Empty Weight + Passengers + baggage	13.00	3355
Empty Weight + passengers + baggage + TFO	12.98	3373
Empty Weight + passengers + baggage + TFO + batteries	12.79	3980

The CG excursion diagram is as follows:

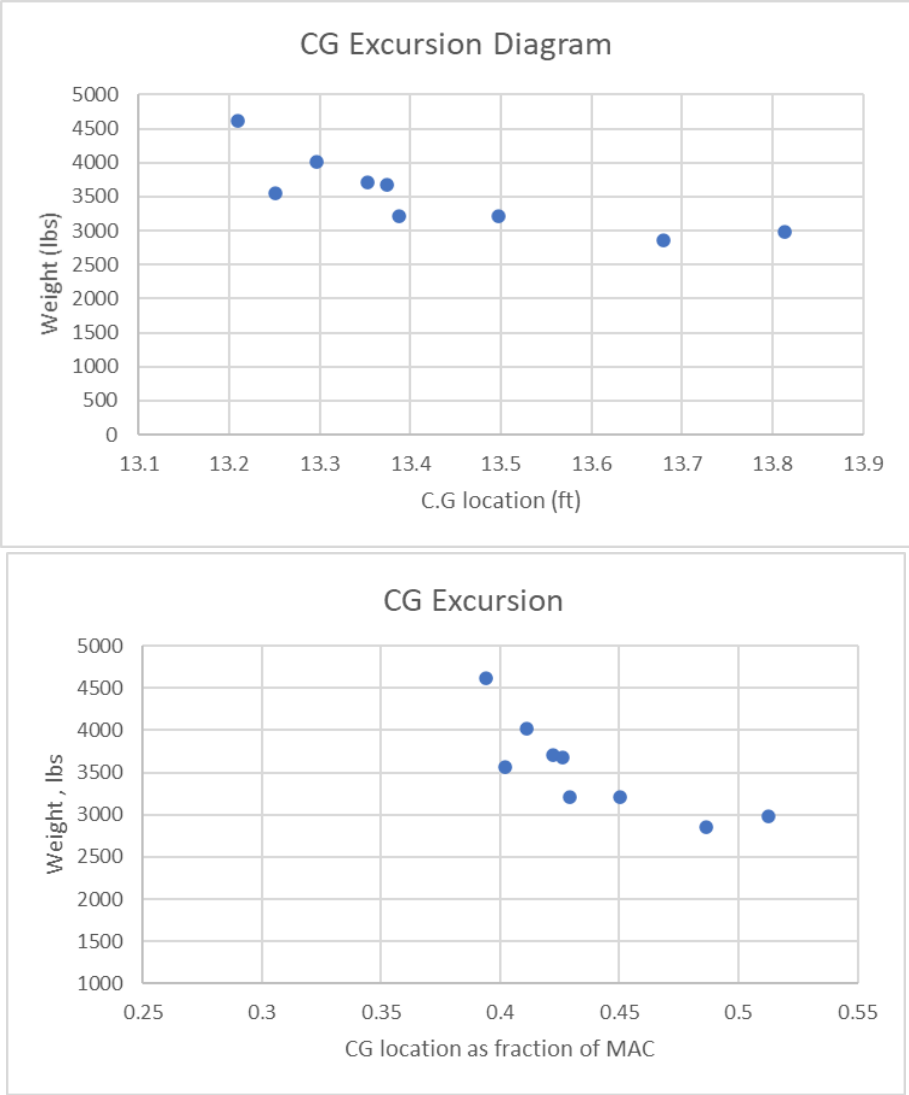


Figure 8.4: CG excursion diagram

**Conclusions from the CG Excursion diagram:**

- Most forward CG location from the nose of the proposed aircraft: 12.79 ft
- Most aft CG location from the nose of the proposed aircraft: 13.40 ft

As per the Roskam [1], the CG range for single engine airplanes is 7 to 18 inches and the obtained range for the proposed aircraft is 7.2 inches.

**CG range as a fraction of Mean Aerodynamic Chord (MAC):**

- Most forward CG as the fraction of MAC: 0.31
- Most aft CG as the fraction of MAC: 0.431

The obtained range for the proposed aircraft is 0.12c, which is within the range mentioned in Roskam [1].

### 8.3 Landing Gear Design

#### 8.3.1 Number, Type, and Size of Tires

The maximum static load per strut can be calculated by using the following equations:

$$\text{Nose wheel strut: } P_n = \frac{W_{TO} * l_m}{l_m + l_n} = 1053 \text{ lbs}$$

$$\text{Main wheel strut: } P_m = \frac{W_{TO} * l_n}{(l_m + l_n) * n_s} = 1465 \text{ lbs}$$

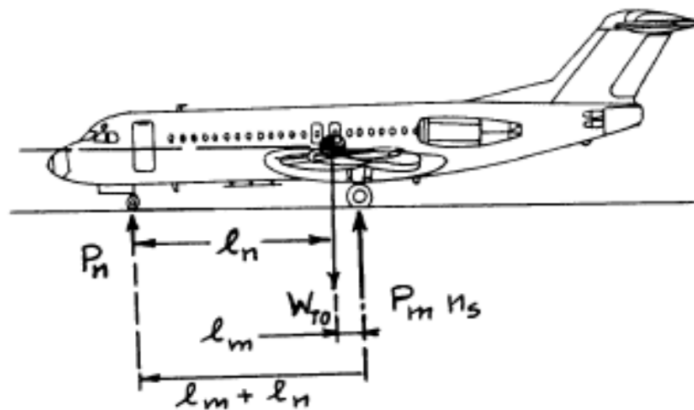


Figure 8.5: Geometry for Static load tricycle gear

$$l_m = 2.7 \text{ ft and } l_n = 7.5 \text{ ft}$$

Here  $n_s = 2$ : two main gear struts are used for the proposed aircraft. One nose gear strut is used based on the maximum static load calculation. The gear ratios are determined as :

$$\frac{n_s * P_m}{W_{TO}} = 0.74: \quad \text{Main Gear tire : } D_t \times b_t = 16.5 \times 6 \text{ inches}$$

$$\frac{P_n}{W_{TO}} = 0.26: \quad \text{Nose Gear tire: } D_t \times b_t = 14 \times 5 \text{ inches}$$

#### 8.3.2 Preliminary Arrangement

The landing gear is designed based on two geometric criteria:

### 1.) Tip-over criteria

- Longitudinal tip-over criterion:

According to this criterion, the main landing gear must be behind the aft CG location for tricycle gear and the angle between the aft CG and the main landing gear should be 15 degrees.

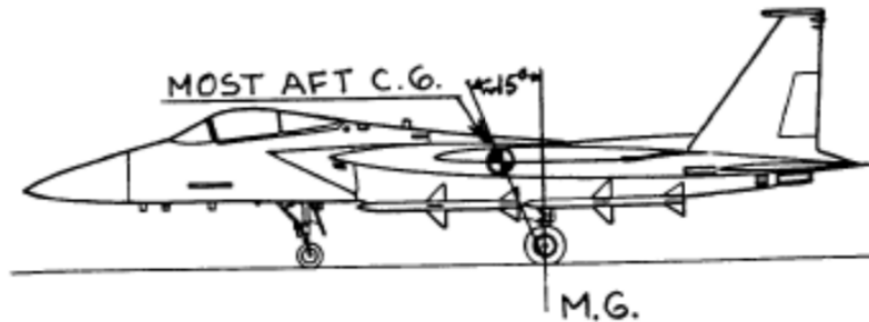


Figure 8.6: Longitudinal tip-over criterion for tricycle gear

The landing gear disposition is rightly placed based on the above geometric criterion. Figure 8.7 shows the proposed aircraft satisfying the longitudinal tip-over criterion.

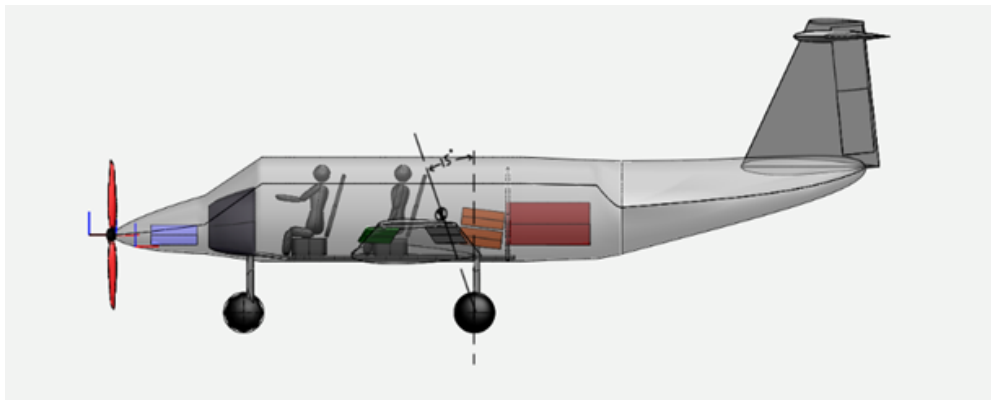


Figure 8.7: Longitudinal tip-over criterion for the proposed aircraft

- Lateral tip-over criterion:

The lateral tip-over criterion is given by the below figure and is dictated by angle  $\psi$ .

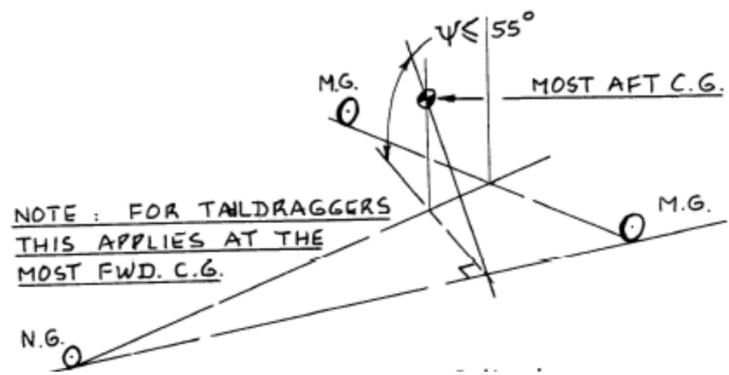


Figure 8.8: Lateral tip-over criterion

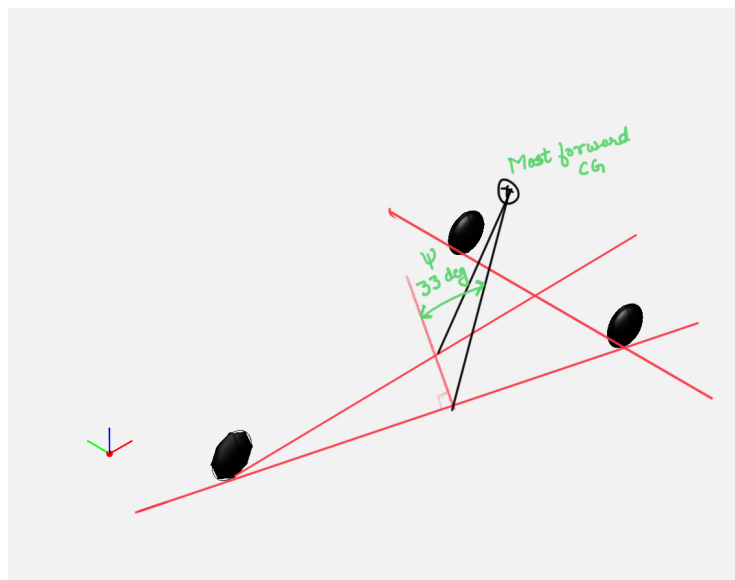


Figure 8.9: Lateral Tip-over criterion for the proposed aircraft

## 2. Ground clearance criteria:

- Longitudinal ground clearance criterion:

The longitudinal ground clearance given for tricycle gear is shown below

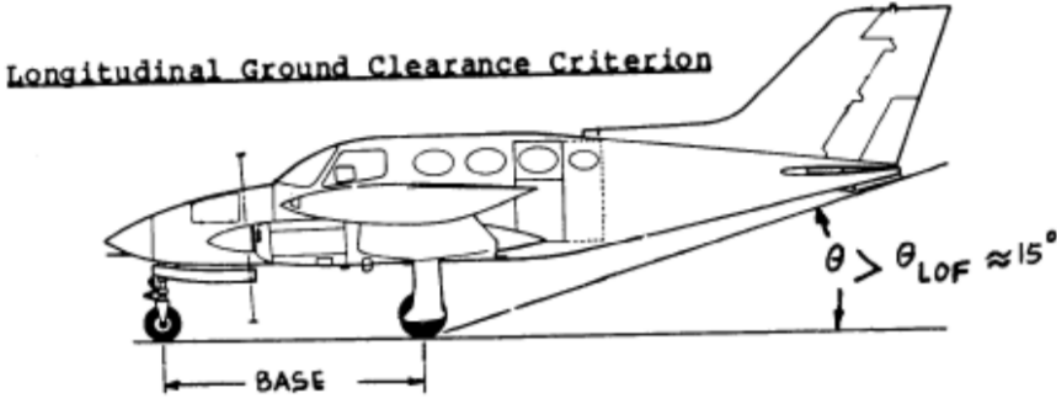


Figure 8.10: Longitudinal ground clearance criterion for tricycle gear [1]

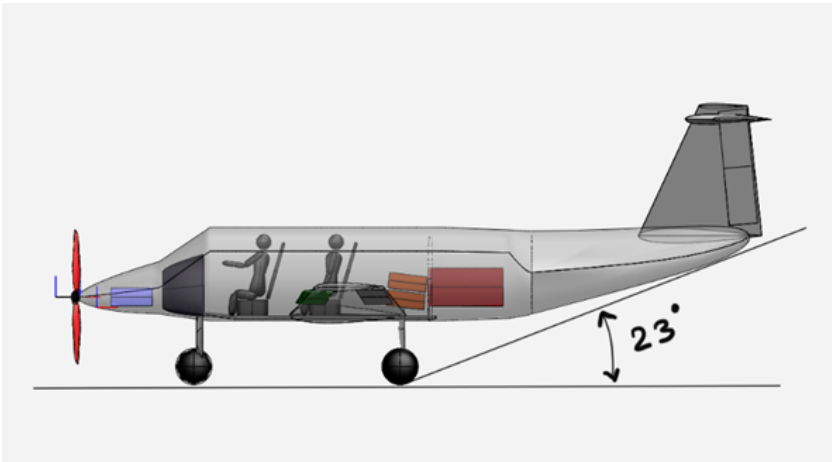


Figure 8.11: Longitudinal ground clearance criterion for the proposed aircraft

- Lateral ground clearance criterion:

The lateral ground clearance given for tricycle gear is shown below:

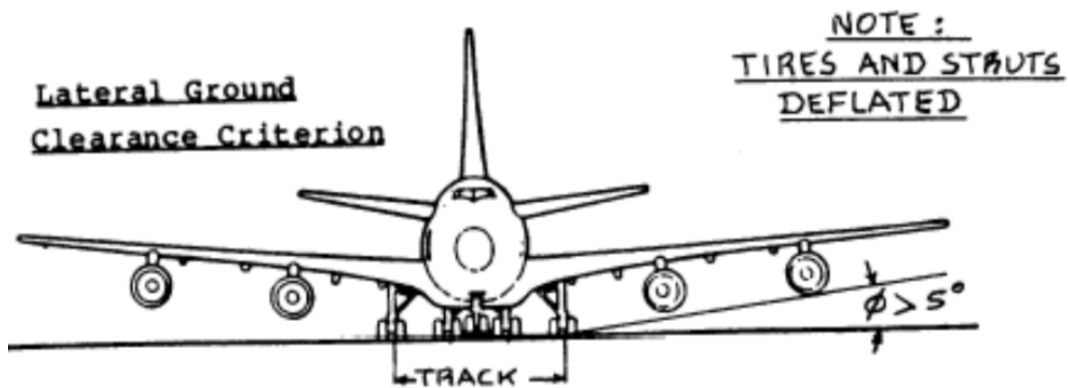


Figure 8.12: Lateral ground clearance criterion for tricycle gear

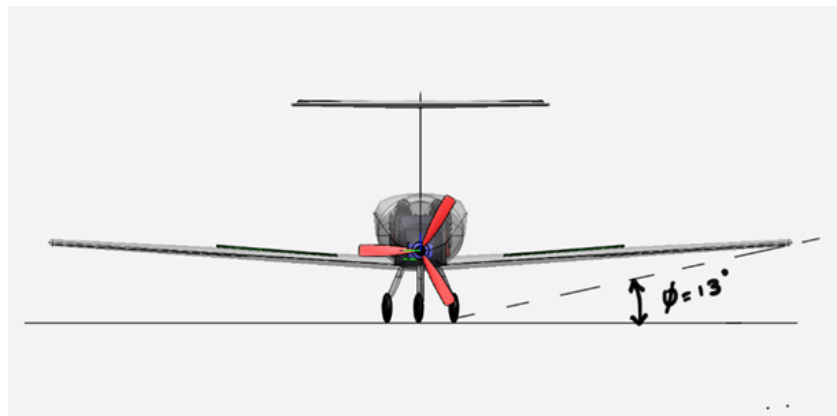


Figure 8.13: Lateral ground clearance criterion for the proposed aircraft

## 8.4 Discussion

An iterative process is carried out for the landing gear disposition satisfying the geometric criteria. The component weights are obtained by using comparable airplanes weight fraction data. Initially, the weight and balance method for subgroups of aircraft is carried out by assuming the landing gear disposition. The main landing gear has shifted 1.5 ft to the front to meet the two geometric criteria mentioned above.

The CAD model of the proposed aircraft with landing gear disposition is shown below:



Figure 8.14: Front view of the proposed aircraft with landing gear disposition



Figure 8.15: Side view of the proposed aircraft

## Chapter 9

### Weight and Balance Analysis

#### 9.1 Introduction

In this chapter, an iterative study will be carried out to determine whether or not the center of gravity of the proposed aircraft is in the right place for different loading scenarios.

#### 9.2 Component Weight Breakdown

The component's final weight and coordinate data are shown below with x and z coordinates based on the updated landing gear disposition. The moment arm data for the landing gear is updated in the table below.

**Table 9.1: Components with final weight and coordinate data**

Type of Component	Weight(lbs)	x(ft)	Wx (ft.lbs)	z (ft)	Wz (ft.lbs)
Wing	460	11.758	5408.68	5	2300
Empennage	99	27.0095	2673.941	16.4	1623.6
Fuselage	428	11.466	4907.448	6.5	2782
Landing Gear: Nose	57	5.88	335.16	1.5	85.5
Landing Gear: Main	228	14.7	3351.6	2.5	570
Powerplant	800	4.41	3528	6	4800
Fixed Equipment	443	11.466	5079.438	6.5	2879.5
Empty Weight	2535	13.23	33538.05	7.38	18708.3
Passengers: Front row	350	10	3500	6.5	2275
Passengers: Rear row	350	12	4200	6.5	2275

Luggage	120	15	1800	6	720
Trapped fuel and oil	18	10	180	6	108
Batteries	620	11.758	7289.96	5.2	3224
Takeoff Weight					3980

### 9.3 Center of Gravity Location for Various Loading Scenarios

The final CG locations are calculated for different loading scenarios as follows:

**Table 9.2 : Final CG location for different loading scenarios**

Loading scenarios	CG locations from nose (ft)	Weight(lbs)
Empty Weight	13.23	2535
Empty Weight + Front Row passengers	12.838	2885
Empty Weight + Rear row passengers	13.081	2885
Empty Weight + Passengers	12.747	3235
Empty weight + Baggage	13.310	2655
Empty Weight + Passengers + Baggage	12.828	3355
Empty Weight + Passengers + Baggage + TFO	12.813	3373
Empty Weight + Passengers + Baggage + TFO + Batteries	12.649	3980

The updated CG excursion diagram based on the final CG locations for different loading scenarios is shown below:

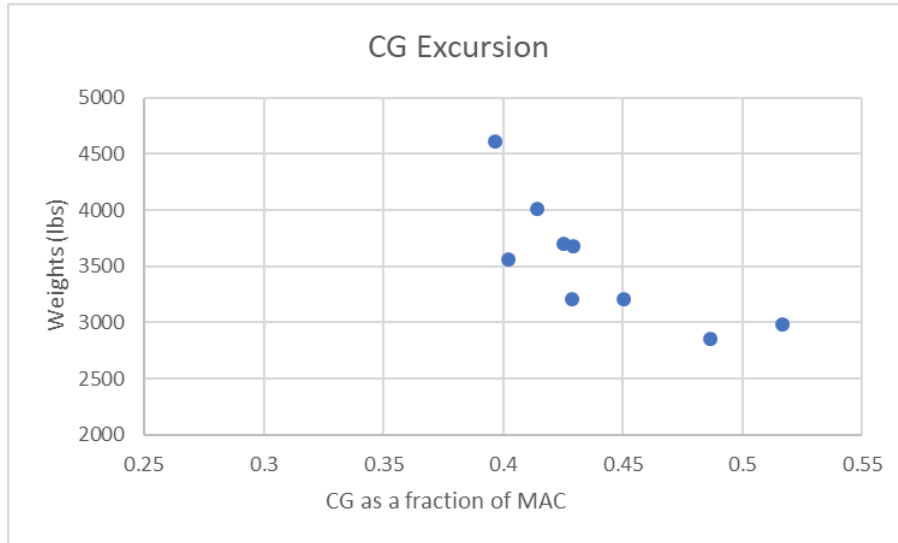


Figure 9.1: CG excursion diagram

Based on the final CG excursion diagram, the CG range for the proposed aircraft is determined as 0.13c.

- Most forward CG location from nose tip: 12.64 ft
- Most aft CG location from nose tip: 13.31 ft

## 9.4 Discussion

In this chapter, an iterative process was carried out for the weight and balance analysis. The CG range for the proposed aircraft is within the acceptable limits of comparable aircraft CG range given by Roskam [1]. Further stability and control analysis will be carried out with more iterations to obtain exact CG location.

# Chapter 10

## Stability and Control Analysis

### 10.1 Introduction

This chapter presents a detailed class-I stability and control analysis for the proposed aircraft configuration. The main objective is to determine the static longitudinal stability and static directional stability for the electric design.

Longitudinal and directional x-plots with respect to horizontal tail and vertical tail area are obtained in this report. The x-plots are used to determine the changes in the horizontal and vertical tail area with respect to the change in the aerodynamic center and center of gravity locations of the proposed aircraft.

### 10.2 Static Longitudinal Stability

The static longitudinal stability is determined in this section with the help of the following two legs of the X:

- The center of gravity leg represents the rate at which the center of gravity moves with respect to the change in the horizontal tail area [1].
- The aerodynamic center leg represents the rate at which the aerodynamic center moves with respect to change in the horizontal tail area [1].

The aft center of gravity location is already obtained in weight and balance analysis and the weight of the empennage is also known. The total empennage weight is obtained as 100 lbs. The horizontal tail weight is calculated as 49.95 lbs with 46.25 sq. ft area. Assuming the weight of the horizontal tail is independent of surface area, then the aerodynamic center is calculated for the proposed aircraft with the following equation:

$$\underline{X}_{a.c_A} = \frac{\{\underline{X}_{a.c_{wf}}\} + \frac{\{C_{L\alpha_h} * (1 - d\epsilon_h/d\alpha) * (S_h/S) * \underline{X}_{a.c_h}\}}{C_{L\alpha_{wf}}}}{\{1\} + \frac{\{C_{L\alpha_h} * (1 - d\epsilon_h/d\alpha) * (S_h/S)\}}{C_{L\alpha_{wf}}}}$$

(1)

**Table 10.1: Static longitudinal stability parameters [Appendix B]**

Parameters	Values
$\underline{X}_{ac_{wf}}$	0.091

$C_{L\alpha_{wf}}$	0.095 per deg
$C_{L\alpha_H}$	0.069 per deg
$\frac{d\varepsilon}{d\alpha}$	0.4
$\underline{X}_{ac_H}$	3.61

The longitudinal x-plot is shown below with the horizontal tail area varying from 0 to 60 sq. ft. Both  $\underline{X}_{ac_A}$  and  $\underline{X}_{c.g}$  are plotted as a function of horizontal tail area.

The proposed aircraft needs to be inherently stable with a static margin of 5 percent as it is a single-engine aircraft. The empennage area for a minimum static margin of 5 percent is the design point.

$$\frac{dc_m}{dc_L} = \underline{X}_{c.g} - \underline{X}_{ac} = -0.05 \quad (2)$$

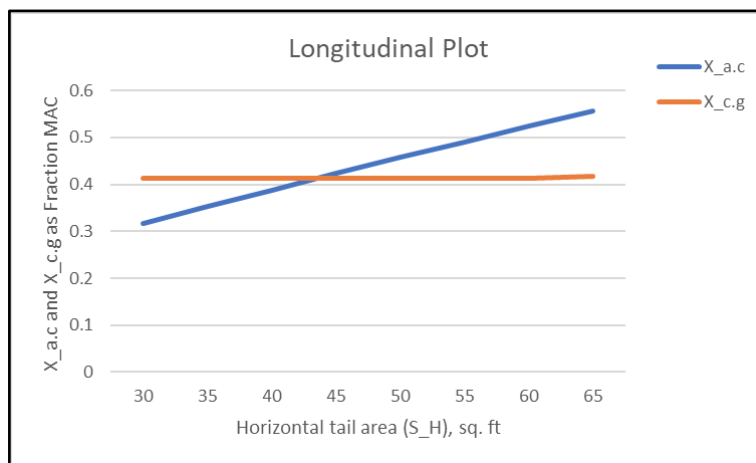


Figure 10.1: Longitudinal stability x-plot

Figure 10.1 shows the static margin of 5 percent at the horizontal tail area of 50.5 sq. ft and area of horizontal tail obtained during empennage design is 46.25 sq. ft. The difference between the estimated and obtained tail areas is within the specified limits as per class-I stability and control analysis. Therefore, the proposed aircraft is longitudinally stable and no iteration is required.

### 10.3 Static Directional Stability

The static directional stability is determined in this section using a directional x-plot with a side slip moment coefficient as a function of the vertical tail area.

The  $C_{n\beta}$  leg of the X-plot follows from:

$$C_{n\beta} = C_{n\beta_{wf}} + C_{L\alpha_v} * \frac{S_v * X_v}{S * b} \tag{3}$$

The Wing-Fuselage contribution in equation 5 can be calculated as:

$$C_{n\beta_{wf}} = -K_n * K_{RI} * \frac{S_{fs} * l_f}{S * b} \tag{4}$$

**Table 10.2: Static directional stability parameters [Appendix B]**

Parameters	Values
$C_{n\beta_{wf}}$	-0.000341 per deg
$C_{L\alpha_v}$	0.035 per deg
$K_n$	0.0011
$K_{RI}$	1.5

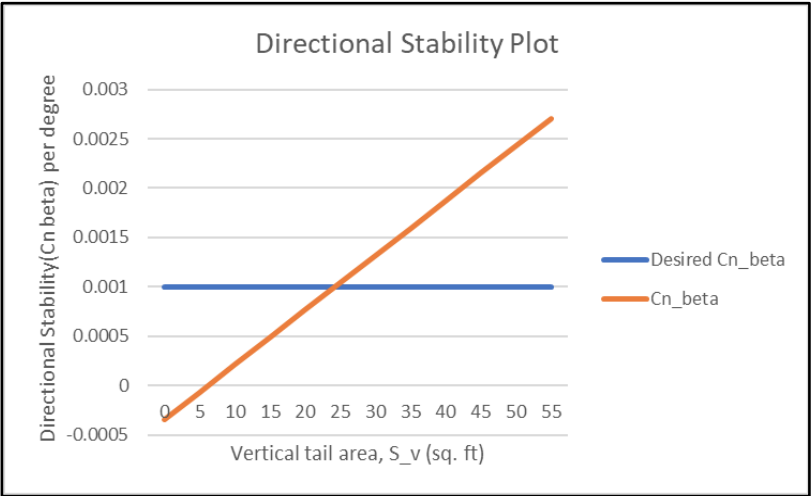


Figure 10.2: Directional stability x-plot

The vertical tail area of 25.2 sq. ft is obtained from the directional x-plot at  $C_{n_{\beta}} = 0.001$  and the value obtained from the empennage design is 26 sq. ft. The difference is quite negligible in the preliminary design of class-I. Hence, the proposed aircraft is directionally stable with no variation in the vertical tail area.

- The proposed aircraft is single-engine propeller-driven aircraft. Thus, the one engine inoperative requirement does not apply.

## 10.4 Conclusion

The plots above clearly indicate that the proposed aircraft is both longitudinal and directionally stable as per class I preliminary design requirements. The vertical tail area does not require any iteration, the horizontal tail area, however, can be resized more precisely to improve the difference. Some components need to be moved to adjust the center of gravity location. The iteration for the proposed aircraft will be explored further in class-II sizing.

# Chapter 11

## Drag Polar Estimation

### 11.1 Introduction

In this chapter, the drag polar estimation of the proposed aircraft is studied. The initial estimation of the drag polar equations is already obtained in the performance analysis chapter. The main objective of this report is to calculate the drag increment due to flaps and landing gear during take-off and landing. The calculated drag polar equations are then plotted for lift coefficient vs drag coefficient for different flight conditions.

### 11.2 Airplane Zero-lift Drag

The airplane zero-lift drag can be determined by calculating the total wetted area for each component that contributes to the wetted area such as:

1. Wing
2. Empennage
3. Fuselage

- **Airplane Total Wetted Area:**

The wetted area for wings, horizontal tail, and vertical tail can be calculated using the following equation:

$$S_{wet_{plf}} = 2 * S_{exp_{plf}} * \left(1 + \frac{0.25 * \left(\frac{c}{c}\right) r * (1 + \lambda r)}{1 + \lambda}\right) \quad (1)$$

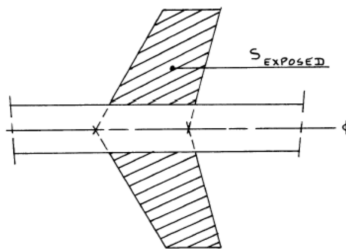


Figure 11.1 Exposed Planform Definition

The wetted area of the fuselage can be calculated using the following formula:

$$S_{wetted_{fuse}} = \pi * D_f * l_f * (1 - \frac{2}{\lambda_f})^{3/2} * (1 + \frac{1}{\lambda_f^2}) \quad (2)$$

The summary of all the component's wetted area of the proposed aircraft is given below:

**Table 11.1 : Summary of components wetted area and total wetted area**

Component	Equation Parameters	Wetted Area (ft <sup>2</sup> )
Wing	S = 194 ft <sup>2</sup> (t/c) <sub>r</sub> = 0.17 (t/c) <sub>t</sub> = 0.13 λ = 0.50 τ = 1.3	406.18
Subtract Intersection of wing and fuselage	Difference = (5.5*5.375)	-29.56
Vertical tail	S <sub>v</sub> = 26.0 ft <sup>2</sup> (t/c) = 0.12 λ = 0.40	53.56
Horizontal tail	S <sub>H</sub> = 46.25 ft <sup>2</sup> (t/c) = 0.12 λ = 0.40	95.275
Fuselage	D <sub>f</sub> = 5.5 ft l <sub>f</sub> = 29.4 ft	437.93
Total Wetted Area		963

The calculated total wetted area of the proposed aircraft is 963 ft<sup>2</sup> and the estimated wetted area from Chapter 3 is 875 ft<sup>2</sup>. This difference needs to be evaluated for any change in L/D ratio.

- **Equivalent parasite drag of the airplane**

The equivalent parasitic area, 'f' of the airplane is estimated from Figure 3.8 as follows.

$$f = 9 \text{ ft}^2$$

- **Clean zero-lift drag coefficient C<sub>D0</sub>**

The clean zero-lift coefficient at low speeds is calculated as:

$$C_{D_0} = \frac{f}{S}$$

$$C_{D_0} = 0.046$$

## 11.3 Low-speed Drag Increments

### 11.3.1 High-Lift Device Drag Increments for Takeoff Flaps, Landing Flaps and Landing Gear

The flap drag increment for take-off and landing can be determined by using the data from Figure 3.9. The estimated values for  $\Delta C_{D_0}$  and  $e$  are as follows

**Table 11.2: Flap drag increment for different flight conditions**

Flight condition	$\Delta C_{D_0}$	Aspect ratio	$e$	Drag Polar
Clean	0	10	0.85	$0.046 + 0.0374C_L^2$
Take-off flaps	0.0165	10	0.80	$0.0625 + 0.0397C_L^2$
Landing flaps	0.0615	10	0.75	$0.1075 + 0.0424C_L^2$
Landing gear	0.0215	10	No effect	$0.129 + 0.0424C_L^2$

## 11.4 Airplane Drag Polar

The following tabulation summarizes the drag polar for the proposed airplane with an aspect ratio of 10 and a wing area of 194 ft<sup>2</sup>.

**Table 11.3: Drag polar equations**

Flight Condition	$C_D$
Clean	$0.0460 + 0.0374C_L^2$
Takeoff Flaps	$0.0625 + 0.0397C_L^2$
Landing Flaps	$0.1075 + 0.0424C_L^2$
Landing Gear	$0.1290 + 0.0424C_L^2$

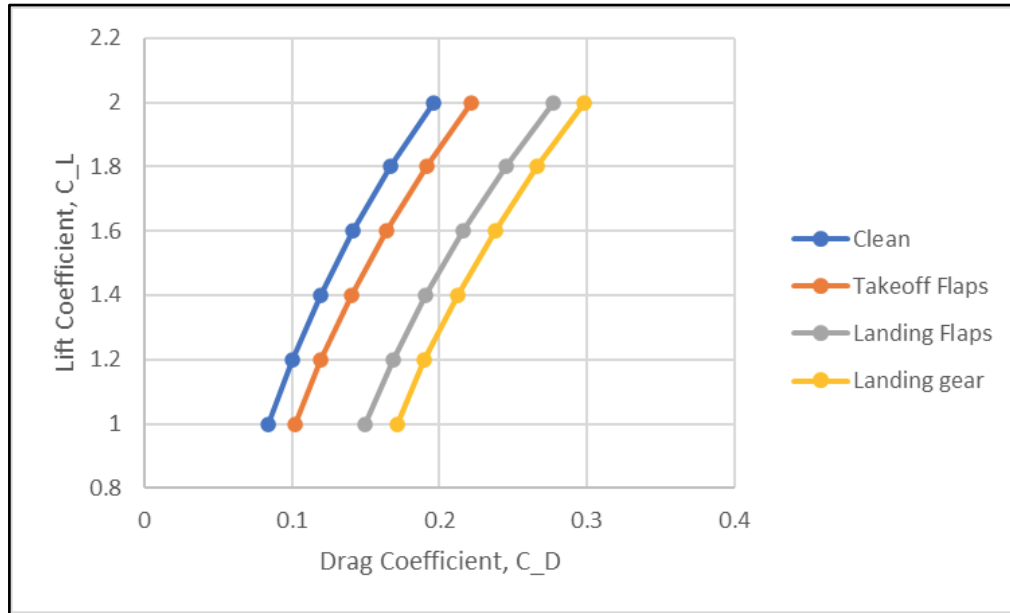


Figure 11.2: Cruise, takeoff and landing drag polar

Table 11.4: Part I and part II L/D values

Flight Condition	L/D Part I	L/D Part II
Clean	11.72	11.50
Takeoff	10.0	9.70
Landing	7.50	7.35

## 11.5 Discussion

In this chapter, drag polar equations for different flight conditions were calculated manually and then plotted using Excel. The data in Table 11.4 indicates that the proposed aircraft has slight reduction in the L/D values than predicted during the performance sizing in chapter 3. From the sensitivity analysis, range is affected by a change in lift-to-drag ratio by a factor of 74 kms for a unit change in lift-to-drag ratio. Therefore, the range for the proposed aircraft will be reduced by 16 km.

Compressibility drag is neglected for this design as  $M \leq 0.3$ . The obtained drag polar equations are acceptable for Class-I preliminary design.

## **11.6 Conclusion**

To summarize, mission specification changes due to the decrease in the final lift-to-drag ratio. However, the difference is quite negligible and can be ignored.

# Chapter 12

## Drawings, Environmental and Safety Considerations

### 12.1 Drawings

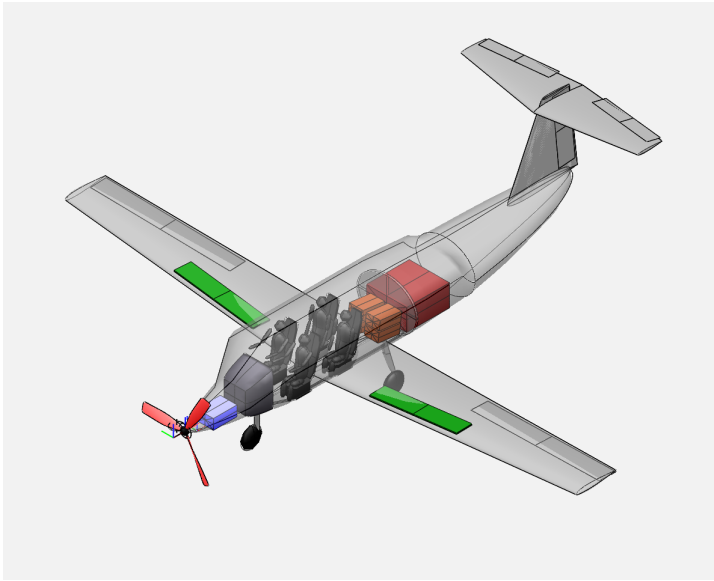


Figure 12.1: Isometric

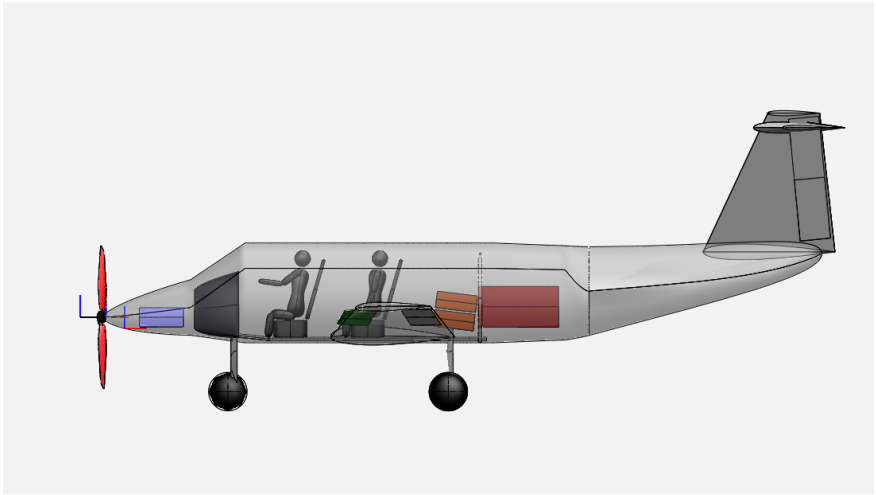


Figure 12.2: Side view of the proposed aircraft

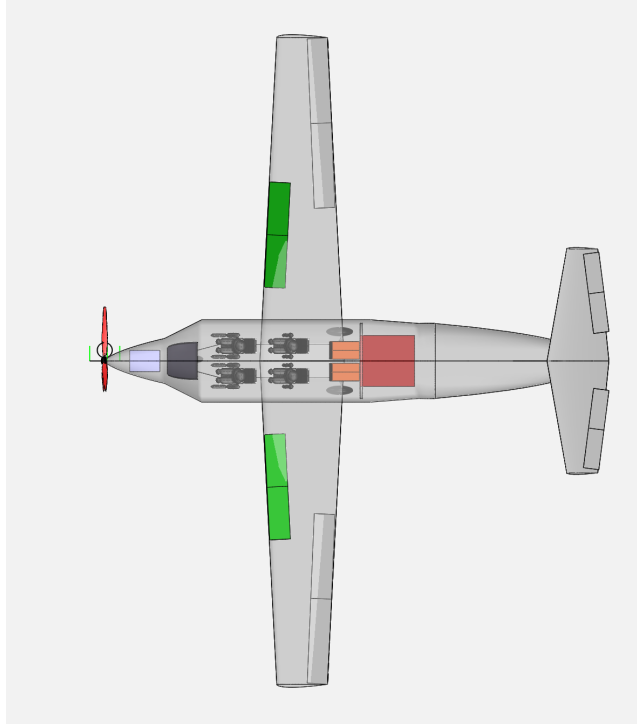


Figure 12.3: Top view of the proposed aircraft



Figure 12.4: Front view of the proposed aircraft

**Table 12.1: Important design parameters**

	<b>WING</b>	<b>HORIZONTAL TAIL</b>	<b>VERTICAL TAIL</b>
<b>Area</b>	194 ft <sup>2</sup>	46.25 ft <sup>2</sup>	26 ft <sup>2</sup>
<b>Span</b>	44 ft	15.20 ft	6.44 ft
<b>Aspect ratio</b>	10	5	1.6
<b>Sweep angle</b>	0 deg	10 deg	15 deg
<b>Taper Ratio</b>	0.50	0.5	0.4
<b>Airfoil</b>	Wing Root: NASA LS-0417 Wing Tip: NASA LS-0413	NACA 0012	NACA 0012
<b>Dihedral Angle</b>	7 deg	0 deg	90 deg
<b>Incidence Angle</b>	2 deg	Variable	0 deg
<b>Root Chord</b>	5.87 ft	4.05 ft	5.76 ft
<b>Tip Chord</b>	2.90 ft	2.02 ft	2.3 ft
<b>FUSELAGE</b>			
<b>Total Length</b>	29.40ft		
<b>Diameter</b>	4.5 ft		
<b>Nose Length</b>	5 ft		
<b>Cabin Length</b>	10.4 ft		
<b>Fineness Ratio</b>	6.53		
<b>Tail Cone Length</b>	14 ft		

### 12.1.1 Areas to improve:

The proposed aircraft is designed based on many assumptions by comparing to similar mission airplanes. The mission requirements seem reasonable for this type of aircraft while trying to push the capabilities of electric propulsion in terms of range.

- The design could be improved by choosing a lower coefficient of lift during takeoff or otherwise going for a larger wing.
- The range specified in the mission directly depends on the battery energy density. Battery system needs further research to improve the battery energy density and weight of the battery.

## 12.2 Environmental Considerations

- The environmental issues associated with the electric aircraft is the disposition process for the batteries. Currently in use, are made of lithium ions and the process associated with the production of lithium batteries emits air pollutants that may affect air quality and health. Moreover, the lifetime of batteries is still short and induces battery waste containing toxic or corrosive materials such as lithium. This hazardous waste could pose threats to health and the environment if improperly disposed.
- To address the battery disposal issue, the rechargeable batteries are suggested in the proposed aircraft, so that the same batteries can be reused multiple times. When no longer viable for aircraft use, it is also possible that these batteries are subsequently re-used in a secondary operation such as backup power for server locations to reduce the impact on the environment.
- Manufacturing cost of the electric aircraft is not going to be high except the integration of avionics and other subsystems with batteries. Once the technology gets matured and validated, the cost will automatically decrease.
- The economic tradeoff for the environmental concern is the cost of research in battery technology and the cost of manufacturing and operating the electric aircraft. Public acceptance can be gained by proving the value and safety of the technology.
- All-electric aircraft could greatly reduce the environmental impact of aviation. Batteries with significantly higher specific energy density and lower cost, coupled with further reductions of costs and CO<sub>2</sub> intensity of electricity, are necessary for exploiting the full range of economic and environmental benefits provided by electric airplanes.[19]

## 12.3 Safety Considerations

- The key hazards identified were lithium-polymer battery thermal runaway and energy uncertainty, common mode power system failure, and vehicle automation failure. Thermal runaway can be caused by a number of factors; over-charging, over-heating, mechanical damage, and manufacturing defects are the most common. [20]
- The safety issue can be addressed by carefully monitoring the battery power and improving electrical protection. Excessive charging brings on thermal runaway so to prevent this problem,

lithium batteries should contain auto shut-off circuits that stops the batteries from overcharging. The discharging rate needs to be controlled by an electronic controller.

- The electric aircraft technology is currently in the development phase and not much data available from the past flights due to battery energy limitations and weight addition.
- The risk of battery thermal runaway is the tension between currently acceptable ways of meeting the requirements and the need to reduce battery weight as much as possible to make the vehicles practically viable. Experimental research has been going on improving the battery technology and it gives the most promise in terms of specific energy density.

## References

1. Roskam, J. (1985). *Airplane Design: Preliminary configuration design and integration of the propulsion system*. DARcorporation.
2. Riddell, A., Ronson, S., Counts, G., & Spenser, K. (2004). Towards Sustainable Energy: The current Fossil Fuel problem and the prospects of Geothermal and Nuclear power. *Journal on trade & environment*.-Stanford University, California, USA.
3. Jardine, C. N. (2005). Calculating the Environmental Impact of Aviation Emissions. Environmental Change Institute, Oxford University Centre for Environment.
4. Air Transport Action Group (ATAG). <https://www.atag.org/facts-figures>
5. Overview of NASA Electrified Aircraft propulsion research for large subsonic transports. <https://arc.aiaa.org/doi/10.2514/6.2017-4701>
6. “Sun Flyer,” *Bye Aerospace* Available: <https://bye aerospace.com/sun-flyer/>.
7. “Aircraft Model Pipistrel aircrafts”: <https://www.pipistrel-usa.com/panthera/>
8. “Aircraft Yuneec E-340”: [https://en.wikipedia.org/wiki/Yuneec\\_International\\_E430](https://en.wikipedia.org/wiki/Yuneec_International_E430)
9. “Aircraft Model Taurus Electro G2”.  
<https://www.pipistrel-aircraft.com/aircraft/electric-flight/taurus-electro/>
10. “Aircraft Model Airbus Vahana” <https://www.airbus.com/innovation/urban-air-mobility/vehicle-demonstrators/vahana.html>
11. Abdel-Hafez, A. (2012). Power generation and distribution system for a more electric aircraft-A review. *Recent advances in aircraft technology*. IntechOpen.
12. M. Hepperle, "Electric Flight - Potential and Limitations," NATO Science and Technology Organization, 2012.
13. T. Engineering, "U.S. Standard Atmosphere," *Engineering ToolBox*.  
[https://www.engineeringtoolbox.com/standard-atmosphere-d\\_604.html](https://www.engineeringtoolbox.com/standard-atmosphere-d_604.html), 2003.
14. D. P. Raymer, "Aircraft Design," in *Aircraft Design: A Conceptual Approach, Fifth Edition*, AIAA Education Series, 2012.
15. Airfoil data Retrieved: <https://ntrs.nasa.gov/archive/nasa/casi.ntrs.nasa.gov/19810003507.pdf>
16. “Design of a 4-Seat, General Aviation, Electric Aircraft.”  
<https://www.sjsu.edu/ae/docs/Viral.Rathod-S18.pdf>
17. “Electric, Hybrid, and Hydrogen Aircraft” – State of Play By ICAO Secretariat.
18. Jardine, C. N. (2005). Calculating the Environmental Impact of Aviation Emissions. Environmental Change Institute, Oxford University Centre for Environment.

19. Schäfer, A. W., Barrett, S. R., Doyme, K., Dray, L. M., Gnad, A. R., Self, R., ... & Torija, A. J. (2019). Technological, economic and environmental prospects of all-electric aircraft. *Nature Energy*, 4(2), 160-166.
20. Courin, C., & Hansman, R. J. (2018). Safety Considerations in Emerging Electric Aircraft Architectures. In *2018 Aviation Technology, Integration, and Operations Conference* (p. 4149).